FINAL REPORT

FOR

STUDY PROGRAM ON LARGE APERTURE ELECTRONIC SCANNING PHASED ARRAY ANTENNAS FOR THE SHUTTLE IMAGING MICROWAVE SYSTEM

PREPARED FOR

JET PROPULSION LABORATORY
4800 OAK GROVE DRIVE
PASADENA, CALIFORNIA 91103

FR - 104
JUNE 1974

SENSE SYSTEMS COMPANY
9162 LA ROSA DRIVE
TEMPLE CITY, CALIFORNIA 91780

Final Report for

A STUDY PROGRAM ON LARGE APERTURE ELECTRONIC SCANNING PHASED ARRAY ANTENNAS FOR THE SHUTTLE IMAGING MICROWAVE SYSTEMS

Final Report FR-104

June 1974

Contract No. 953921

Prepared for

JET PROPULSION LABORATORY
4800 Oak Grove Drive
Pasadena, California 91103

This work was performed for the Jet Propulsion Laboratory, California Institute of Technology, sponsored by the National Aeronautics and Space Administration under Contract NAS 7-100.

Prepared by

SENSE SYSTEMS COMPANY
9162 La Rosa Drive
Temple City, California 91780

CONTENTS

CONTENTS (Continued)

1.0 INTRODUCTION

This study investigates the potential use of large electronically scanned phased arrays as components of the multispectral antenna system for SIM S. While emphasis is placed on array antennas for 70, 21, 6 and 3 cm wavelengths, the material, in general, is presented in a format which allows extrapolation to shorter wavelengths.

The report is organized in five sections with the central topic of each section corresponding to the topics of the five weekly technical briefings. Section 2 introduces basic phased array theory and discusses performance parameters with emphasis on those parameters relating to microwave radiometry. Section 3 contains brief descriptions of four scanning phased arrays representing current examples of state-of-the-art phased array technology. A discussion of problem areas, both in performance and fabrication, is also included. Section 4 presents extrapolations of performance characteristics of phased array antennas expected with increased "sizes" up to 20 m x 20 m. Section 5 discusses the possibility of interlacing two or more phased arrays to achieve a multi-frequency aperture. Section 6 with a recommended antenna system to be used for SIMS, and Section 7 with conclusions and recommendations.

Section 2

PHASED ARRAY ANTENNA CHARACTERISTICS

2.1 FUNDAMENTAL ARRAY THEORY

A phased array antenna is an array of radiating elements aligned in such a manner that the energy from each of the radiators adds in-phase to produce a relative maximum or main beam in some desired direction. The radiation pattern of the phased array may be expressed as the array factor

$$A(\theta) = \sum_{n=0}^{N} E_n \left[\exp j\, n\psi \right]$$

where E_n are the individual element excitation coefficients, Ψ is the phase factor, and n is the number of radiating elements.

2.1.1 PHASE REQUIREMENTS

The location of the main beam peak is controlled by the inter-element phase relationship of the array which is the phase factor, Ψ. This factor can be written

$$\psi = k\, d \sin$$

where θ is the direction of the main beam relative to the array broadside, k is the wave number, $2\pi/\lambda$, and d is the inter-element spacing.

If there is assumed to be some constant phase difference, βd, between adjacent elements due to an interconnecting transmission line, then the relation becomes

$$\psi = k\, d \sin = \beta d$$

or

$$k\,d\sin\theta = \beta\,d$$

where $\beta = 2\pi/\lambda_g$ with λ_g the wavelength in the transmission line. Thus, for the linear array shown in Figure 2-1a, the location of the main beam is given by

$$\sin\theta = \lambda/\lambda_g$$

If phase reversal is added at each element as in the case of a waveguide array with slots alternately inclined about the waveguide centerline as shown in Figure 2-1b, then the above equation becomes

$$\sin\theta = \lambda/\lambda_g - \lambda/2d$$

Carrying the example one step further, assume that phase shifters are added at each radiating element as shown in Figure 2-1c, then

$$\sin\theta = \lambda/\lambda_g - \lambda/2d + \Phi/\frac{2\pi d}{\lambda}$$

where Φ is the added inter-element phase differential due to the phase shifter.

2.1.2 AMPLITUDE DISTRIBUTION

The above section describes the phase relations required to form a peak at some given location. It is equally important to control the width of that beam and the relative level of the beam peak to the highest sidelobe formed. The amplitude distribution is a controlling factor for both beamwidth and sidelobe level.

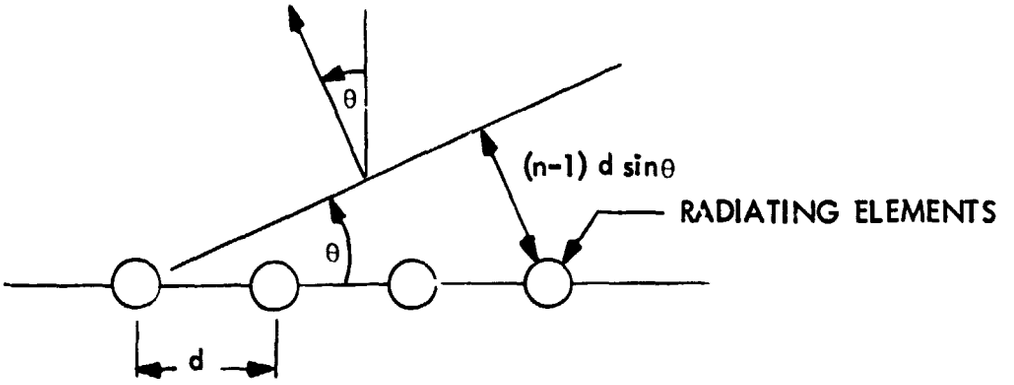

$k\ d \sin\theta = \beta d$

(a)

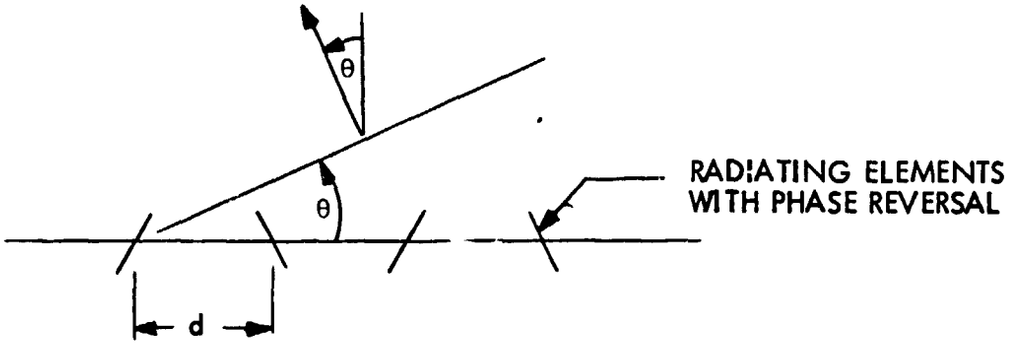

$k\ d \sin\theta = \beta d - \pi$

(b)

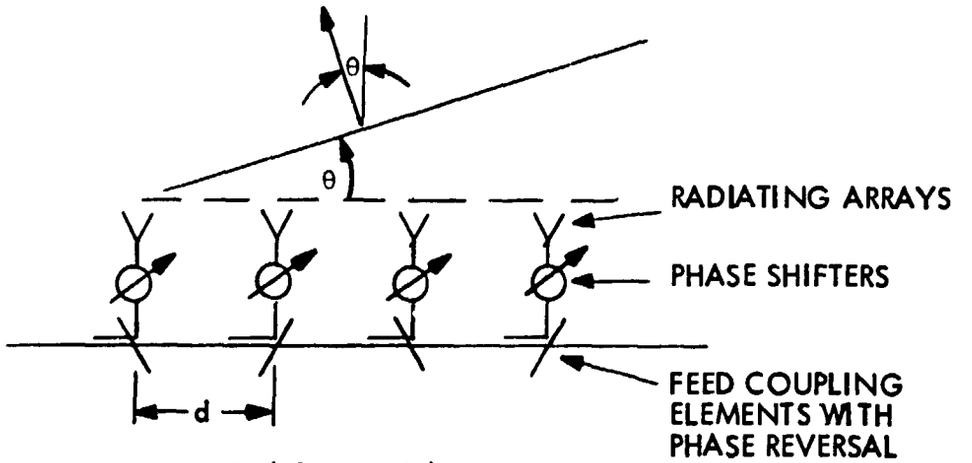

$k\ d \sin\theta = \beta d - \pi + \Phi$

(c)

Figure 2-1. Beam Angle

There are several amplitude distributions discussed in the literature, but the most important are the (1) uniform distribution, (2) Dolph Chebyshev (Ref. 1) distribution, (3) Taylor (Ref. 2) distribution, and (4) cosine-on-a-pedestal distribution.

The uniform distribution as its name implies requires that equal power be radiated from each element. This distribution provides the narrowest beamwidth for a given array size, hence maximum aperture efficiency. The disadvantage of the uniform distribution is its relatively high peak sidelobe level, -13.6 dB. However, for comparisons of amplitude distributions, the beamwidth of the uniform distribution is often used as a baseline or reference.

The Dolph-Chebyshev (D-T) distribution is a tapered amplitude distribution in which the excitation coefficients are made to coincide with the Chebyshev polynomial. This distribution yields a minimum beamwidth w hen the sidelobe levels are fixed and a minimum sidelobe level when the beamwidth is specified. The sidelobes are theoretically of equal amplitude over all space.

The Taylor distribution is a tapered amplitude distribution which is a modification of the D-T distribution. This distribution while similar to the D-T distribution, is more easily physically realizable. The Taylor distribution has only a finite number of equal amplitude sidelobes adjacent to the main beam. The number of equal level sidelobes and the peak sidelobe level are variables which specify the Taylor distribution. In the limit, as the number of equal level sidelobes approaches infinity, the Taylor distribution approaches the D-T distribution.

Figure 2-2 shows the relation between aperture length and beamwidth for both a Taylor and a D-T distribution with -35 dB peak sidelobes. The uniform distribution is included for reference.

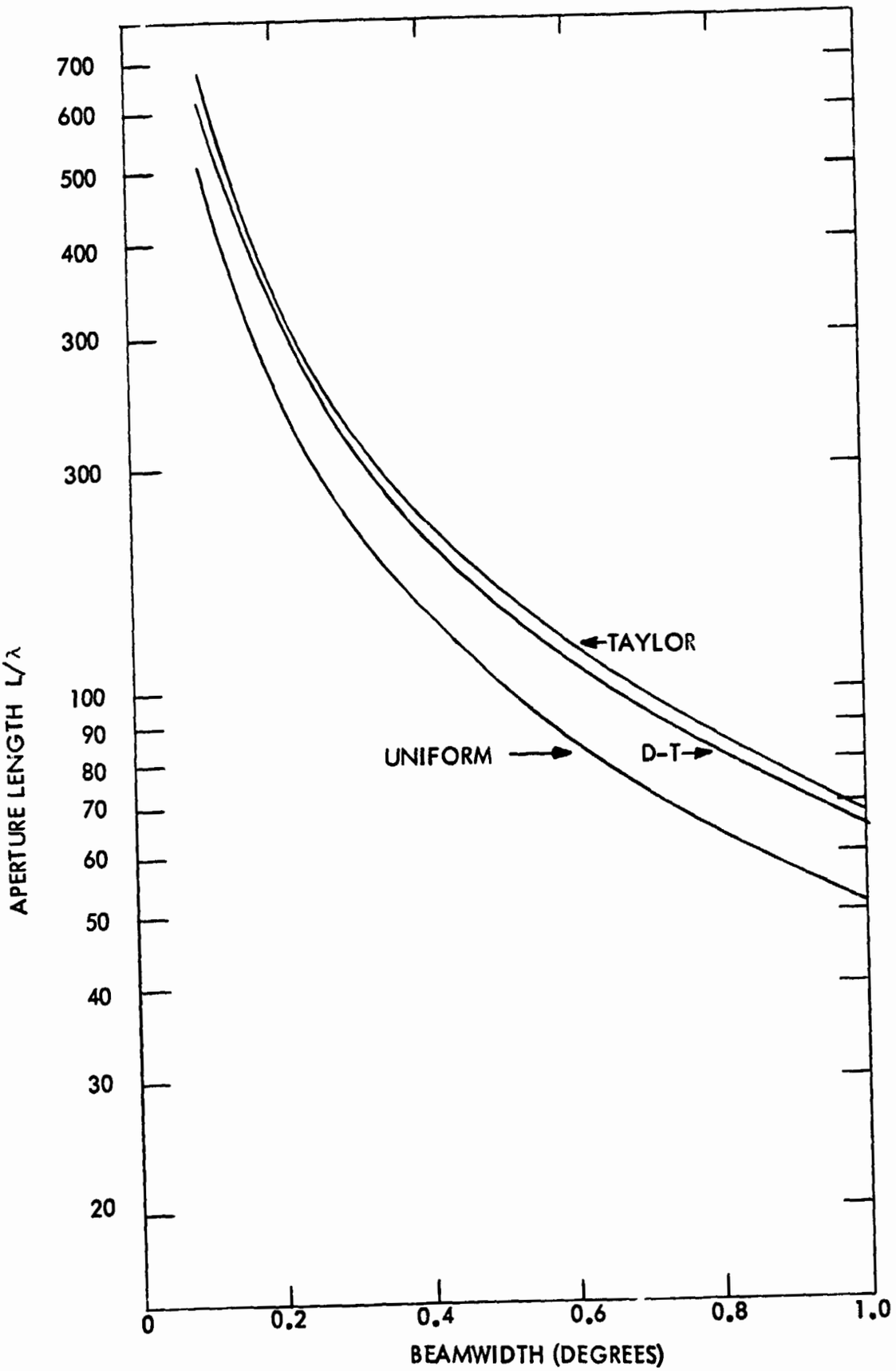

Figure 2-2. Beamwidth versus Aperture Length for Various Distributions

The cosine-on-a-pedestal distribution is, as the name implies, an amplitude distribution tapered to follow a cosinusoidal pattern, $\cos(\theta)$, with the limits

$$-\pi/2 \leq \theta \leq \pi/2$$

The term, pedestal, refers to a normalizing factor which in effect prevents a zero radiation condition from appearing at the end elements. The sidelobe level is controlled to some extent by the height of the pedestal.

2.1.3 ELEMENT FACTOR

The linear phased array, discussed above, has been assumed to have isotropic radiating elements, i.e., elements which radiate equally over all space. Since the practical element radiates with some specific pattern shape the linear array pattern will be modified accordingly as shown in Figure 2-3. The actual array pattern $A(\theta)$ is the result of pattern multiplication of the element factor $E(\theta)$ with the linear array factor. Hence,

$$A(\theta) = E(\theta) \sum_{n=0}^{N} C_n \left[\exp j\, n\, k\, d \sin\theta \right]$$

It can be seen from the figure that the element factor can cause a reduction in gain as the beam is scanned off broadside.

2.1.4 TWO-DIMENSIONAL ARRAY (Ref. 3)

The two dimensional or planar array is a grouping of individual radiators arranged in a rectangular array as shown in Figure 2-4. Assume that the array consists of

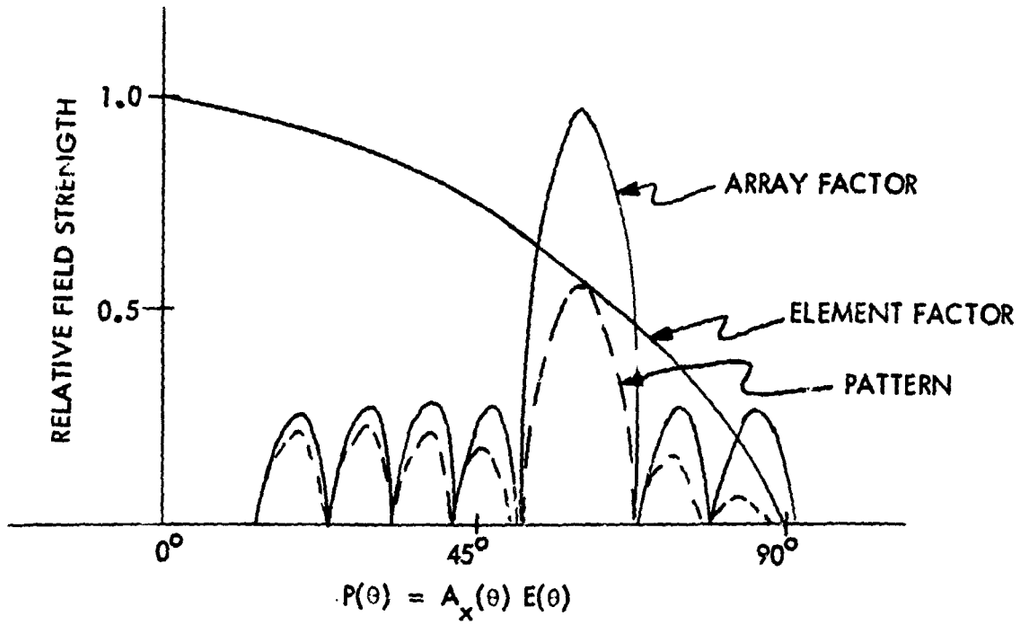

Figure 2-3. Effect of the Element Factor on the Pattern of a Linear Array

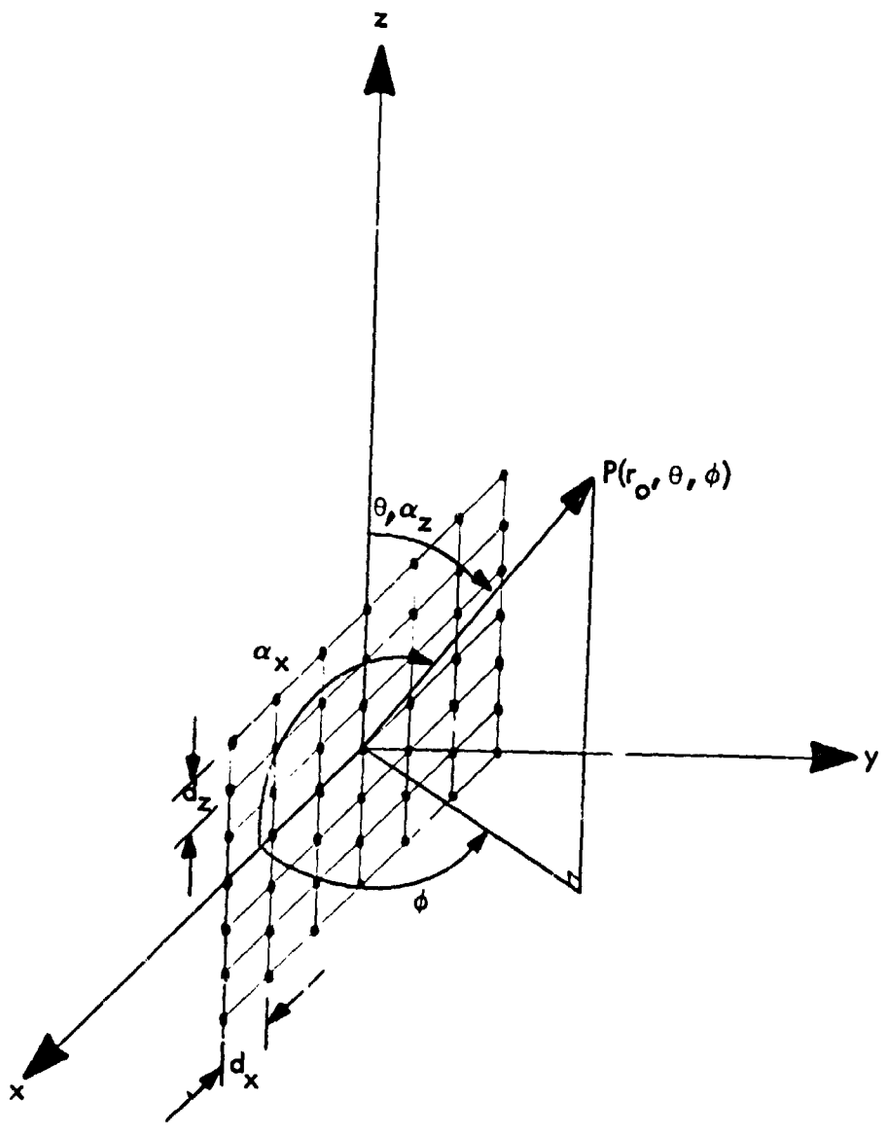

Figure 2-4. Array Geometry

$2N_z+1$ rows of elements with common spacing, dz , and that each row contains $2N_x+1$ elements with spacing, dx . The mnth element can then be defined as the element located at

$$x_m = md_x \, , \; z_n = nd_z$$

Also assume that the voltage (or current) amplitude at the mnth element is E_{mn} . The total array factor can then be written

$$A(\theta,\phi) = \sum_{m=-N_x}^{N_x} \sum_{n=-N_z}^{N_z} (E_{mn}/E_{oo}) \exp\left[j\, k\, (md_x \cos\alpha_x + nd_z \sin\alpha_z) \right]$$

If each row has the same amplitude distribution, then the array factor is separable and can be written as the product of the individual linear array factors.

$$A(\theta,\phi) = A_x(\theta,\psi)\, A_z(\theta,\Psi)$$

where

$$A_x(\theta,\phi) = \sum_{-N_x}^{N_x} E_m \exp(j\, m\, k\, d_x \cos\alpha_x)$$

$$A_z(\theta,\phi) = \sum_{-N_z}^{N_z} E_n \exp(j\, n\, k\, d_z \sin\alpha_z)$$

with E_m and E_n being the normalized amplitude distribution of the elements parallel to the x-axis and z-axis respectively.

If a uniform phase progression is imposed on the array and the amplitude distributions are symmetric, then the linear array factors A_x and A_z produce patterns which consist of conical main beams and sidelobes symmetric about the linear array axis.

The planar array factor $A = A_x A_z$, being the product of the two linear array factors has several important properties. Both of the linear array factors produce beams that are narrow in one angular dimension and fanned out over a conical surface in the other. The main beam is the result of the intersection of the two conical surfaces as shown in Figure 2-5. All significant sidelobes result from the product of the main beam of one array and the sidelobes of the other and must lie along the surface of the cones. Sidelobes which are a product of the individual array sidelobes are negligibly small. The majority of the radiated power is therefore contained within the regions defined by the conical main beams of the linear arrays. This of course is not true of rotationally symmetric antennas such as conical horns, reflector antennas, etc., where sidelobes occur as rings about the main beam. For this reason phased arrays have higher beam efficiencies than circularly symmetric antennas for a given maximum sidelobe level.

2.1.5 PHASED ARRAY BEAM SCANNING

The conical patterns of the two orthogonal linear array factors will have half cone angles α_x and α_z defined by the phase progression Ψ, along the x-axis and z-axis respectively, as shown by the following equations

$$\cos\alpha_x = \Psi_x / k\, d_x = \sin\theta \cos\psi$$

$$\cos\alpha_z = \Psi_z / k\, d_z = \cos\theta$$

By varying either Ψ_x or Ψ_z, the main beam will scan in either the α_x or α_z directions. Thus, for example, a waveguide array scanning in one dimension, α_x, with phase

PATTERN MULTIPLICATION

$$P(\alpha_x, \alpha_y) = [P_1(\alpha_x)] \times [P_2(\alpha_y)]$$

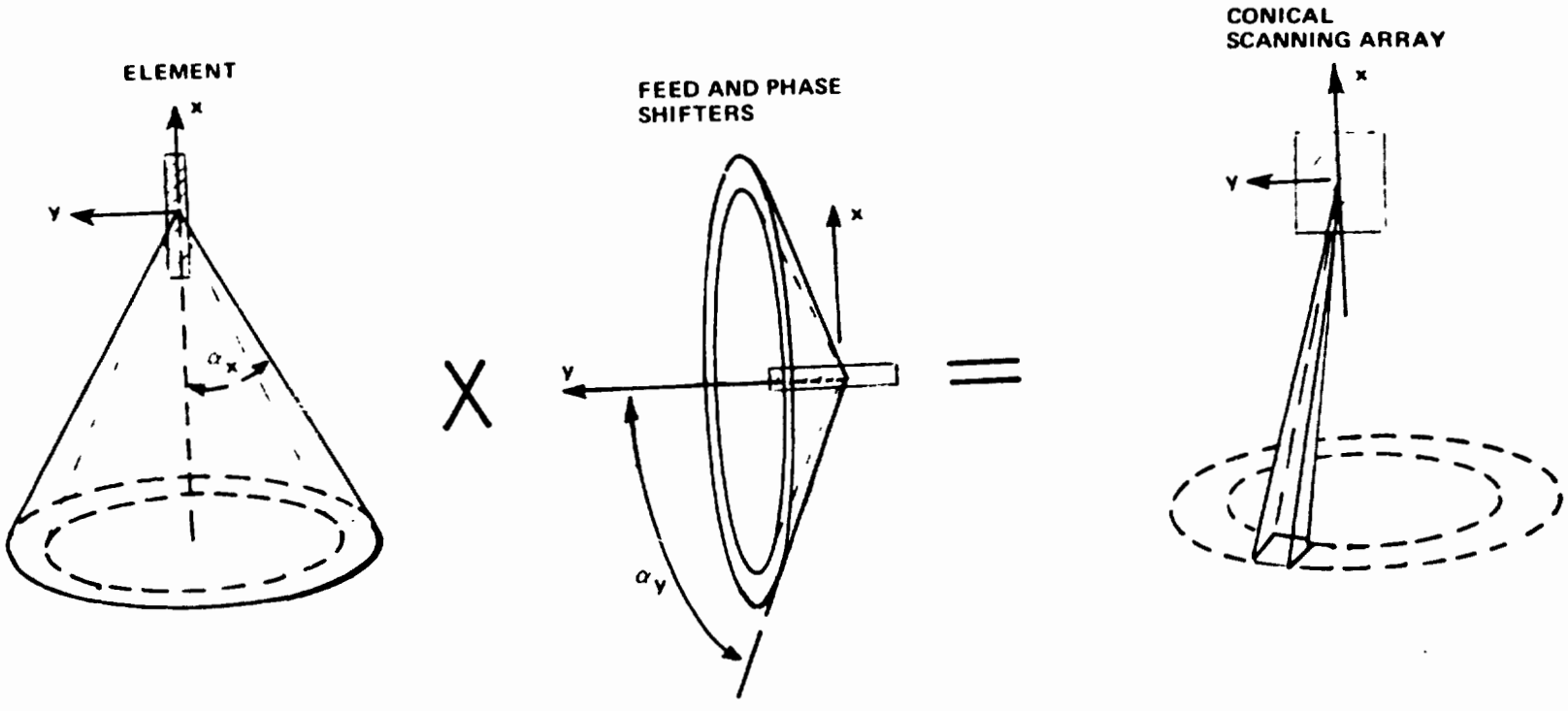

Figure 2-5. Theory of Operation

reversal between slots and a variable phase shifter at each port, will have a phase progression in the x direction, Ψ_x given by

$$\Psi_x = \beta d_x - \pi + \Phi$$

hence

$$\cos\alpha_x = \Psi_x / k d_x = \lambda/\lambda_g - \lambda/2_{dx} + \frac{\Phi}{2\pi d_x/\lambda}$$

where $k = 2/\lambda$, $\beta = 2/\lambda_g$ and Φ is the phase shift due to the variable phase shifter. Note that α_x is 90° at broadside as indicated in Figure 2-4. The above relationship can be extended to a two-dimensional scan by adding a variable phase shift term into the Ψ_z phase progression.

2.1.6 GRATING LOBE LIMITATIONS

The phase factor Ψ in the preceding discussion has been assumed to be

$$\Psi = k d \sin\theta$$ (referring once again to a linear array with $= 0^\circ$ at broadside)

However, by rewriting this equation

$$\Psi - k d \sin\theta = 0$$

and realizing that the above expression is the phase difference between two adjacent elements in the far field, then it follows that the array factor is maximum whenever the difference $\Psi - k d \sin\theta$ is an integral number of wavelengths (Ref. 4).

Hence,

$$\Psi - k\,d\sin\theta_m = 2\pi m$$

where $m = 0, \pm 1, \pm 2, \ldots$, and θ_m is the direction of the corresponding beam peak. The beams corresponding to $|m| > 0$ are second order beams or grating lobes. By letting $\Psi = k\,d\sin\theta_o$ and substituting $k = 2\pi/\lambda$, the above equation becomes

$$\sin\theta_m = \sin\theta_o \pm \frac{m}{d/\lambda}$$

If the first grating lobe, $m = |1|$ is set at $\theta_1 = 90^\circ$

$$d/\lambda = \frac{1}{1 + |\sin\theta_o|}$$

Hence, to maintain $\theta_1 \geq 90^\circ$ (outside of the visible region of the antenna), the spacing between elements must be

$$d/\lambda < \frac{1}{1 + |\sin\theta_o|}$$

Note that if $d < \lambda/2$ the grating lobe will always remain outside of the visible region regardless of the scan angle, θ_o, of the main beam.

It follows from the above equations that the grating lobe will scan with the main beam, hence it is necessary to insure that the grating lobe is suppressed over the total scan range. Van Aulock (Ref. 5) has devised a graphical technique which depicts the main beam/grating lobe relationship for a two-dimensional array.

Utilizing this technique, see Figure 2-6, the null contours of the main beam and the grating lobes are plotted as a function of cosine α_x and cosine α_z where α_x .

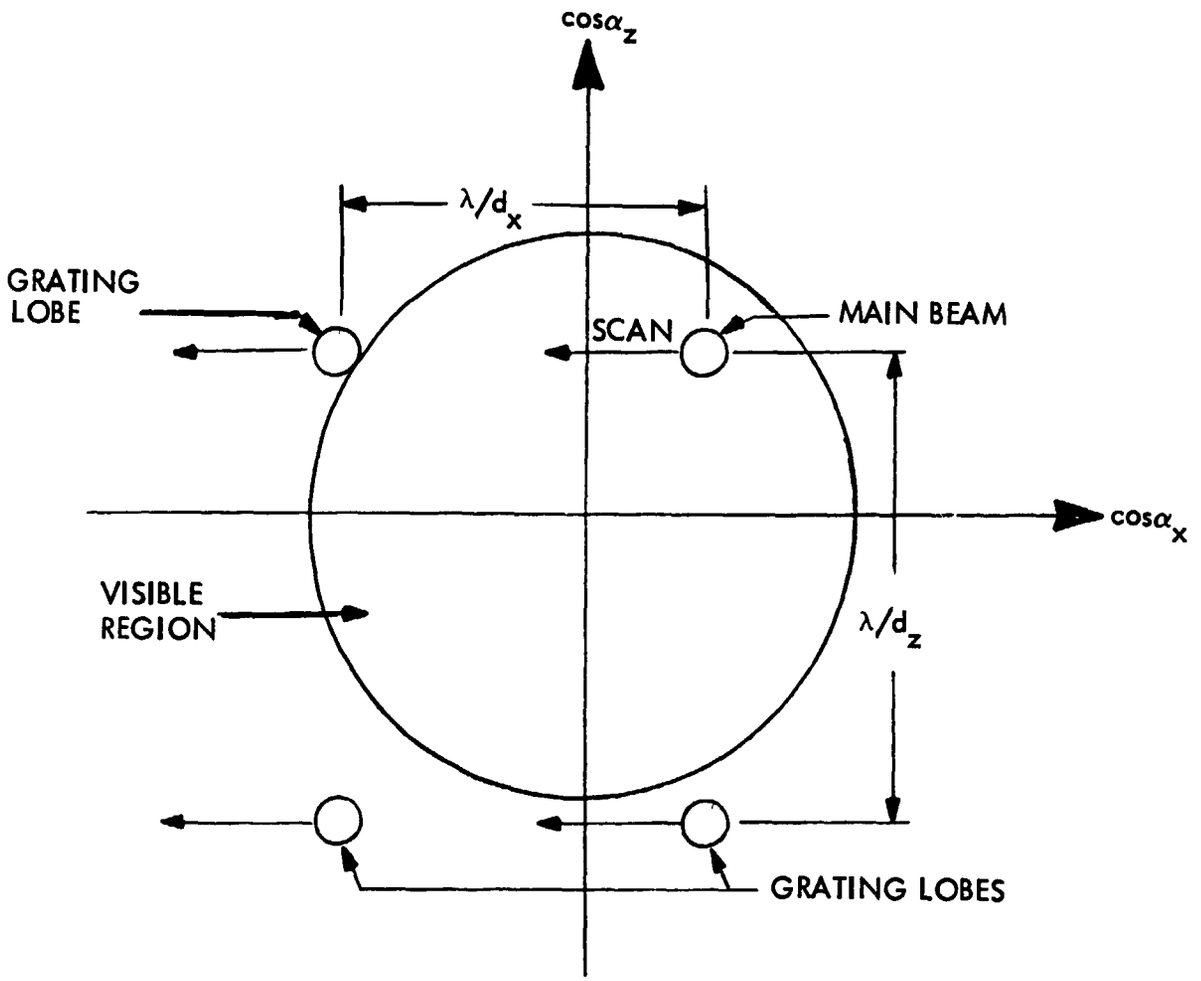

Figure 2-6. Grating Lobe Diagram

and α_z are the angles from the beams to the x and z axes respectively. The antenna is assumed to be oriented as shown in Figure 2-4. The example shown in Figure 2-6 assumes one-dimensional scan in the α_x direction with a fixed α_z angle.

The criteria for grating lobe suppression, derived in a manner similar to the one-dimensional case given above, are

$$d_x/\lambda < \frac{1}{\sin\theta(1+\cos\psi)}$$

and

$$d_z/\lambda < \frac{1}{1+\cos\theta}$$

The above equations are used to determine the maximum spacing of elements for a given scan angle and conversely to determine the maximum scan angle given the element spacing.

2.2 TYPES OF ARRAYS

Phased arrays can be generally classified in two categories: (1) one-dimensionally fed arrays and (2) space-fed arrays. A space-fed array is a two-dimensional array fed by a source located some distance from the array as shown in Figure 2-7a. A one-dimensionally fed array is one in which collimation is provided in only one dimension and collimation in the orthogonal dimension must be obtained from the aperture that is being fed. An example of a one-dimensional array is shown in Figure 2-7b.

2.2.1 SPACE-FED ARRAY

An obvious advantage of the space-fed array is the capability to scan in two dimensions; however, this advantage is usually offset by the fact that there must be

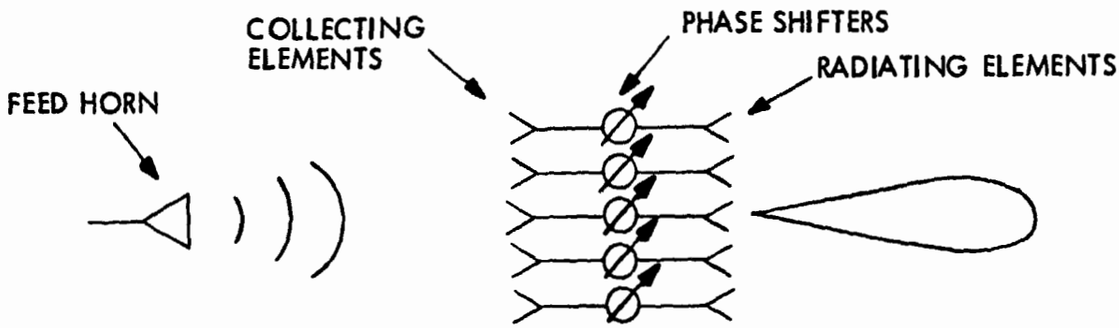

Figure 2-7a. Space-Fed Aperture

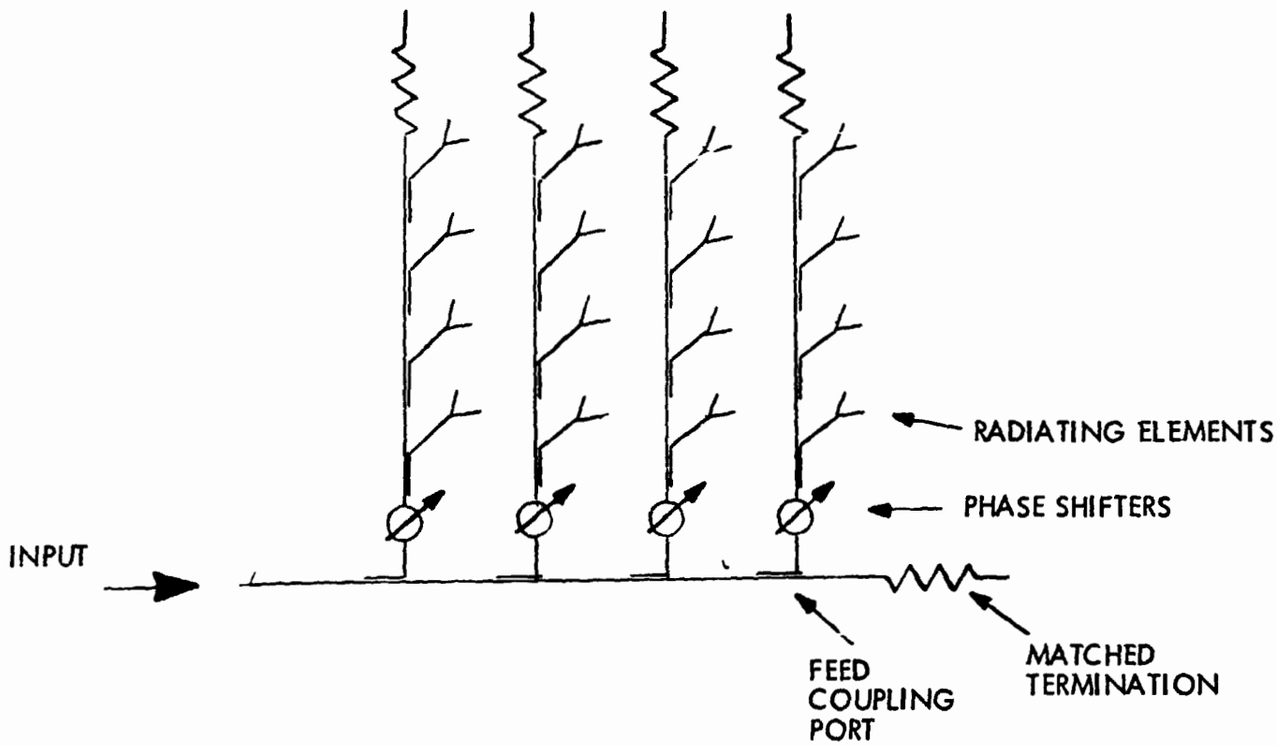

Figure 2-7b. One Dimensionally Fed Aperture

phase control at each element of the array. Since phase errors are the principal cause of increased sidelobe levels and lower beam efficiencies, the space-fed array is not a practical choice for a microwave radiometer system.

2.2.2 ONE-DIMENSIONAL FED ARRAY

There are many types of one-dimensional feeds but in general they can be classified as (1) an optical feed, (2) a corporate feed, or (3) a series feed. The optical feed utilizes a microwave lens to collimate the energy in one plane and feeds a two-dimensional radiating aperture consisting typically of slotted waveguide linear arrays. Scanning is accomplished via phase shifters at each linear array. A schematic diagram of the optical feed is shown in Figure 2-8a.

The corporate or parallel feed as shown in Figure 2-8b utilizes power dividers to couple energy from a single input via a branching transmission line structure, to the radiating elements. The corporate feed is a broadband device but can be quite lossy when used to feed a large antenna due to the long lengths of transmission line required.

The series feed, shown in Figure 2-8c, can be either end-fed or center-fed and functions as either a standing wave (resonant) device or as a traveling wave (non-resonant) device. The resonant series feed requires the radiating elements to be spaced 1/2 wavelength apart with the end of the feed terminated in a short circuit. The resonant array produces a beam broadside to the array and is well matched at the design frequency but operates over a very narrow bandwidth.

The non-resonant series feed is terminated in a matched load and, due to its traveling wave nature, requires that the radiating elements be spaced other than 1/2 wavelength apart to prevent multiple reflections at the coupling ports from adding in phase at the input port. This means that the beam must be squinted off broadside to

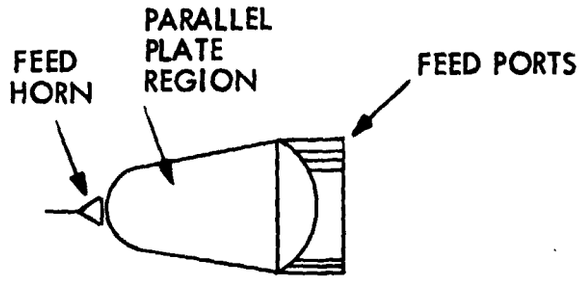

Figure 2-8a. Optical Feed

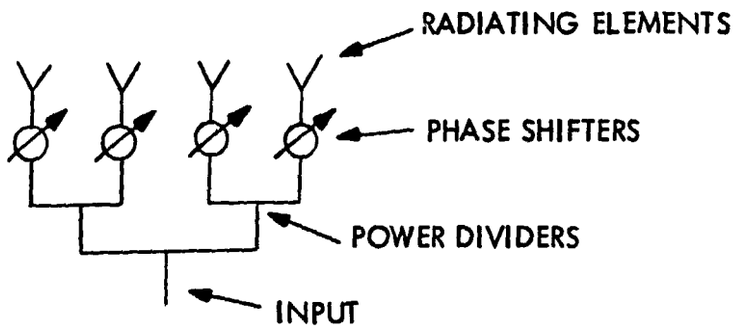

Figure 2-8b. Corporate Feed

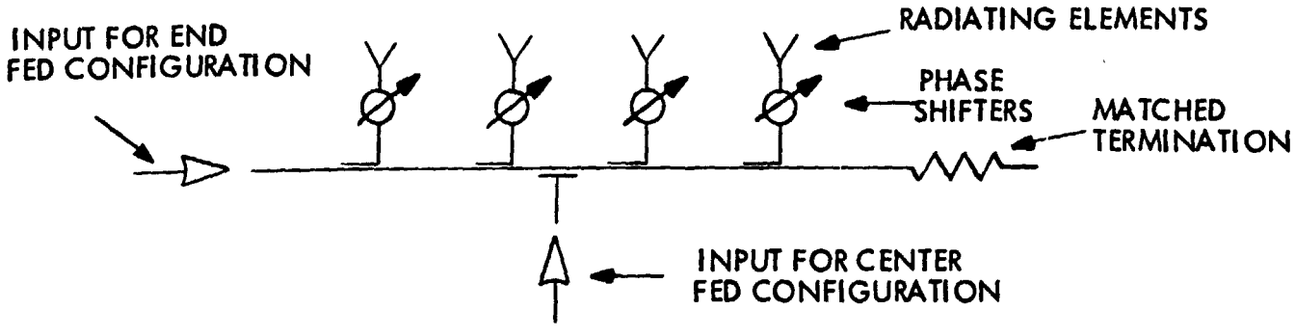

Figure 2-8c. Series Feed

maintain a good impedance match. However, with proper design, the non-resonant feed can have a very low VSWR over a broad bandwidth, low insertion loss, and provide excellent amplitude taper control.

2.3 RADIATING ELEMENTS

The radiating element is used to couple energy from a transmission line into free space. As was previously mentioned in Section 2.1.3, the radiating element is an individual antenna which radiates energy with some characteristic pattern shape and due to pattern multiplication affects the total array factor. While there are many types of radiating elements, the discussion here will be limited to some of the more common elements used in phased arrays.

2.3.1 THE DIPOLE

The most basic element is of course the dipole. Its usefulness is limited to the lower frequencies generally X-band and below. It can be fed by either coaxial or strip-line transmission lines. Dual linear polarization can be achieved by interleaving arrays of orthogonally oriented dipoles.

2.3.2 WAVEGUIDE HORNS

Waveguide horns make excellent radiators for linear arrays and have been used for linear phased arrays. However, due to their size, it is difficult to place them close enough together to allow wide angle scanning. They are also costly and difficult to fabricate in the large numbers needed for large aperture, two dimensional arrays.

2.3.3 WAVEGUIDE SLOT RADIATORS

The waveguide slot radiator is a slot cut through the wall of a waveguide. The slot can be either resonant or non-resonant, shunt or series. The type of slot is determined by which wall of the waveguide it is cut into and by its orientation relative to the waveguide axis. The different types of slot radiators are shown in Figure 2-9. The principal advantage of the slot radiator is the relative ease with which the degree of coupling at each individual slot can be controlled.

Typically, slot radiators are resonant length slots which radiate a single linear polarization. However, dual linear polarization can be achieved by radiating from a crossed-slot pair of non-resonant slots cut into the wall of a square waveguide. The square waveguide is designed to support two orthogonal modes (TE10 and TE01) simultaneously with each mode coupling to only one slot in the crossed slot pair.

2.4 BEAMWIDTH

The beamwidth of an array is usually defined as the width of the far field main beam at the half power or 3 dB points and is measured in degrees. It is inversely proportional to the aperture length (in wavelengths) and is given by the formula

$$\theta_{HP} = \frac{A}{L/\lambda}$$

where L/λ is the aperture length in wavelengths and A is a constant whose magnitude is dependent on the amplitude distribution imposed on the array.

This formula can be applied independently to each orthogonal axis of a two-dimensional array to determine the cross-sectional dimensions of the main beam. It is important to remember that the beamwidths determined in this manner are measured along the conical surface on which the main beams form.

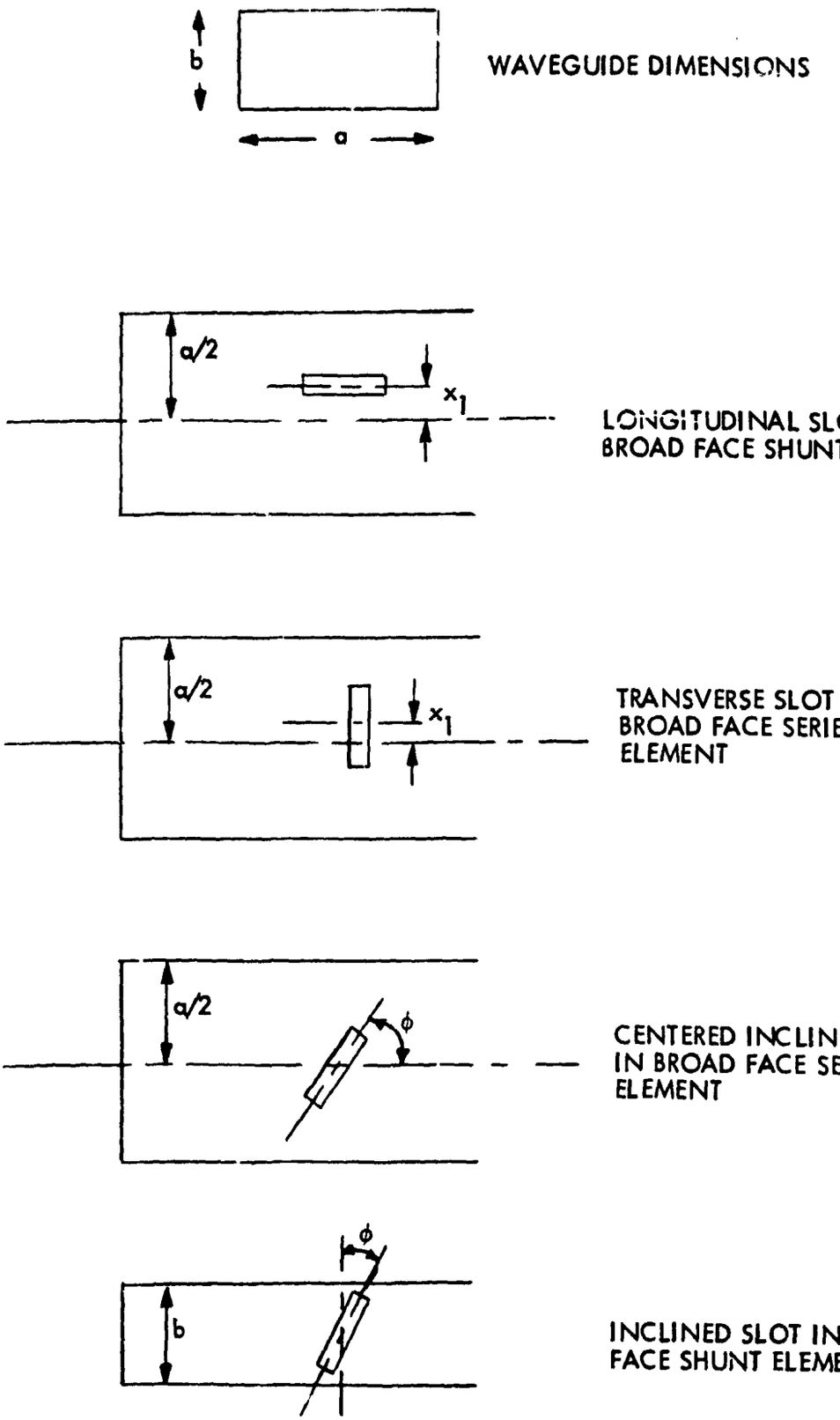

Figure 2-9. Slot Radiators

2.4.1 EFFECTS OF AMPLITUDE DISTRIBUTION ON BEAMWIDTH

As seen in the above formula, once an aperture length is specified, the beamwidth is strictly a function of the constant, A. This constant is at a minimum and is independent of sidelobe level only for the uniform distribution. Thus, the beamwidth of a uniform array is the minimum achievable beamwidth for a given aperture length. Unfortunately a uniform distribution provides no control on sidelobe level and produces peak sidelobes of -13.6 dB. However, it provides the baseline beamwidth with which to measure the beam broadening produced by amplitude tapering to achieve lower sidelobes.

Values of the constant, A, can be calculated for both the Dolph-Chebyshev and the Taylor distributions as a function of peak sidelobe level. Table 2-1 below shows a comparison of the constant, A, for the three distributions at various sidelobe levels.

Sidelobe Level (dB)	A (in degrees) Uniform	D-T	Taylor ($\bar{n} = 6$)
-13.6	50.9		
20	-	51.1	55.00
30	-	60.6	64.23
40	-	68.7	71.72

Figure 2-10 is a plot of beamwidth versus aperture length showing the relative beam broadening of the D-T and Taylor distributions for 25 dB and 40 dB sidelobe levels as compared to the beamwidth of the uniform distribution. Figure 2-11 shows the effect of decreasing sidelobe levels on beamwidth for various aperture lengths (the aperture length shown represents 20-meter apertures at the wavelengths of interest). Figure 2-12 is a

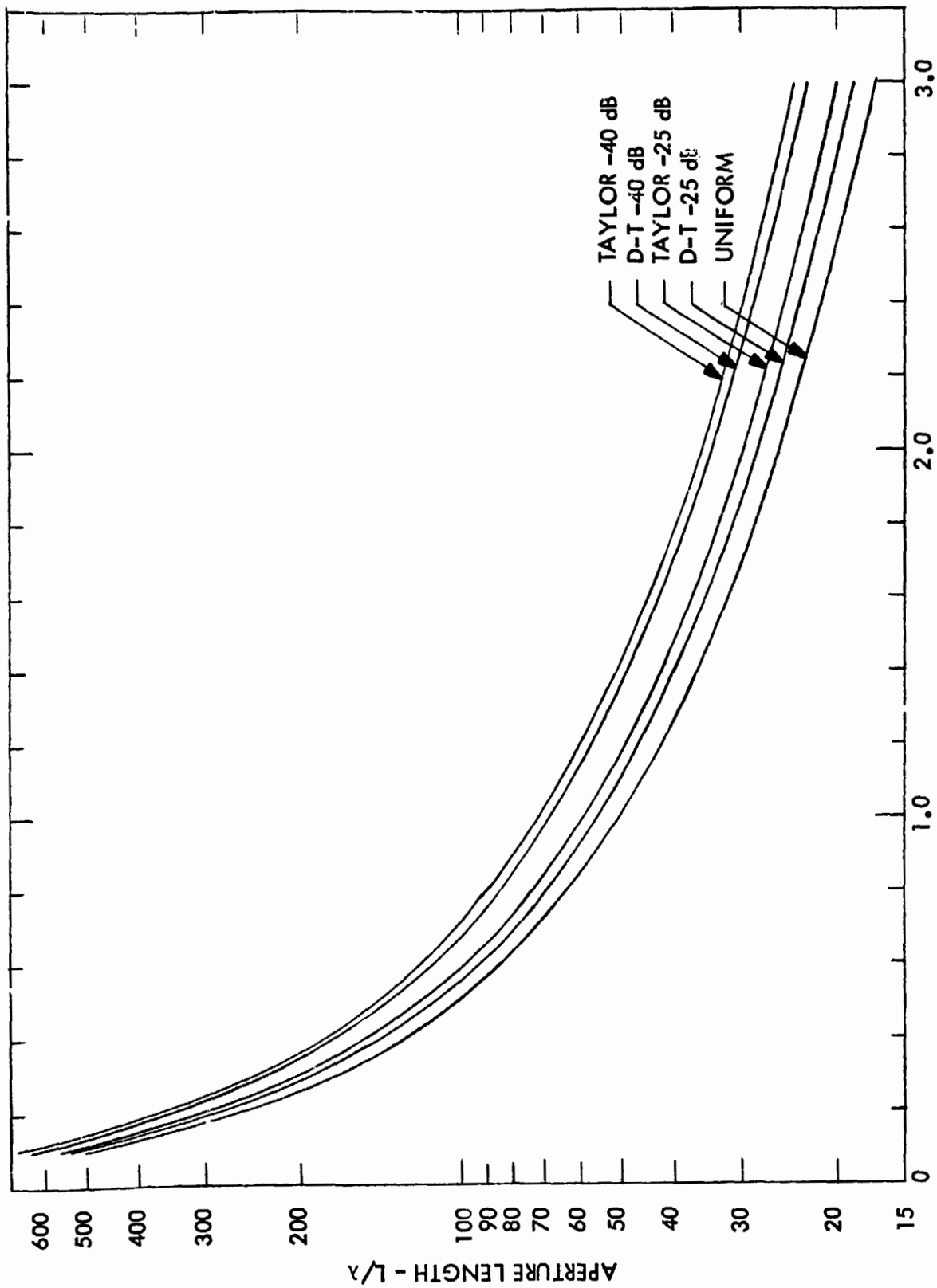

Figure 2-10. Beamwidth versus Aperture Length for Various Distributions

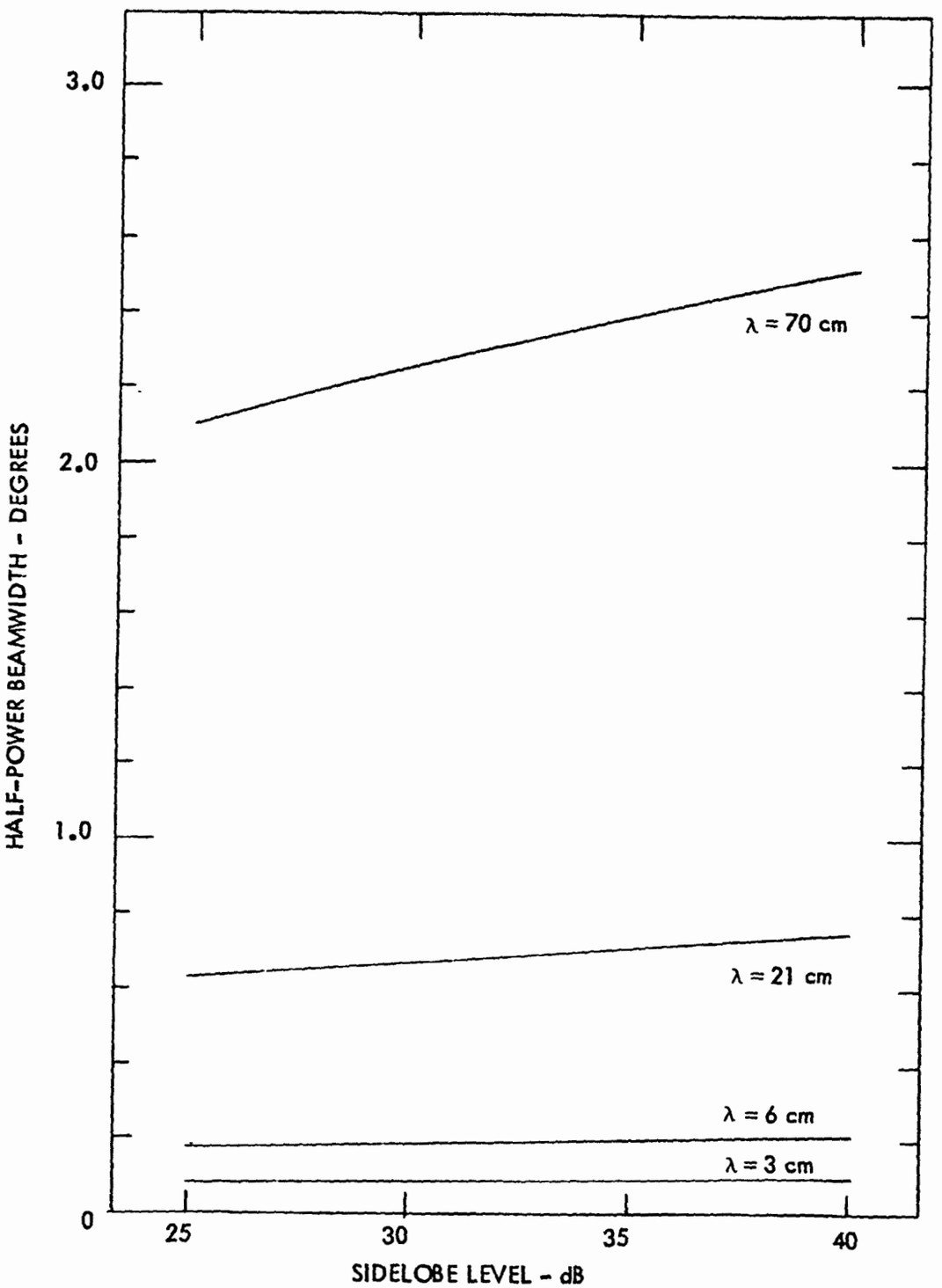

Figure 2-11. Beamwidth versus Sidelobe Level for a Taylor Distribution

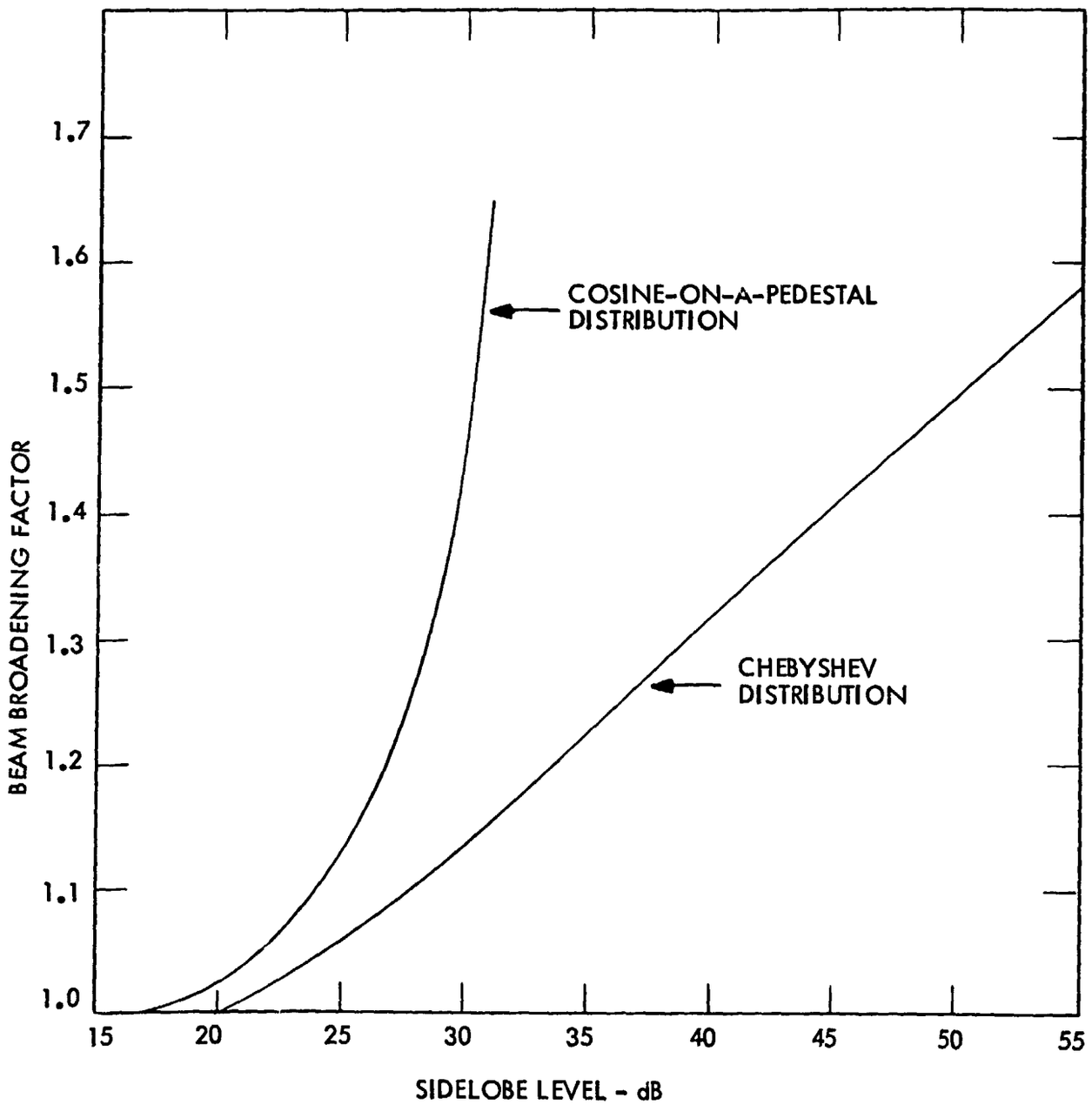

Figure 2-12. Beam Broadening Factor

plot of beam broadening (the ratio of "A" for a given distribution to A = 50.9 for a uniform distribution) versus sidelobe level for the D-T distribution and the cosine-on-a-pedestal distribution. The cosine-on-a-pedestal is a typical distribution for reflector type antennas and is included here to provide a comparison of beam broadening for reflector antennas and phased arrays.

2.4.2 EFFECTS OF SCAN ANGLE ON BEAMWIDTH

The equation for beamwidth indicates that the half-power beamwidth is a function only of the physical aperture length of the antenna. This is true only when the beam is broadside to the antenna. As the beam is scanned off broadside, the effective aperture length is the length of the aperture projected onto a plane normal to the beam. Hence, for a scanning beam the half-power beamwidth is

$$\theta_{HP} = \frac{A}{(L/\lambda)\cos\theta}$$

where θ is the angle of the main beam relative to the array broadside. Figure 2-13 shows the effective beam broadening of an array as a function of scan angle.

2.5 BEAM EFFICIENCY

The beam efficiency of an antenna is defined as the ratio of the power radiated in the main lobe of the antenna to the total power radiated by the antenna. It describes the degree of concentration of power in the main beam and is useful in the determination of brightness temperature from antenna temperature measurements. The main beam is defined to be that part of the power pattern including the beam peak and bounded by the first nulls measured on the two orthogonal principal plane patterns.

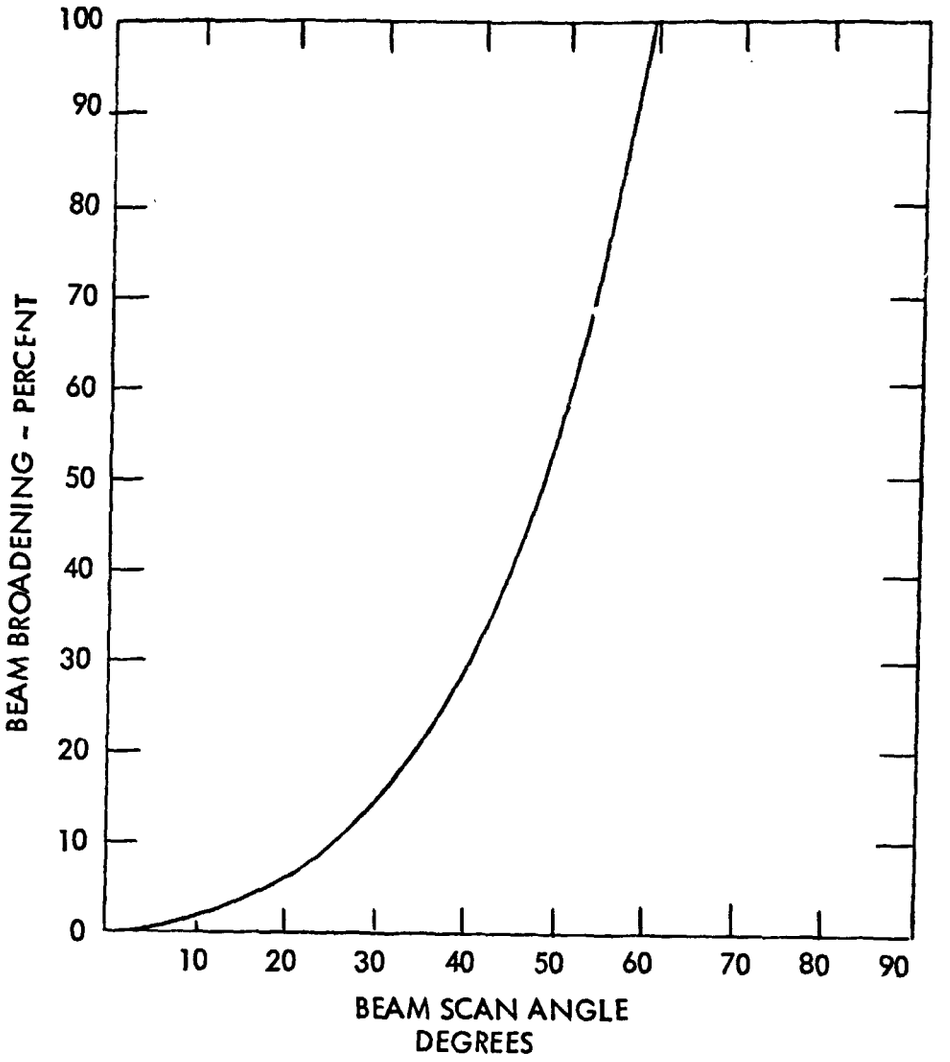

Figure 2-13. Beam Broadening as a Function of Scan Angle

The beam efficiency is expressed as

$$\eta = \frac{\int_{\Omega_o} F(\theta,\phi)\, d\Omega}{\int_{4\pi} F(\theta,\phi)\, d\Omega}$$

where

$F(\theta,\phi)$ = the antenna power pattern (array factor)

$d\Omega$ = incremental solid angle

Ω_o = the main beam solid angle

The assumption is made that the amplitude distribution is such that the array factor $F(\theta,\phi)$ is separable and can be written

$$F(\theta,\phi) = F_x(\theta,\phi)\, F_z(\theta,\phi)$$

where $F_x(\theta,\phi)$ and $F_z(\theta,\phi)$ are the individual linear array factors along the orthogonal axes of the planar array. Now, by transforming the coordinate system from θ and ϕ to the directional angles α_x and α_z, the array factor can be rewritten

$$F(\alpha_x,\alpha_z) = F_x(\alpha_x,\alpha_z)\, F_z(\alpha_x,\alpha_z)$$

The beam efficiency, η, can now be expressed as

$$\eta = \frac{\iint_{\Omega_o} F_x(\alpha_x,\alpha_z)\, F_z(\alpha_x,\alpha_z)\, d\Omega}{\iint_{2\pi} F_x(\alpha_x,\alpha_z)\, F_z(\alpha_x,\alpha_z)\, d\Omega}$$

The power patterns of F_x and F_z have been shown to lie along conical surfaces symmetrical about the x and z axes respectively. It has also been shown that the pattern, F_x, is independent of α_z and, similarly, the pattern F_z, is independent of

α_x. Thus, F_x and F_z can be expressed as a function of one angle only, allowing the equation for beam efficiency to be rewritten as

$$\eta = \frac{\iint_{\Omega_o} F_x(\alpha_x, \alpha_{z_o})\, F_z(\alpha_z, \alpha_{x_o})\, d\Omega}{\iint_{2\pi} F_x(\alpha_x, \alpha_{z_o})\, F_z(\alpha_z, \alpha_{x_o})\, d\Omega}$$

where α_{x_o} = beam pointing angle of F_x

α_{z_o} = beam pointing angle of F_z

2.5.1 SIDELOBE LOCATION

It is obvious from the theory of pattern multiplication that only those sidelobes lying along the conical surfaces described by the main beams of the two linear array factors, F_x and F_z, will contribute any significant sidelobe energy to the total array power pattern since the sidelobes not on the conical surfaces can only multiply with other sidelobes resulting in negligible energy levels. Thus, if the visible region of a planar array is plotted as a function of directional angles α_x and α_z, then strips laid out along the α_{x_o} and α_{z_o} ordinates with widths corresponding to the null beamwidths of the arrays will contain all of the significant sidelobe energy of the array. This is shown graphically in Figure 2-14.

2.5.2 BEAM EFFICIENCY VERSUS SIDELOBE LEVEL AND BEAMWIDTH

Referring to the above equation for beam efficiency, it can be seen that by relating the area of the main beam to the numerator and the total area of the radiated energy to the denominator, an empirical relationship can be derived for expressing beam efficiency as a function of average sidelobe level and beamwidth. Based on this approach

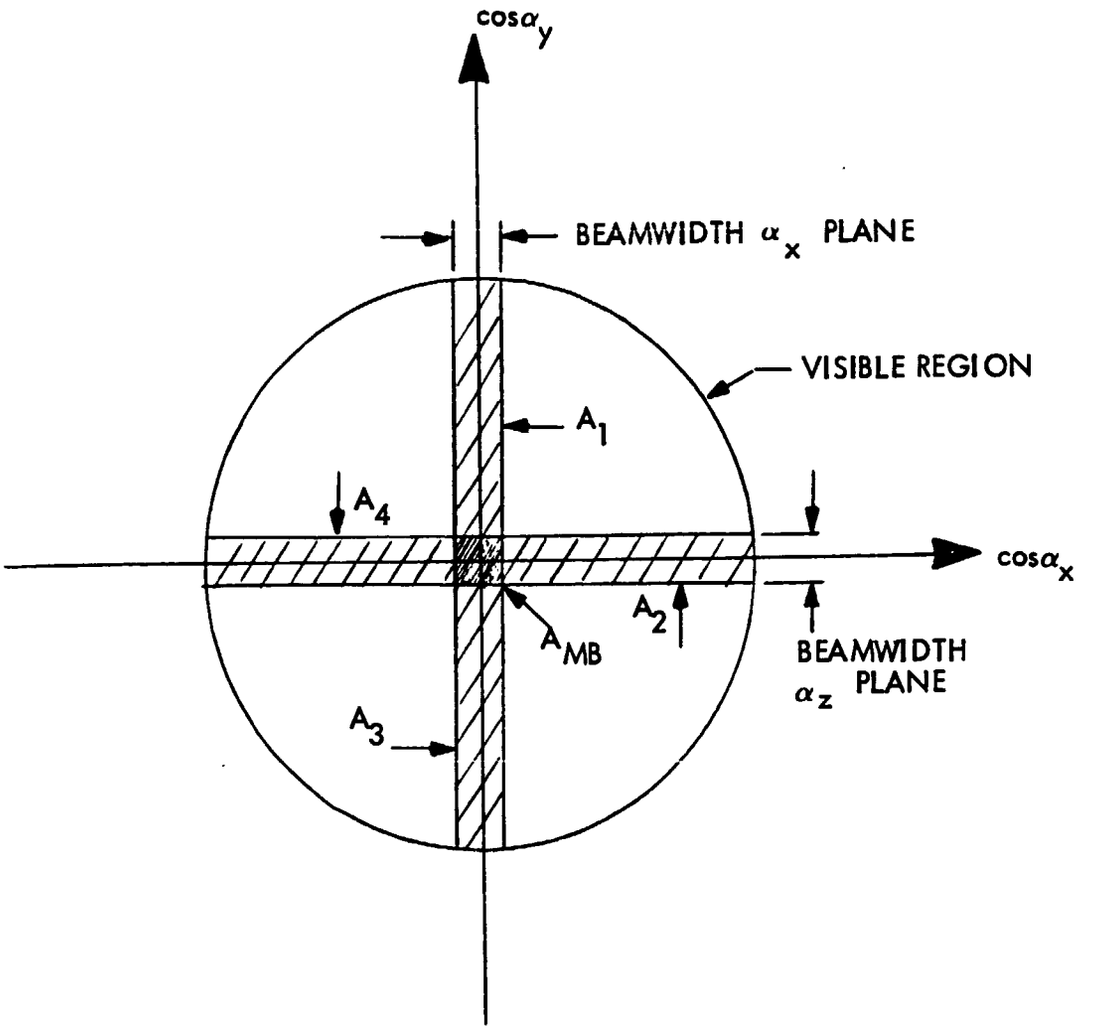

Figure2-14. Energy Distribution

a graph relating beam efficiency to average sidelobe level and beamwidth was plotted as shown in Figure 2-15. It should be emphasized that the sidelobe level referred to is average sidelobe level, not peak sidelobe level. As expected, the graph shows that for a constant average sidelobe level, the beam efficiency increases with increasing bandwidth.

The most significant aspect of the data presented in Figure 2-15 is the fact that once the beamwidth and sidelobe level are specified for an array, the beam efficiency is also specified. Hence, when specifying an array for high beam efficiency, e.g., > 95%, and narrow beamwidth, e.g., < 1.0°, it should be realized that one is also specifying an array whose average sidelobe level does not exceed -33 dB.

2.5.3 LOSS OF GAIN VERSUS BEAM EFFICIENCY AND PHASE ERRORS

Much work has been done to relate tolerance errors, especially phase tolerance errors, to loss of gain for reflector-type antennas. Ruze (Ref. 6) has shown that the reduction of gain due to phase errors is given by

$$G/G_o = \overline{\delta_o^2}$$

where G_o is the theoretical antenna gain, G is the actual gain and $\overline{\delta_o^2}$ is the weighted mean-square phase error. This reduction in gain for a reflector antenna is attributed to a scattering of energy resulting from the error phase front. This scattered energy is radiated in the form of increased sidelobe levels.

It is obvious, then, that the loss of gain of an antenna and commensurate increase in sidelobe level must be accompanied by a similar decrease in beam efficiency. Nash (Ref. 7) has developed a relationship between beam efficiency of a rectangular aperture and phase error as a function of amplitude taper. Using this relationship, and

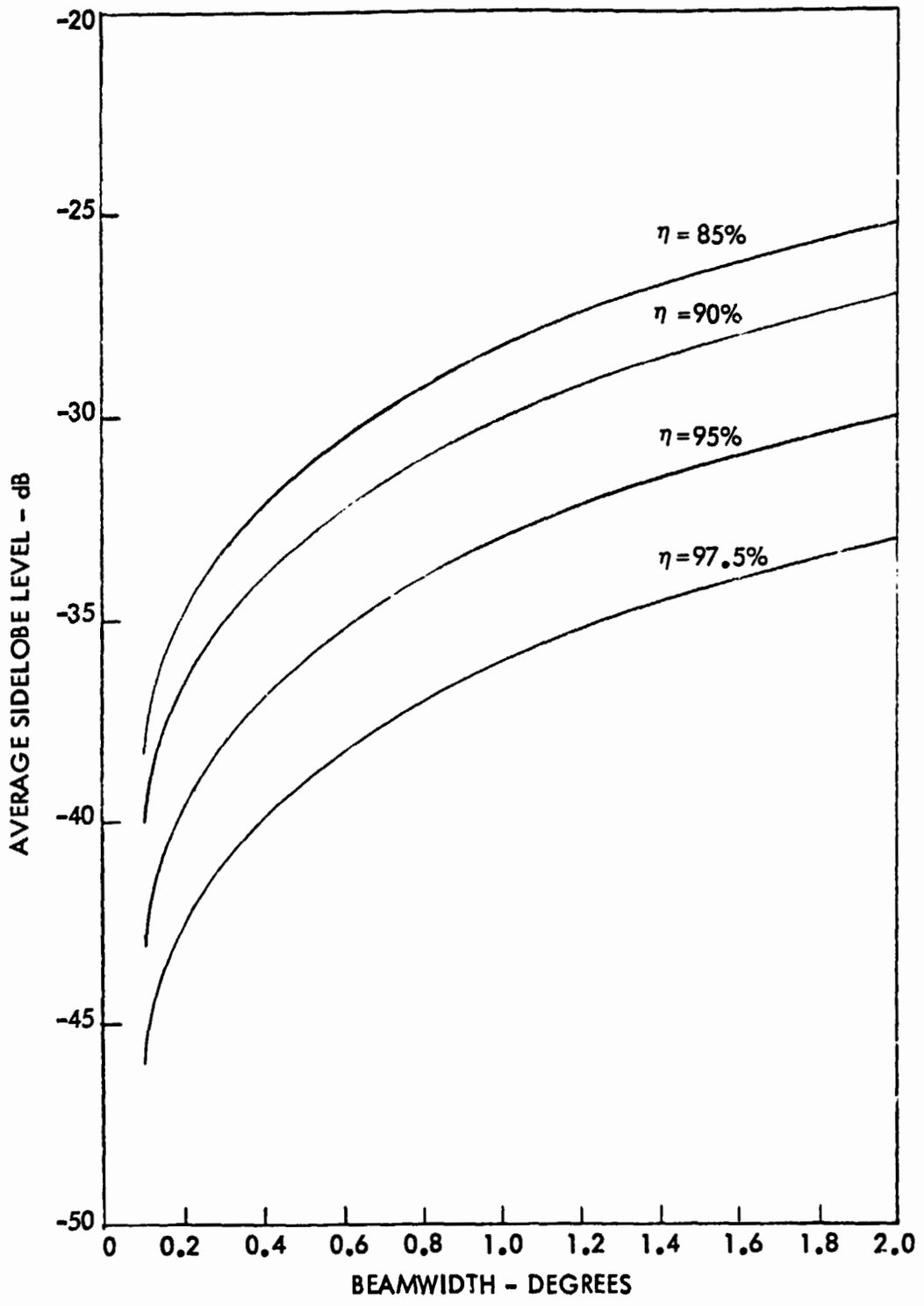

Figure 2-15. Beam Efficiency as a Function of Beamwidth and Average Sidelobe Level

the above equation for gain loss (and remembering that the phase error for a phased array is one-half that of a reflector since the reflector sees the error for both the incident and reflected wave), it is possible to relate gain loss to beam efficiency directly as shown in Figure 2-16.

Elliot (Ref. 8) has derived equations relating increase in sidelobe level to both phase and amplitude errors for planar arrays with Chebyshev amplitude distribution. From these relationships, it is possible to go one step further and relate beam efficiency to phase error for specific Chebyshev distributions as a function of beamwidth. Figure 2-17 is a graph of beam efficiency versus phase error for a planar array with a 40-dB Chebyshev distribution plotted for three different beamwidths, 0.5, 1 and 2 degrees. Figure 2-18 is a similar graph showing instead the difference in beam efficiency between a 40-dB Chebyshev distribution and a 45-dB Chebyshev distribution both with one-half degree beamwidth.

2.6 BEAM BROADENING

The radiation characteristics of a phased array are usually described at discrete frequencies. However, if the array is to be used in a system that operates over a finite bandwidth, then the frequency dispersive characteristics of the array, if any, will affect the radiation characteristics. The most significant effect will be the movement of the beam peak as a function of frequency.

2.6.1 BEAM POSITION VERSUS FREQUENCY

Referring once again to the phase term of the array factor

$$\psi = K d \sin\theta = \beta d$$

and rewriting

$$\sin\theta = \beta d / Kd = \lambda/\lambda_g$$

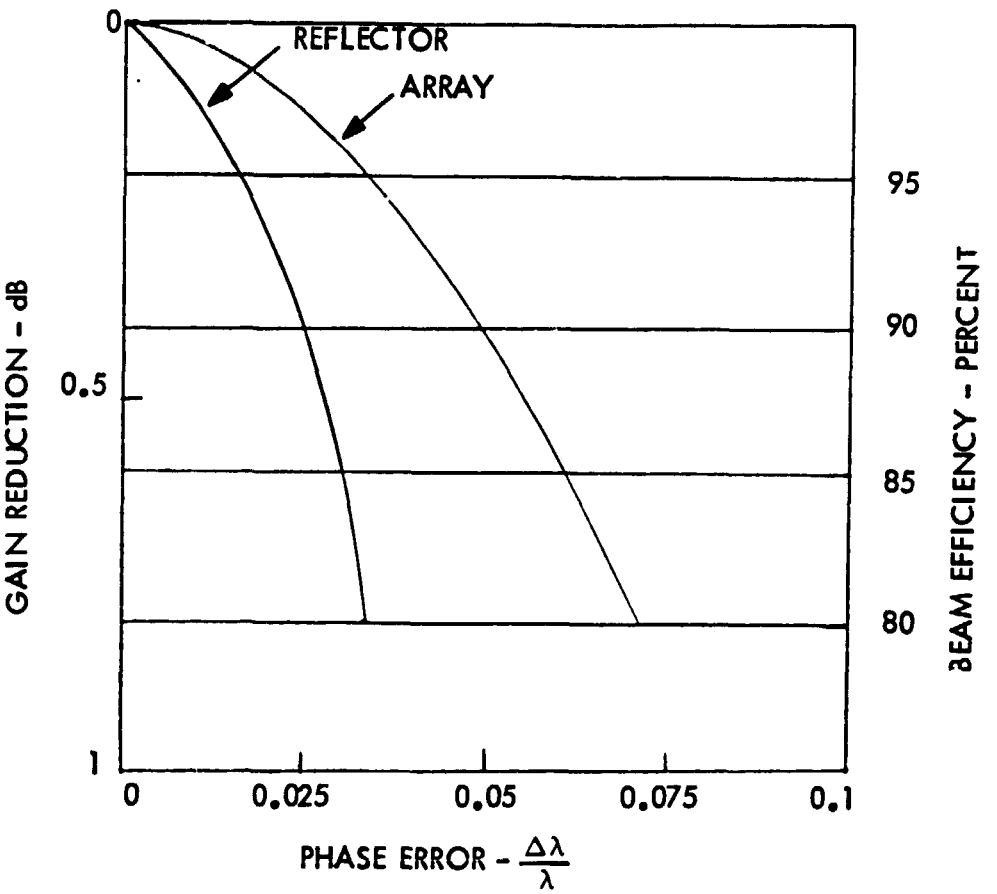

Figure 2-16. Gain-Beam Efficiency versus Phase Error

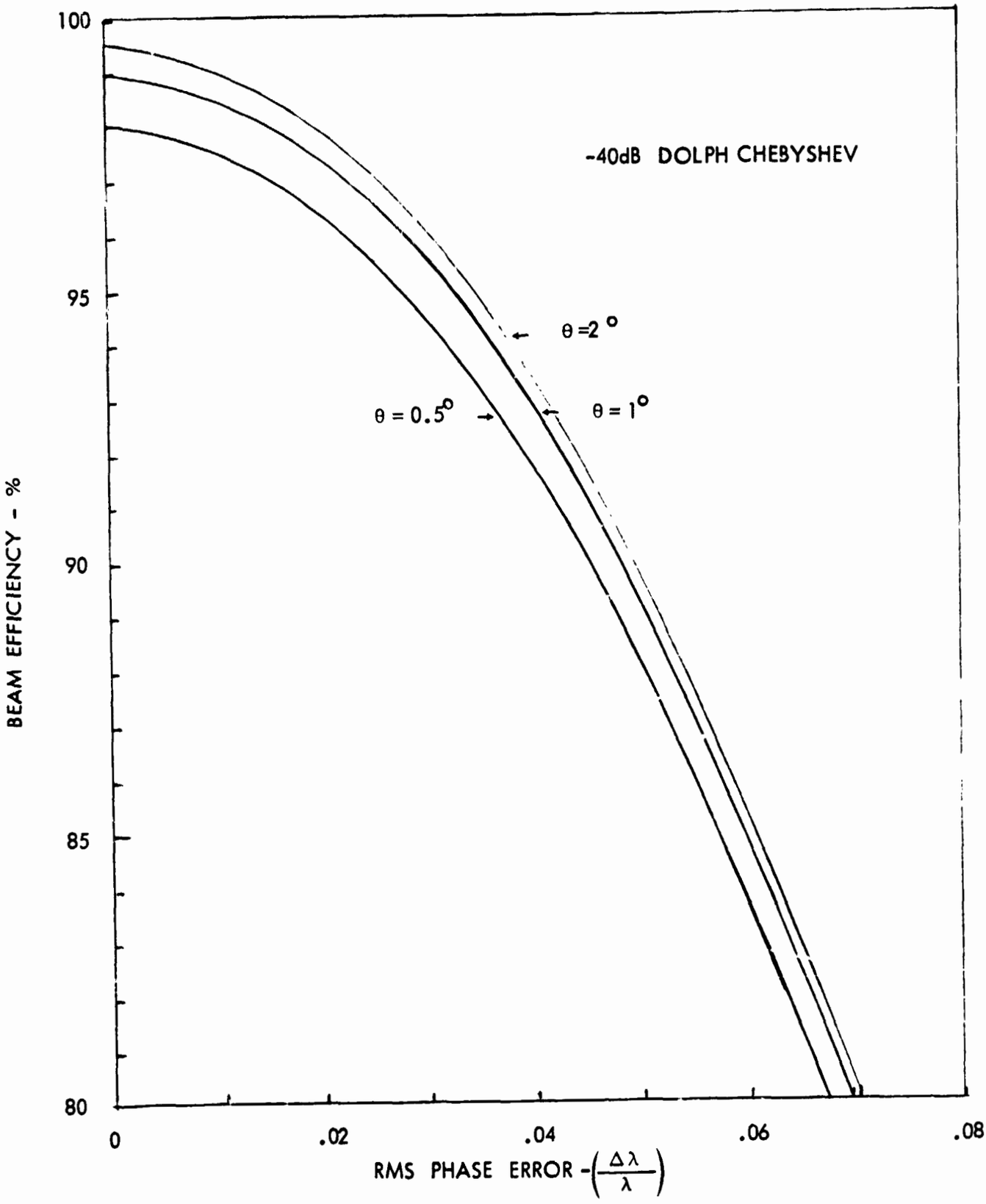

Figure 2-17. Beam Efficiency versus Phase Error

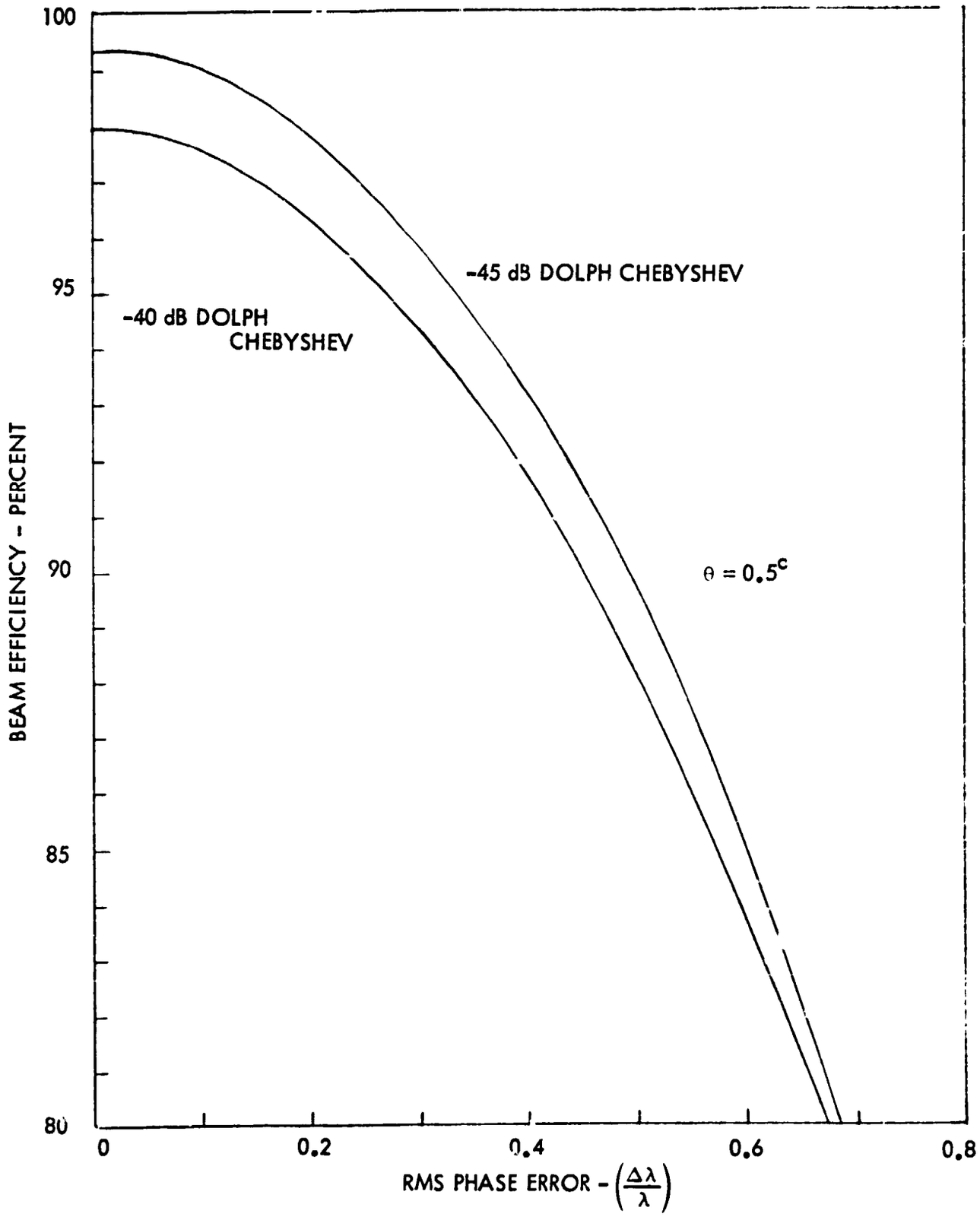

Figure 2-18. Beam Efficiency versus Phase Error

it is obvious that a change in frequency can affect the beam pointing angle directly. For example, assume that the transmission line utilized by the antenna is waveguide with the guide wavelength given by

$$\lambda_g = \frac{\lambda}{\sqrt{1 - (\lambda/2a)^2}}$$

with a = long dimension of the waveguide, then

$$\sin\theta = \lambda/\lambda_g = \sqrt{1 - (\lambda/2a)^2}$$

Now, assigning to "a" some fractional value of a wavelength at the center frequency, the beam pointing angle, θ_o, can be calculated

$$\sin\theta_o = \sqrt{1 - (\ /2a)^2}$$

where $a = x_o(\lambda)$, and x is limited to values between 0.5 and 1.0 for rectangular waveguide (these limits establish the frequency boundaries for a waveguide propagating a single mode above cutoff). By varying the operating frequency about the center frequency, the movement of the beam can be calculated. Figure 2-19 is a plot of beam movement versus percent change in frequency for different values of a/λ.

If there is phase reversal between radiating elements then the phase term is

$$K\,d\sin\theta = \beta d - \pi$$

or rewriting in terms of

$$\sin\theta = \sqrt{1 - (\lambda/2a)^2} - \lambda/2d$$

where d is the inter-element spacing. Figure 2-20 shows beam movement as a function

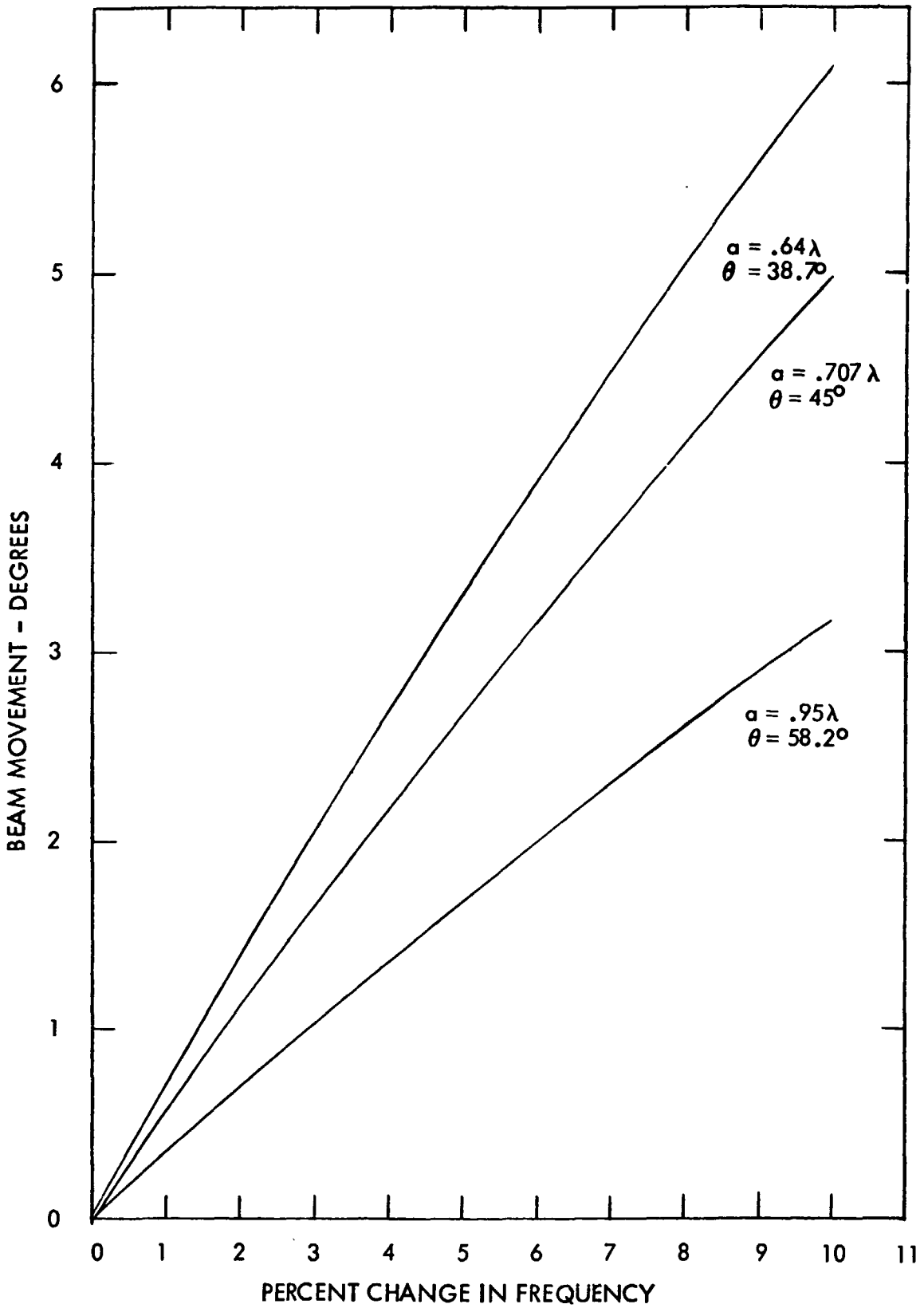

Figure 2-19. Beam Movement versus Percent Frequency Change (No Phase Reversal)

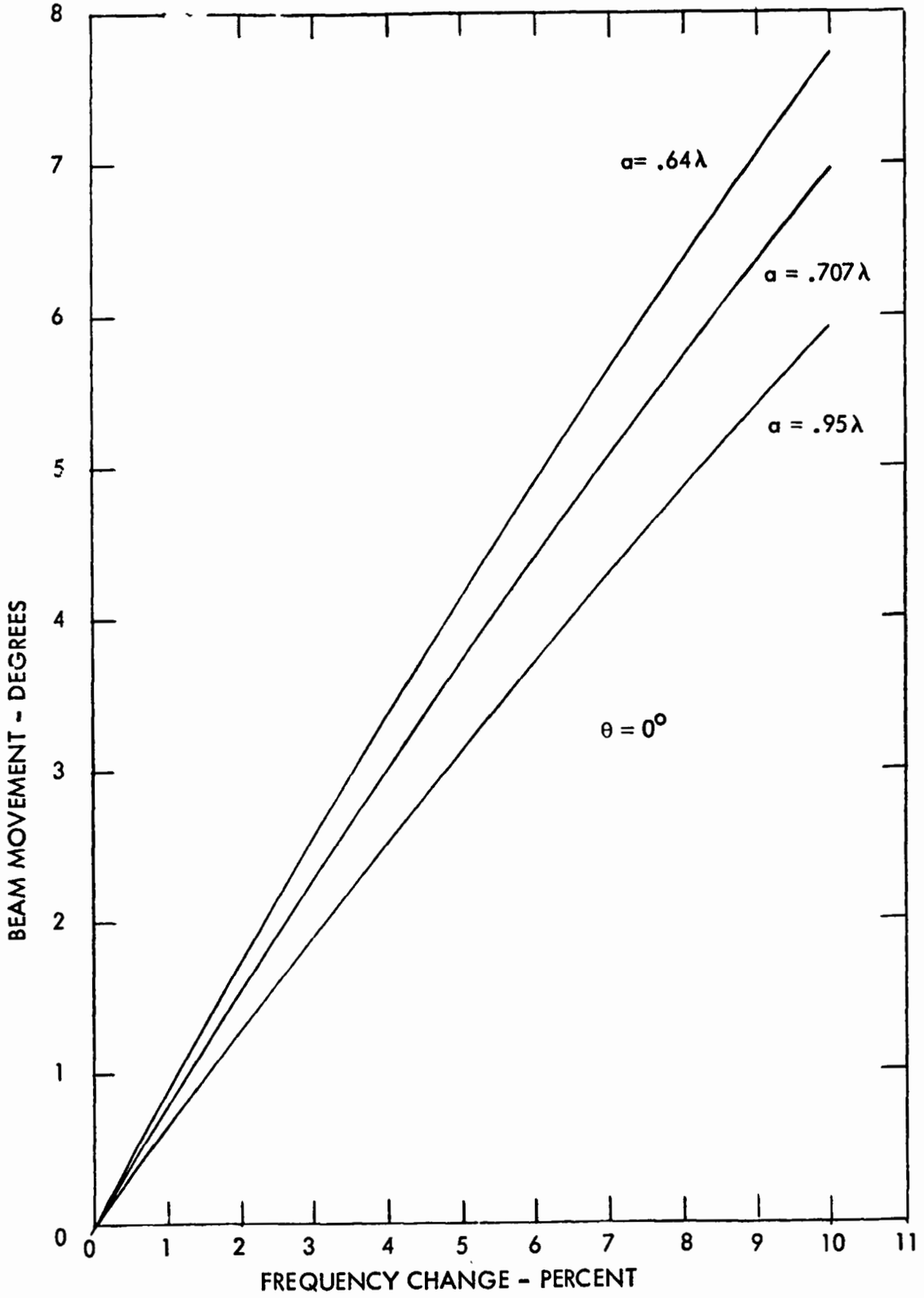

Figure 2-20. Beam Movement versus Percent Frequency Change (with Phase Reversal)

of frequency for different values of a/λ with the value of d selected in each case to produce a broadside beam at the center frequency.

2.6.2 BEAM BROADENING DUE TO FINITE BANDWIDTH

Since the radiometer is receiving the entire bandwidth of frequencies simultaneously, the array produces a main beam which is a composite of the beams it would produce at each of the discrete frequencies. The beam is thus "smeared" or broadened compared to the design beamwidth at the center frequency.

The relationship of the beam broadening to the beam pointing position movement is plotted in Figure 2-21.

The beam position movement is normalized to the center frequency 3 dB beamwidth. This is based on a rectangular RF bandpass with all frequencies in the bandpass contributing. There is no notch in the center of the RF bandpass as would occur in a double sideband superheterodyne receiver.

Figure 2-22 relates the 3 dB beamwidth to the percentage RF bandwidth for various amounts of beam broadening.

2.7 APERTURE EFFICIENCY (LOSS)

The aperture efficiency or loss of an array can be expressed as the summation of all the resistive losses in the array system. The loss mechanisms naturally vary from system to system, depending on the type of aperture, type of transmission line and method of scan utilized. For the two basic array types, the space-fed array and the one-dimensionally fed array, the nature of the loss mechanisms vary significantly. In

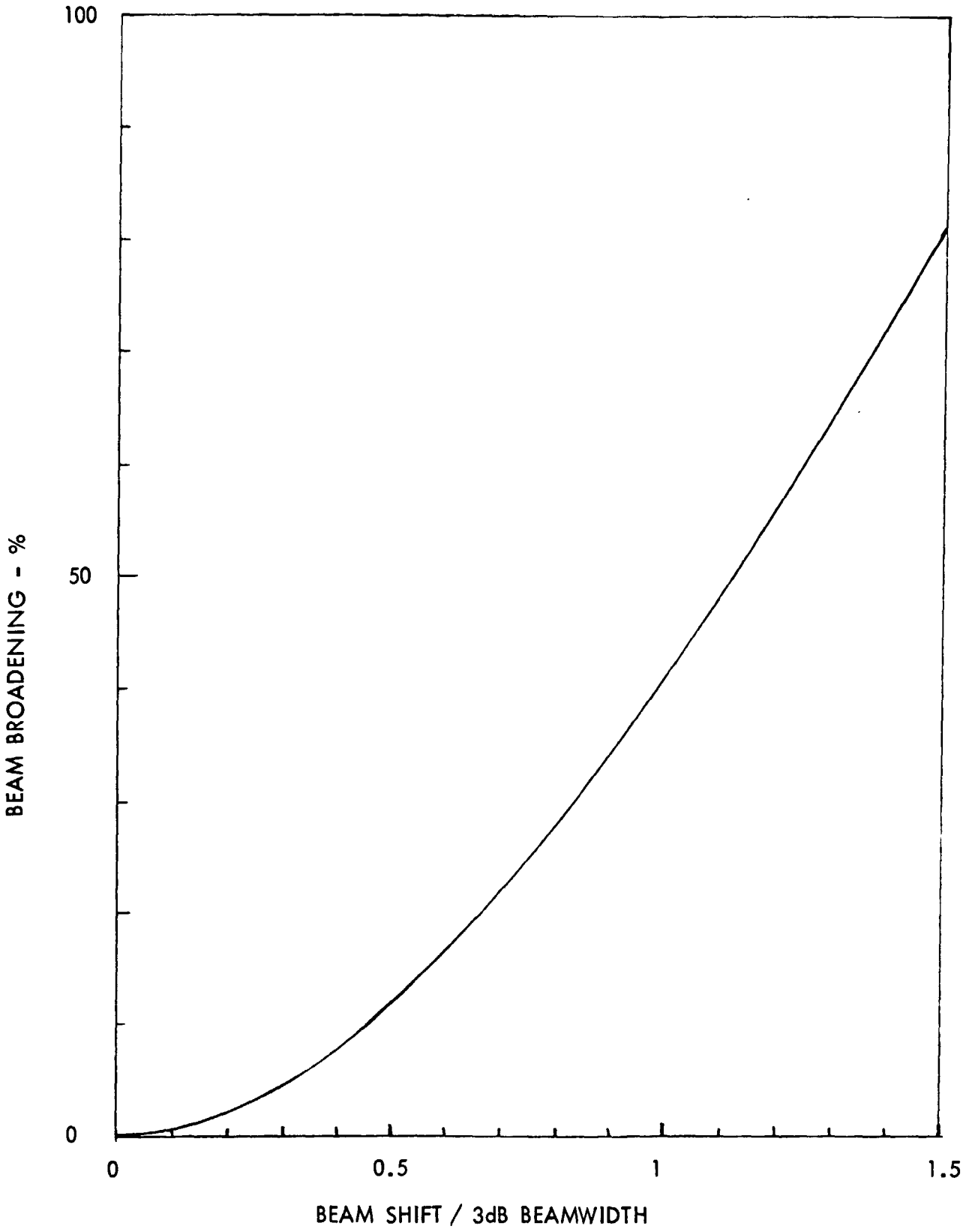

Figure 2-21. Beam Broadening versus Beam Shift

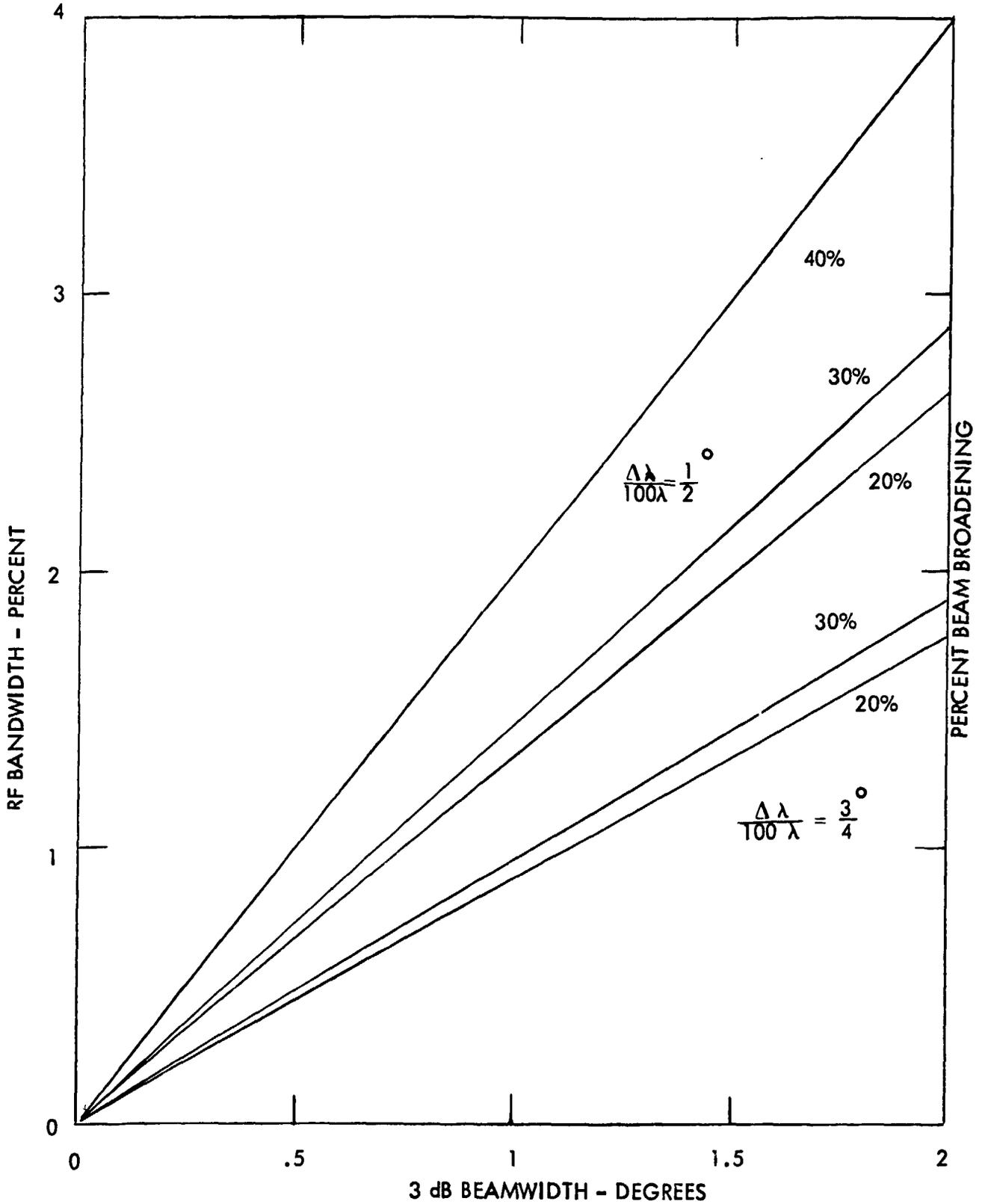

Figure 2-22. Beam Broadening versus Bandwidth

the space-fed array the feed illumination factor and related spillover have perhaps the greatest impact on aperture efficiency. The one-dimensionally fed array, on the other hand, is most sensitive to transmission line losses. Since the one-dimensionally fed array appears to be the optimum system for radiometric applications, the following discussion on loss mechanisms will emphasize the components which make up a typical one-dimensionally fed array.

2.7.1 TRANSMISSION LINE LOSSES

2.7.1.1 WAVEGUIDE LOSS

Attenuation of a wave propagating within a waveguide is the result of two factors; dielectric loss and conductor loss. Dielectric loss is a factor only if the medium of propagation within the waveguide is something other than air. Since losses in dielectric result in very rapid attenuation of the transmitted waves, dielectric loading of a waveguide is not a normal practice. Thus, the attenuation of waves within a waveguide is generally a function only of conductor, or wall losses.

For a rectangular, copper air-filled waveguide operating in the dominant or TE_{10} mode, the attenuation is given by [9]

$$\alpha_c = \frac{0.011707}{a^{3/2}} \left[\frac{1/2 \; b/a \; (\lambda_c/\lambda)^{3/2} + (\lambda_c/\lambda)^{-1/2}}{\sqrt{(\lambda_c/\lambda)^2 - 1}} \right] \text{ dB/Ft}$$

where λ is the wavelength at the operating frequency, λ_c is the cutoff wavelength of the waveguide. The inner dimensions of the guide, "a" and "b", are in inches with, "a", the larger dimension. If a metal other than copper is used the attenuation given by this equation should be multiplied by the square root of the ratio of the resistivities.

Attenuation has been plotted as a function of waveguide length for several waveguide sizes in Figure 2-23.

By setting "a" equal to "b" in the above equation, the attenuation of square waveguide can be calculated. A plot of attenuation versus guide length for square waveguide in frequency bands corresponding to those of Figure 2-23 is given in Figure 2-24.

2.7.1.2 COAXIAL LINE LOSS

The attenuation of a wave propagating within a coaxial transmission line is also the sum of the dielectric loss and the conductor loss. The attenuation resulting from conductor losses is given by [9]

$$a_c = 13.6 \frac{\delta \mu}{\lambda} \frac{1}{b} \left(1 + \frac{b}{a}\right) \frac{\sqrt{\epsilon_1}}{\ln (b/a)} \text{ dB/unit length}$$

where δ is the skin depth, λ is the wavelength, b and a are the outer and inner radii of the line, μ is the permeability of the conductors, and ϵ_1 is the dielectric constant of the medium separating the conductors.

If the conductors are assumed to be copper the formula reduces to

$$a_c = 2.98 \times 10^{-9} \sqrt{f} \; 1/b \; (1 + b/a) \frac{\sqrt{\epsilon_1}}{\ln (b/a)} \text{ dB/cm}$$

Thus, the attenuation increases as the square root of frequency, assuming that ϵ_1 is independent of frequency, and also varies as the square root of the resistivity of the conductors.

An optimum ratio, $b/a = 3.6$, exists for a fixed dimension, b, of the outer radius with minimum attenuation occurring at this value.

The dielectric attenuation in a dielectric filled coaxial line is given by

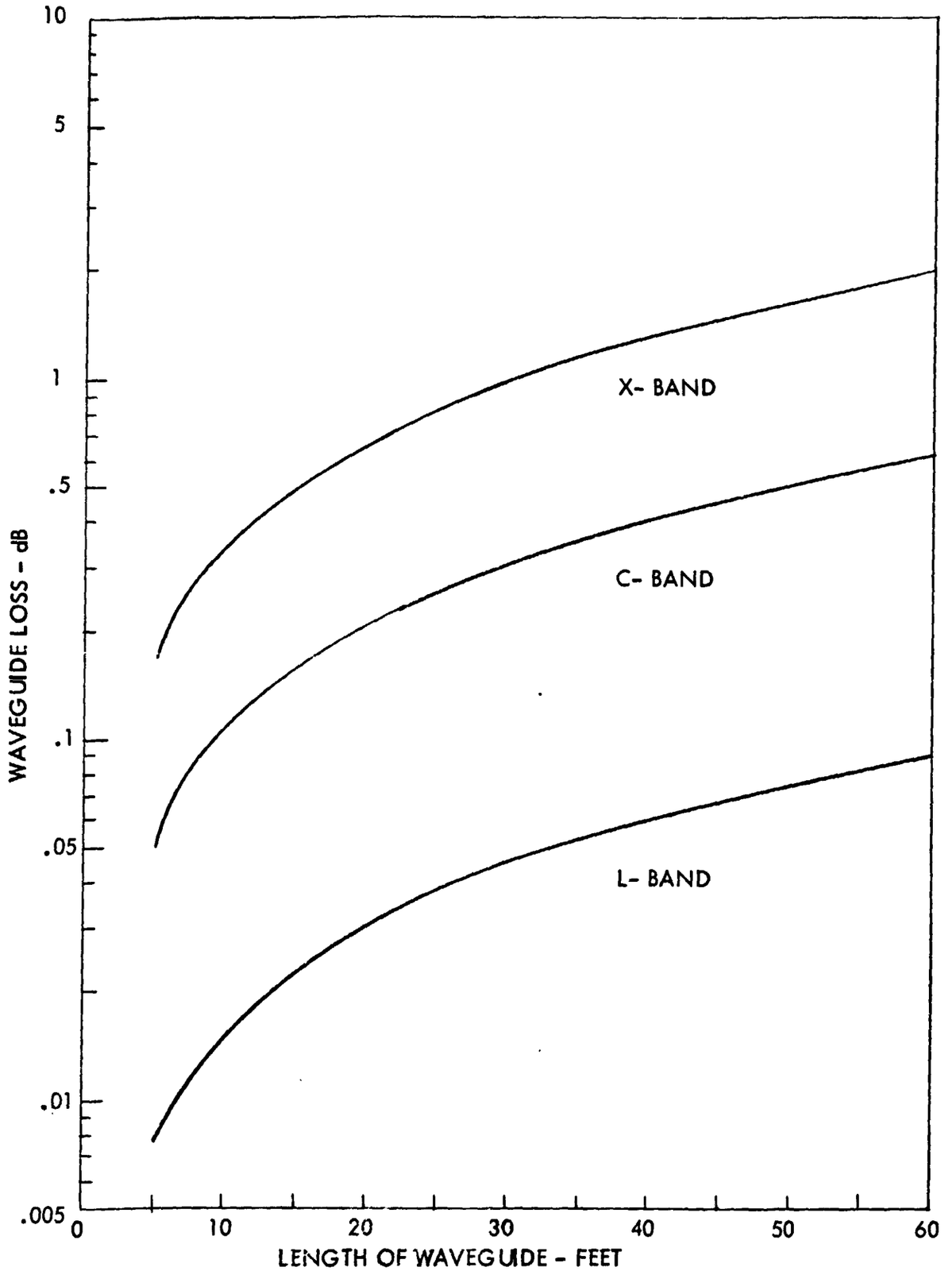

Figure 2-23. Waveguide Loss, Standard Rectangular Guide (Copper)

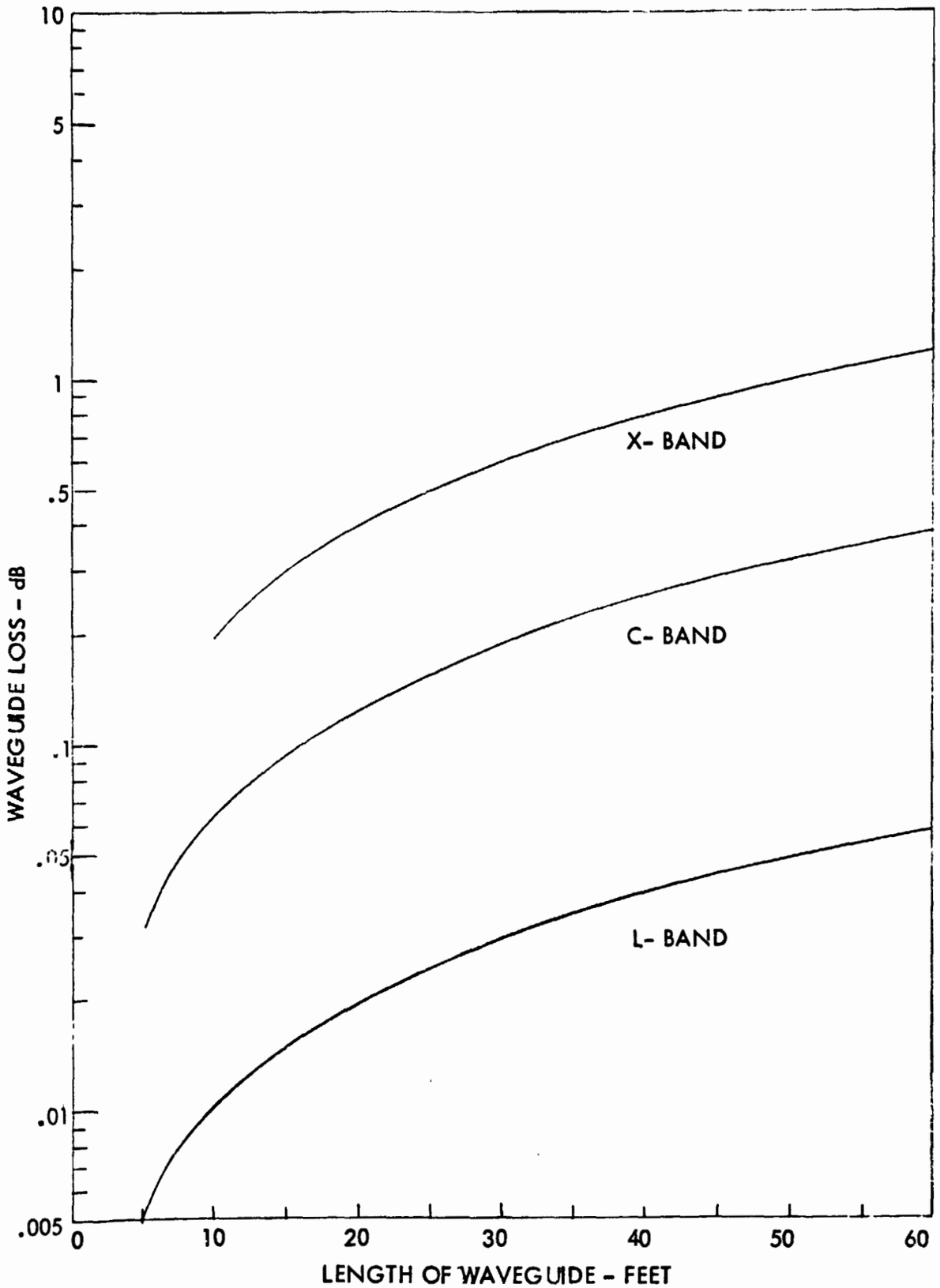

Figure 2-24. Waveguide Loss, Square Waveguide (Copper)

$$\alpha_D = \frac{27.3\sqrt{\epsilon_1'}\tan\delta}{\lambda} \quad \text{dB/unit length}$$

where ϵ_1' is the dielectric constant of the material and $\tan\delta$ is the loss tangent of the material.

The total attenuation in a coaxial line is then the sum of the conductor losses and the dielectric losses, i.e.,

$$\alpha_T = \alpha_c + \alpha_D$$

2.7.1.3 STRIPLINE LOSS

An expression for the conductor loss of stripline has been derived by where

$$\alpha_c = \frac{2.02 \times 10^{-6}\sqrt{\epsilon_r}\; f(\sqrt{\epsilon_r}\, Z_o)}{b}\left[\frac{1}{1-t/b} + \frac{2\,w/b}{(1-t/b)^2} + \frac{1}{\pi}\,\frac{1+t/b}{(1-t/b)^2}\,\ln\left[\frac{\frac{1}{1-t/b}+1}{\frac{1}{1-t/b}-1}\right]\right] \quad \text{dB/unit length}$$

with the following stripline geometry

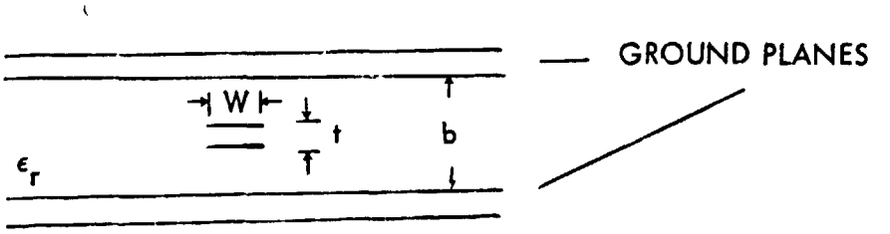

The dielectric loss is similar to that given for coaxial line

$$\alpha_D = \frac{27.3\ \sqrt{\epsilon_r}}{\lambda} \tan \delta$$

And the total loss is

$$\alpha_T = \alpha_c + \alpha_D$$

2.7.2 PHASED ARRAY LOSS LOCATIONS

Identification of all the losses in a phased array must be done on an individual array basis since there can be many variations in such array parameters as types of transmission line used, method of feeding the aperture, types of phase shifting devices and so forth. However, in order to provide some insight into the loss characteristics of phased arrays, an example consisting of a traveling wave, one-dimensionally fed array will be used to identify loss mechanisms and their relative magnitudes. The array will consist of a one dimensional non-resonant traveling wave feed element which will distribute energy properly phased to a two dimensional array of linear radiating elements. The linear arrays will also be non-resonant, traveling wave devices.

The loss components for this array are:

Effective linear array transmission line loss	L_L
Effective feed array transmission line loss	L_F
Linear array termination loss	L_{LT}
Feed array termination loss	L_{FT}
Phase shifter loss	L_S
Connector loss	L_C

The total array loss, L_T, is then the sum of the above component losses

$$L_T = L_L + L_F + L_{LT} + L_{FT} + L_S + L_C$$

The effective feed-line loss for a symmetric aperture distribution is one-half the loss of the unloaded (non-radiating) loss[1].

2.8 BEAM FORMING METHODS

In general a phased array is designed to form one beam in space and wide angle coverage is achieved by scanning the beam in either one dimension or two dimensions. Inertialess scanning of the beam is accomplished by changing the phase progression along the orthogonal axes of the array. Another method of providing wide angle coverage from a phased array is to generate multiple beams from the array, thus providing simultaneous wide angle coverage. A multiple beam array has the advantage from the radiometric standpoint, of allowing longer integration times at each beam position. The disadvantage of the multiple beam array is the complexity of the antenna system required to implement it.

The following discussion will be devoted to methods of scanning a single beam from the view point of the electronics required to implement a phase scanning system, and various methods of implementing a multiple beam array.

2.8.1 SINGLE BEAM SCAN

Scanning the beam, one-dimensionally, requires control of the interelement phase difference along the array axis. Phaser requirements to form and scan a single beam are best illustrated with the aid of Figure 2-25.

Forming a beam in the spatial direction k is equivalent to requiring an equiphase front normal to k. This equiphase front is generated by introducing phase delays $\Delta\phi n$ along the linear arrays. The required phase delay, $\Delta\phi n$, for the n^{th} element (relative to a convenient reference, chosen here to be the center element) is

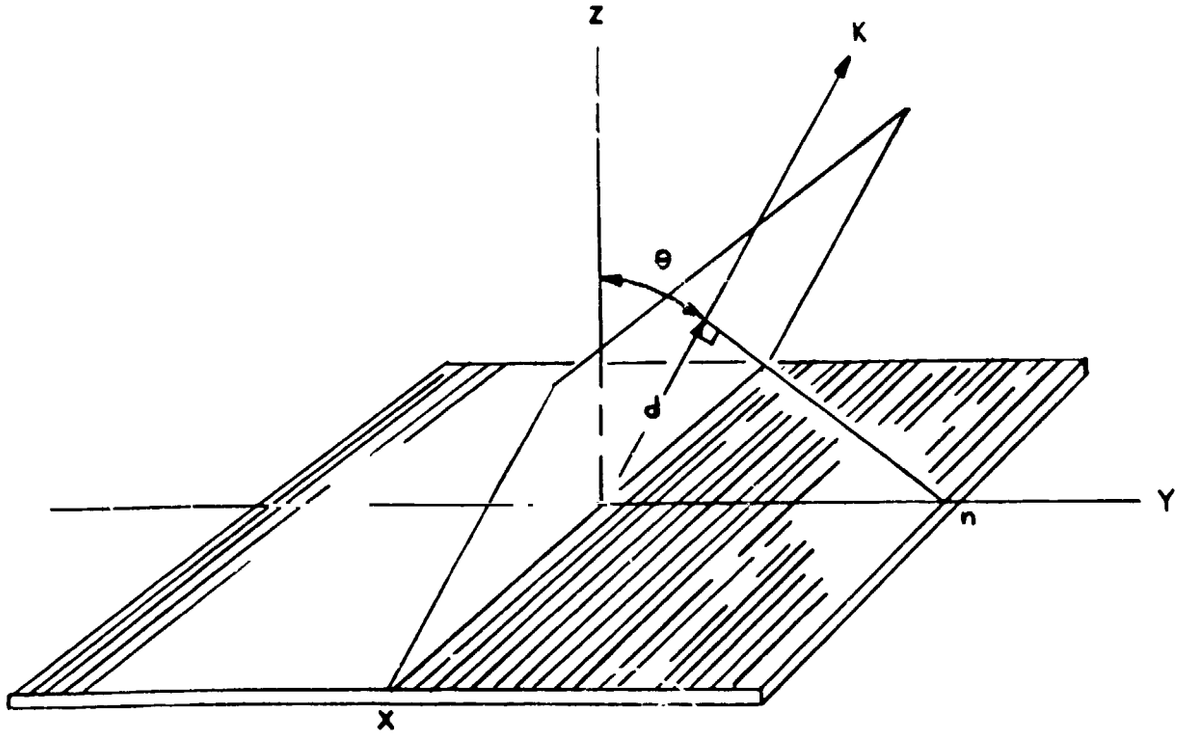

Figure 2-25. Wavefront Geometry

found in terms of the required beam angle from Equation (2.8.1).

$$d = n r \lambda \sin\theta \qquad (2.8.1)$$

where

d = the distance which the wave must lead that of the nth array from the reference array

r = the number of wavelength spacings between arrays

θ = the required beam pointing angle

$$\theta n = k d = 2\pi n r \sin\theta$$

Multiplying both sides of Equation (2.8.1) by the wave number $k = 2\pi/\lambda$ yields the expression for the phase shift required. For reasonable scan angles and large arrays the phase shift requirement ϕn of most phasers will exceed 2π radians. However, since $f(\theta) = f(\theta + 2m\pi)$, the actual phase shift employed $\Delta\phi n$ is

$$\phi n - 2m\pi = \Delta\phi n$$

where m is the number of integral multiples of 2π radians in ϕn. The final result is

$$\Delta\phi n = 2\pi (n r \sin\theta - m) \qquad (2.8.2)$$

Figure 2-26 shows typical phaser requirements as defined by Equation (2.8.2).

It is clear from the foregoing that establishing an equiphase front, with equally spaced phasers, requires generation of incrementally increasing phase shifts from phaser to phaser across the antenna aperture. The magnitude of the phase increment will determine the angle of the equiphase front and hence the angle of the beam normal to the front. Computation of the phase requirement for each specific phaser requires digital

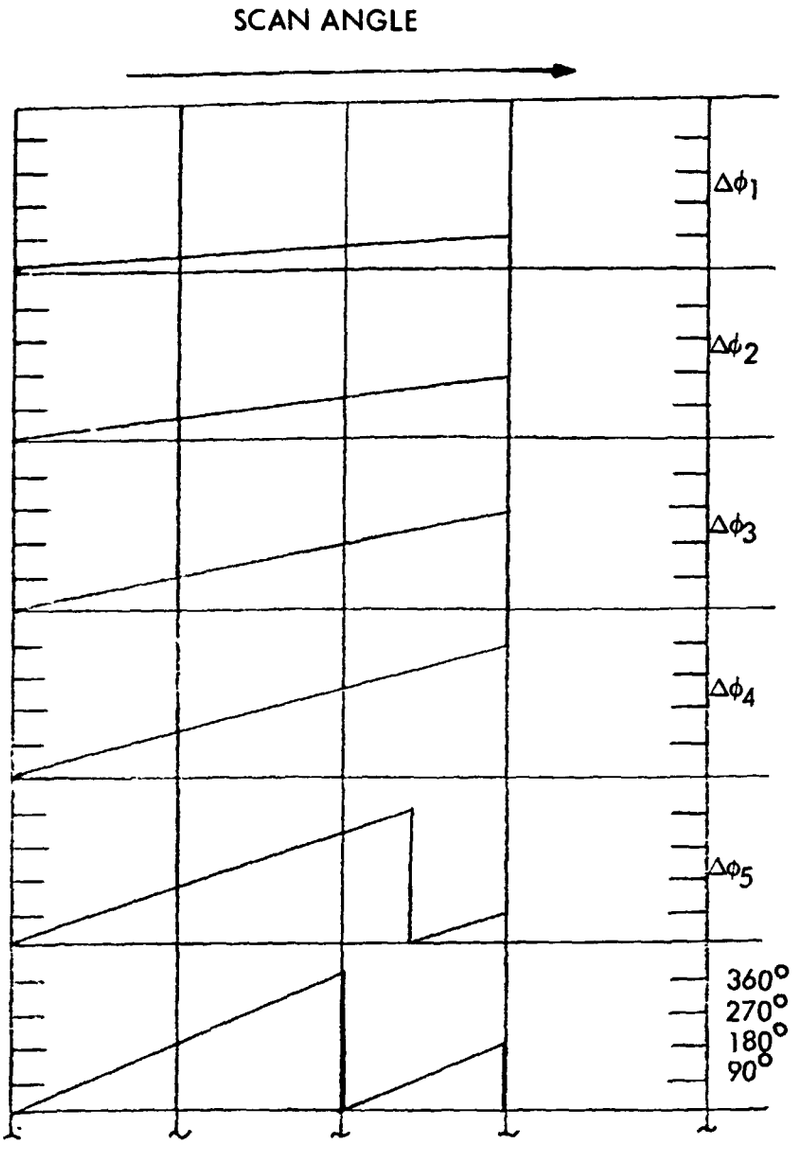

Figure 2-26. Phaser Requirements

techniques to provide the necessary phase accuracy. This is especially true of large arrays incorporating many phasers. Two configurations of beam forming networks which accurately and efficiently generate required phase shifts for stepped scan operation are presented below.

2.8.1.1 CYCLIC BEAM FORMING NETWORK

The configuration of this beam forming network utilizes a natural relationship between the characteristic of a modulo n counter and the phase requirements of equally spaced phasers in forming a planar array beam.

A functional block diagram of the Cyclic Beam Forming Network is presented in Figure 2-27. The k bit adder-storage register combination provides the mechanism essential in generation of incrementally increasing phase shifts from phaser to phaser along the antenna aperture; and therefore the essential element in forming a single beam. The adder-register combination operates in the following manner.

Prior to forming a beam at a new scan angle, the storage register is cleared to zero by a Beam Step input pulse. Inputs to the adder are a constant (N) from the beam translation read only memory (ROM) and the storage register output (zero). Storage register input is the output of the adder which equals N, (N+O). Upon the first clock pulse to follow the register clear, the storage register input is transferred to the register output. The register output becomes N and inputs to the adder N and N. The adder output and register input becoming 2N, (N+N). The following clock pulse shifts 2N to the register output and the adder output becomes 3N, (N+2N). In like manner, each succeeding clock pulse increments the magnitude of the storage register output by a factor of N. The register output therefore may be expressed as Nm, where m equals the number of clock pulses following the register clear. Linearly translating this incre-

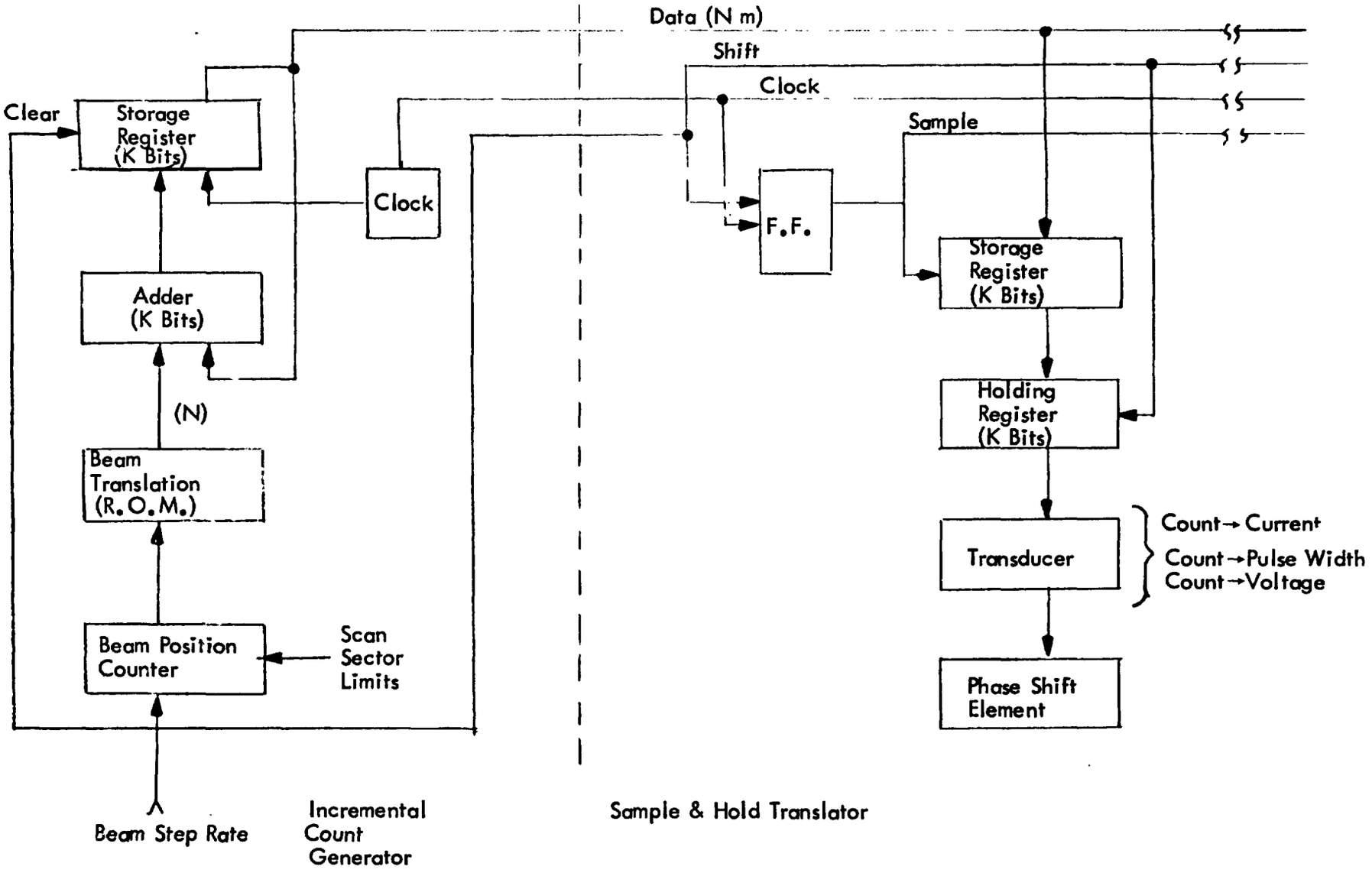

Figure 2-27. Cyclic Beam Scanning Network

menting output to incrementing phase shifts, from phaser to phaser along the array, generates an equiphase front and single beam normal to that front. To limit the differential operating phase shift of any phaser to 2π radians, the gain of each transducer must be adjusted such that maximum storage register capacity (2^k) provides exactly 2π radians of phase shift to any phaser. When the adder-register combination increments past its maximum capacity of 2^k ($N m > 2^k$) it recycles modulo 2^k, through zero, providing an output of $N m - \ell 2^k$ (where ℓ is the integral number of 2^k in N m). Likewise, the phase shift requirement of a given phaser ($B\pi$ radians) which exceeds 2π radians is equivalent to a phase shift of $B\pi - \ell 2\pi$ radians. It is this natural relationship existing between the recycling characteristic of a binary adder and the recycling phase requirement of the phasers along an array that the Cyclic Beam Forming Network utilizes.

Translation of the storage register output (N m) to incrementing phase shifts from phaser to phaser is accomplished by means of one transducer, two registers and one flip-flop, associated with each phaser. Each flip-flop operates as one stage of distribution shift register. In forming a beam, the storage register is cleared to zero and a logical "one" is presented to the first flip-flop of the distribution register. The first clock pulse following register clear, shifts the "one" to the output of flip-flop #1 clocking data (N) from the incrementing register output (data buss) into the storage register associated with phaser #1. The following clock pulse shifts the "one" to the output of the second flip-flop of the distribution shift register and thereby clocks data from the storage register output (2N) into the storage register associated with phaser #2. In like manner, each succeeding storage register acquires an incrementing count; 3N, 4N, 5N, etc. Generation and distribution of incrementing counts to each of the storage registers is accomplished without interruption of the previously formed beam. When all storage registers are filled and the data integration period of the existing beam position is com-

plete, data held in the storage registers is simultaneously transferred to all holding registers; by means of the Beam Step Rate pulse. This data, translated through the phaser transducers, generates the appropriate incremental phase shifts to form a beam at the new scan angle. The data is held in the holding registers for the integration interval of the beam position, during which time the storage registers are sequentially accumulating data for the following beam position.

It is interesting to note that the circuitry associated with each phaser is identical. Each phaser is fed by means of a four-line distribution buss and any number of phasers may be employed within the constraint that, minimum clock interval, times the total number of phasers, is less than the data integration period of each beam position.

From Equation (2.8.2) the angle at which the beam is formed is a function of the differential phase shift from phaser to phaser which, in turn, is proportional to the incrementing magnitude of the storage register (N•m) which, ultimately is a direct function of the constant N from the beam translator ROM. A unique constant must therefore be stored in the ROM for each discrete beam angle within the scan sector. The beam is step scanned through a given sector by means of the beam translation ROM and beam position counter, combination. For each state of the beam position counter, the appropriate constant (required to form a beam at an angle corresponding to the counter state) is addressed by the beam position counter and presented to the adder input by the ROM. The number of beam positions per scan (total scan angle) and initial scan angle, may easily be selected by digitally limiting the operating range of the beam position counter. By this means instant selection of any sector within the total (maximum) scan angle is possible.

Circuit configuration of the transducer (employed to translate the holding register output to the appropriate phaser phase shift) is dependent upon the type of phaser

selected for the array. For a Reggia-Spencer type phase shifter, the translator must linearly translate holding register count to solenoid coil current. For single flux drive type ferrite torroid phasers, the translator linearly translates holding register count to fixed voltage variable pulse widths. Multisection torroid phasers require direct translation of register count to saturation level pulses. Binary weighted multi-diode phasers require direct translation of holding register count to forward bias current and reverse bias voltage levels.

2.8.1.2 PROGRAMMED BEAM FORMING NETWORK

The Programmed Beam Forming Network utilizes a pre-programmed memory containing appropriate phase information for each beam position and phaser in the array. Presently CMOS integrated circuit read only memories (pre-programmed) appear to be the most efficient means of storing this information.

A functional block diagram of the Programmed Beam Forming Network is presented in Figure 2-28. In this configuration one addressable ROM and phase transducer is required for each phaser. All ROMs are addressed in parallel from the output of the beam position counter (beam position buss). For each state of the beam position counter the appropriate word (data) is stored in each of the ROMs to provide phaser phase shifts forming a beam at an angle which corresponds to the counter state. The number of words of memory capacity is therefore equal to the number of beam positions in the total (maximum) scan. Transducers of the Programmed Network are identical to those of the Cyclic Network above. Operation of the beam position counter is also identical to that of the Cyclic Network, such that any sector within the total maximum scan angle may be selected digitally.

The Cyclic Beam Forming Network is less expensive and requires less operating

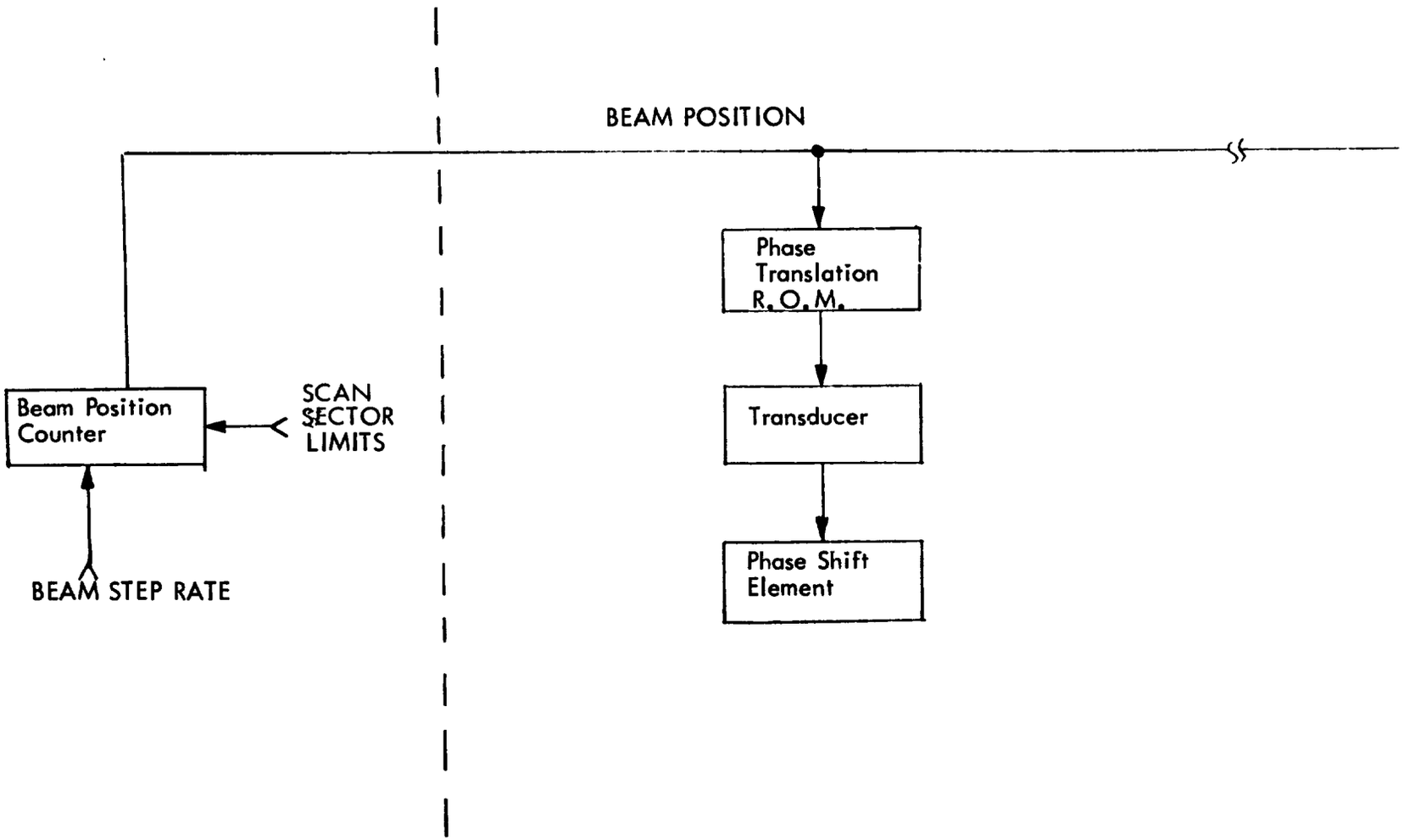

Figure 2-28. R.O.M. Beam Scanning Network

power than the Programmed Beam Forming Network. In addition, the task and expense of programming each ROM is eliminated. However, the Cyclic Network requires phaser linearity over a 2 radian operating range. Phase translations due to temperature effects (predominant in ferrite phasers) must also be included within the linear region. Programmed data in the memories of the Programmed Beam Forming Network may, on the other hand, be tailored to the phaser characteristics and phaser linearity is not a requirement.

2.8.1.3 PHASERS

Within the frequency range of interest, there are generally two types of phase shifting devices which will provide an alterable phase distribution across a planar array aperture. These are semiconductor diode devices and ferrite devices.

Semiconductor phase shifters utilize a p-n or PIN diode junction as the control element in a microwave phaser. The p-n junction of varactor diodes exhibits gradual parameter changes with reverse bias voltage which, in turn, allows low power continuous analog phase shifting. High reverse bias breakdown voltage and relatively constant parameters in both forward and reverse bias states are characteristic of PIN diodes. PIN diodes are therefore generally used in a digital phaser configuration. In such a configuration, a series of diodes, each usually capable of an incremental binary weighted phase shift, are employed. Total insertion loss of the incremental PIN diode phaser is generally greater than the analog phaser, however, higher power capability and linearity of digital drive to phaser phase shift are attributes of the PIN diode.

Ferrite phase shifters presently utilize latching (torroid) and non-latching configurations. Inherent memory (remanent magnetization) following excitation of a current pulse is the principle of latching ferrite operation. Latching phasers consist of a toroid formed from a ferrite or garnet possessing a reasonably rectangular hysteresis

loop (with inherently large remanence) and an axial wire through the center of the torroid for field excitation. Both analog (continuous) and digital (incremental) latching Ferrite phasers are available. Digital configurations consist of a series of different length ferrite toroids, usually binarily weighted as to remanence flux level following saturation. Analog configurations consist of a single ferrite toroid capable of a differential 2π radian phase shift. The method of analog phase shifting is based upon the linear dependence of phase shift or internal flux density of the toroid. Analog phase shift control is therefore dependent uponmagnetic flux provided by the driver circuit. This configuration (flux drive) operates below saturation such that prescribed changes generated in the remanent magnetization level produce proportional levels of differential phase shift in the device. The Reggia-Spencer type non-latching Ferrite phase shifter consists of a cylindrical Ferrite rod, supported in the center of a waveguide section, with a coil wound around the waveguide. Variation of the longitudinal magnetic field changes the effective permeability of the ferrite, providing a continuous (analog) differential phase shift as a function of coil current.

Although more expensive, the flux drive latching phase shifter provides faster response and requires less drive power than the non-latching device. A toroid possessing a rectangular hysteresis loop does not require holding current to retain the desired magnetization level (as does the Reggia-Spencer device), resulting in a considerable saving of drive power. Also, since the toroidal geometry minimizes the reluctance of the magnetic circuit, the current which the driver must supply to the magnetizing coil is correspondingly reduced. Configuring the phaser such that the entire Ferrite magnetic circuit (toroid) is within the waveguide eliminates induced current, which would otherwise flow in the metallic boundary, when switching magnetic flux. Such a configuration provides minimum switching response time.

Operating frequency is probably the most important factor in the choice of diode or ferrite phasers. At lower microwave frequencies (to about 2 GHz) the diode phaser is unquestionably superior. Diode phasers have lower insertion loss than ferrite phasers at lower frequencies, since the diode loss decreases with decreasing frequency. An analog diode phase shifter figure of merit is defined as the number of degrees of phase shift per dB of insertion loss. The figure of merit (F) is related to diode parameters and operating frequency f by

$$F = (6.6^\circ/\text{dB}) \qquad Fc\,(1 - \frac{1}{M})/f$$

where Fc is the varactor cutoff frequency $= 1/2\pi$ Cmin R, and M = Cmax/Cmin, where Cmax and Cmin are the maximum and minimum diode capacitance respectively. Maximizing the Cmax/Cmin ratio maximizes the figure of merit (M). For values of M greater than about 10, the figure of merit is primarily a function of the ratio of the diode cutoff frequency to the operating frequency, or diode Q. For 2π radians of phase shift per dB of loss, a diode Q greater than 55 is required.

The phase shift obtained from an analog diode phase shifter is not linear with applied voltage since the capacitance is related to the control voltage V by

$$C \propto K/(V + V\phi)^n, \qquad 1/3 < n < 1/2$$

where V is the bias voltage, $V\phi$ is the junction contact potential and K and n are constants related to the diode area and function profile, respectively.

In addition to low insertion loss at lower microwave frequencies diode phasers require low drive power (~ 0.1 mw), exhibit fast switching times (microseconds), and mechanical and thermal stability normally associated with semiconductor devices. Non-linearity of phase shift with control voltage, will, however, eliminate the "Cyclic" beam forming drive configuration.

In the 2.5 to 3.5 GHz frequency range, both diodes and ferrites can perform effectively. At higher microwave frequencies diode phasers are eliminated due to excessive insertion loss.

2.8.2 MULTIPLE BEAM ARRAYS

2.8.2.1 IF BEAM FORMING

IF beam forming is a technique that utilizes frequency down conversion so that the formation of multiple beams can be accomplished at a frequency much lower than that received at the antenna aperture. This low frequency (IF frequency) is generated via mixer/amplifier networks at the antenna ports. The IF energy from each antenna port is then fed into a multiple beam forming network. The multiple beam forming network, in this case the Butler Matrix [10], then generates simultaneous multiple beams each with the full gain of the antenna aperture. It is assumed here that the aperture will consist of a two dimensional array of radiating elements made up of linear arrays each of which is terminated at one end by a matched load and at the other end by a mixer/amplifier network as shown in Figure 2-29a.

The Butler Matrix provides a uniform illumination to the array. Amplitude tapering is accomplished by variable attenuators in the IF line. The network utilizes 90 degree hybrids for power division with mechanical phase shifters inserted for phase trimming. A 4-element, 4-beam network is shown in Figure 2-29b.

In a Butler Matrix of 90 degree hybrids the interelement phase shift equals

$$\Delta\phi = \frac{180\ k}{2^n}$$

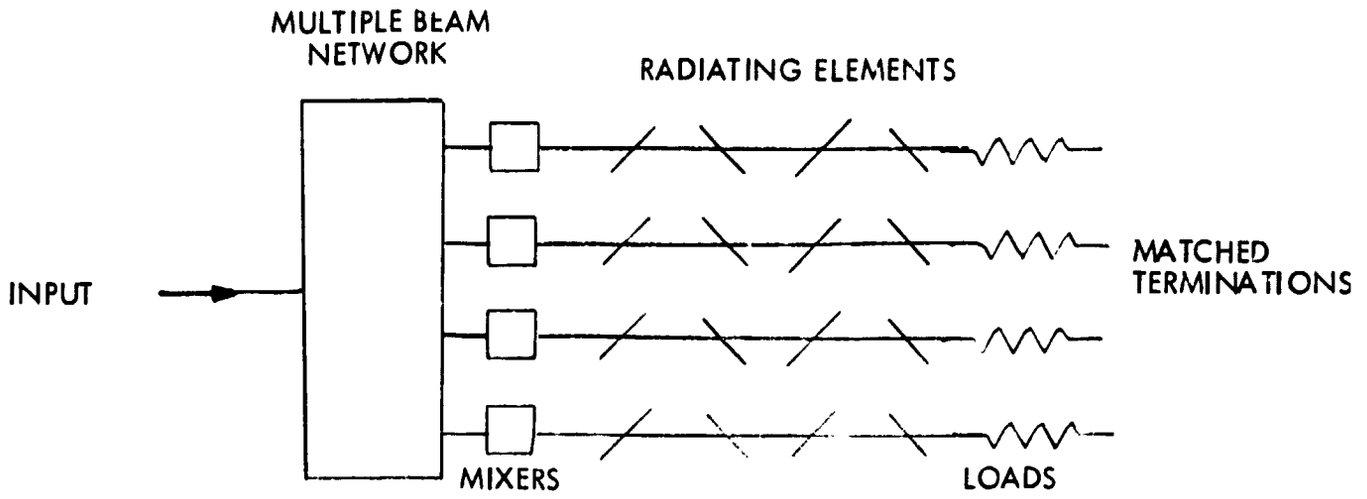

Figure 2-29a. Phased Array with Multiple Beam Forming Network

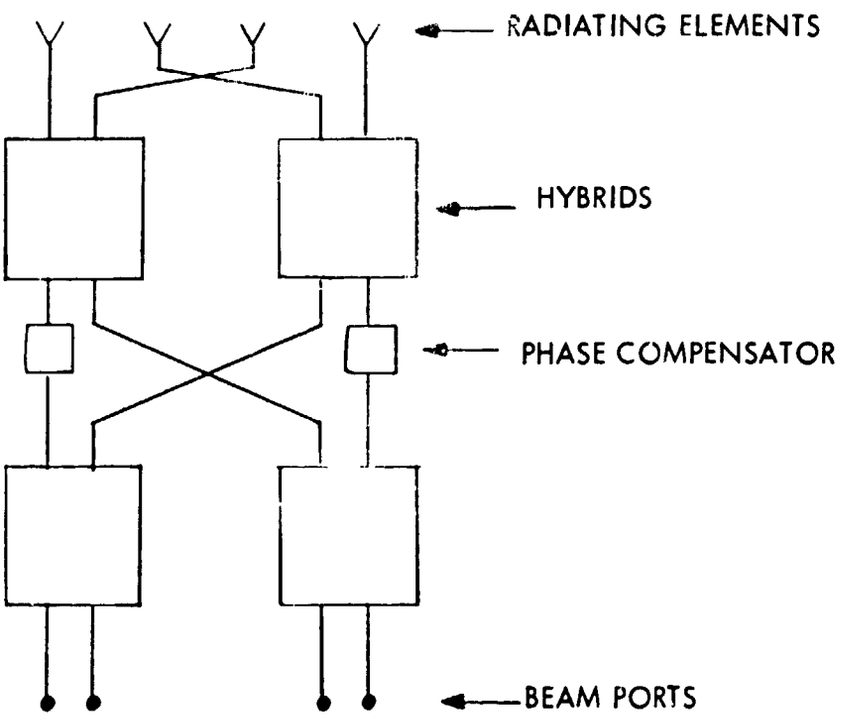

Figure 2-29b. Butler Matrix Beam Forming Network

where k is the beam number equal to $\pm 1, \pm 2, \ldots \pm 2^{n-1}$, and $2^n = N$ is the number of output ports and n is the order of the Butler Matrix. For a one-to-one correspondence between the Butler Matrix and the RF array ports, the array will see the same interelement phase difference of $\Delta\phi$, and the array will point in the direction γ, equal to

$$\gamma = \sin^{-1} \frac{\Delta \phi \lambda}{360\, d}$$

$$\gamma = \sin^{-1} \frac{\Delta \phi \lambda}{2 N d}$$

where d = interlement spacing of the array. Thus, the Butler Matrix beam forming network will form one beam per linear array element. As an example, assume the array consists of 100 elements with an interelement spacing of 0.5λ. The beams will then cover an angular range of ± 30 degrees with the beams spaced an average of 0.6 degrees apart. The half-power beamwidth of the broadside beam will be approximately 1.3 degrees.

2.8.2.2 RF LENS BEAM FORMING

The RF lens beam forming network is a parallel plate metallic lens with multiple feeds; each feed corresponding to a beam position. In this configuration, shown in Figure 2-30, a parallel plate region is used as a transmission line path between each feed horn and the RF lens. By using parallel plates, the energy is constrained to flow only from lens to feed.

The lens [11] itself is made up of sections of waveguide whose lengths are adjusted to provide the desired phase delays. Within the lens a TEM wave is propagated such that the rays through the lens are "constrainted" to follow a path

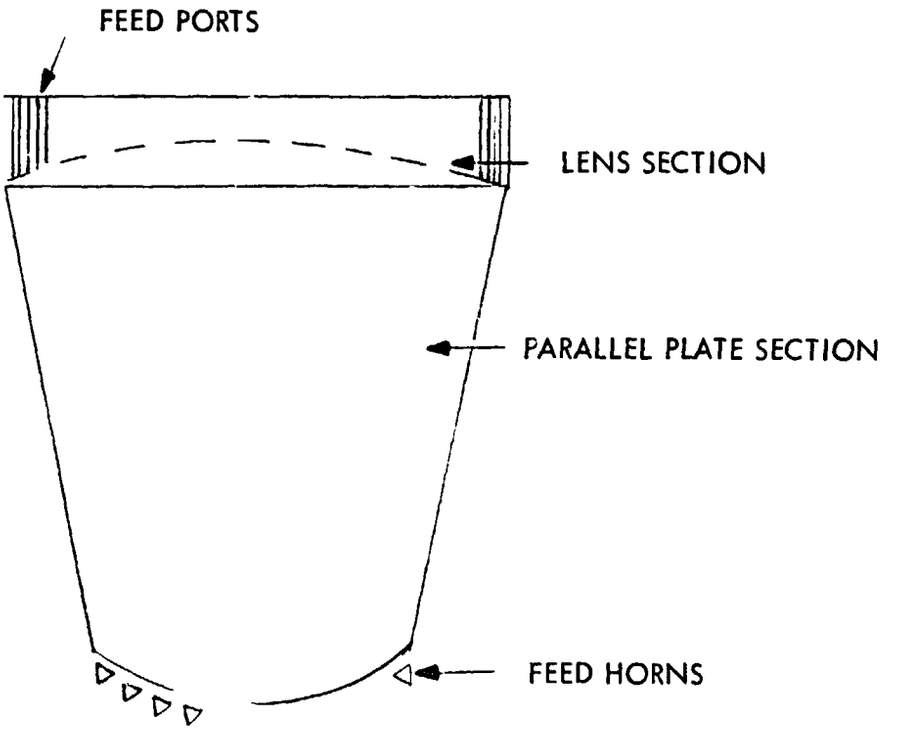

Figure 2-30. RF Lens Multiple Beam Forming Network

parallel to the metal plates that make up the lens. The electrical path lengths through the lens therefore are independent of the angle of the incident wave.

By placing feed horns around the focal arc of the lens, may independent beams can be formed. The number of beams and the angular spacing of the beams is limited, however, due to the finite size of the feed horns. In fact, the size of the feed horns is such that, in general, the beams formed will be spaced many beam-widths apart necessitating the use of some method of scanning the beams to provide continguous coverage.

2.8.2.3 FREQUENCY SCANNING

Frequency scanning is a technique that makes use of the frequency dispersive nature of a traveling wave array to cause the beam to scan. This technique can be thought of as either a method to scan a single beam or as a method of forming multiple beams.

The mechanism by which a beam scans with changing frequency has been discussed in Section 2.6. However, it is obvious that by increasing the length of transmission line between elements the array can be made extremely sensitive to frequency changes. If the antenna feed is increased in length between elements as shown in Figure 2-31, the equation for the beam pointing angle is

$$\theta = \sin^{-1} \frac{D}{d}\left[\left(\frac{\lambda}{\lambda g} - \frac{\lambda}{\lambda g'}\right)\right]$$

where d is the interelement spacing, D is the length of transmission line between elements and $\lambda g'$ is the guide wavelength at the center frequency. If D is on the order of several wavelengths then the angle θ will vary significantly with small changes in wavelength.

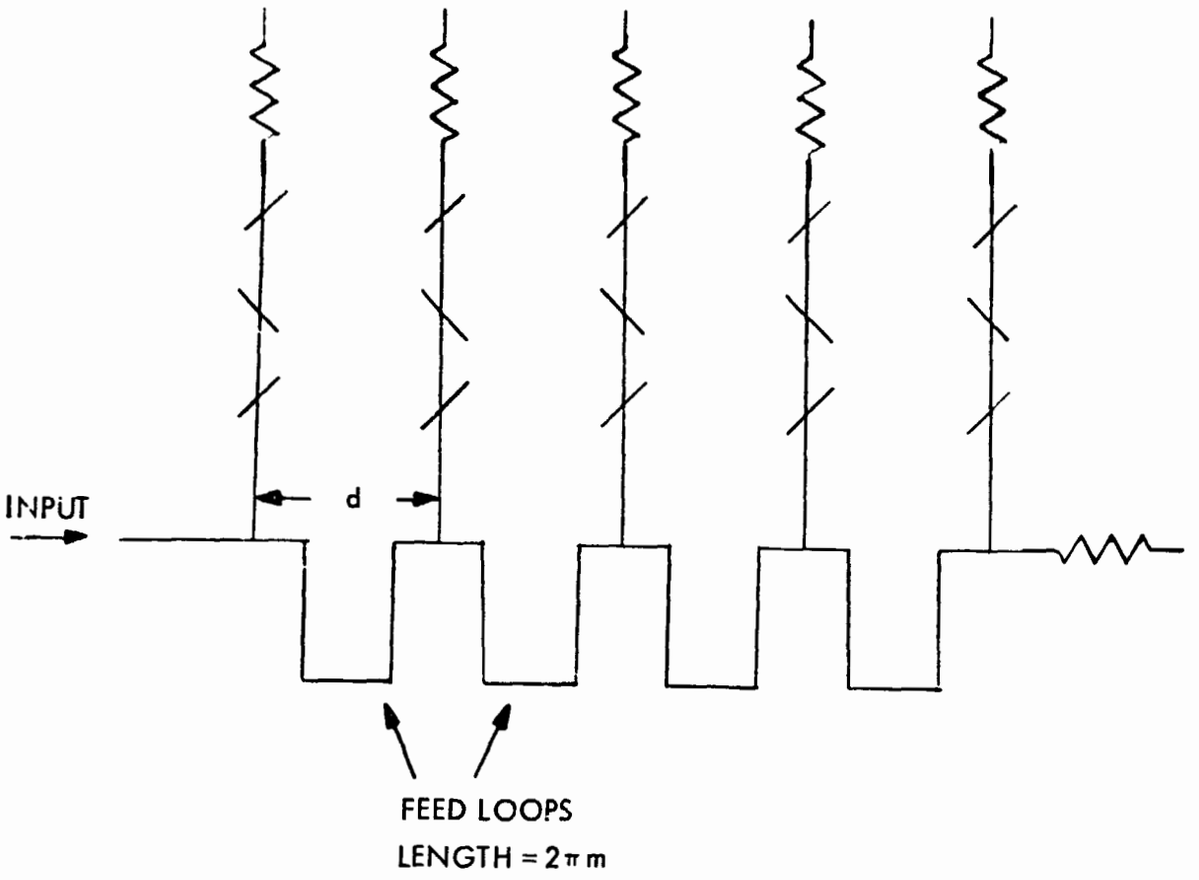

Figure 2-31. Frequency Dispersive Feed

A multiple beam array can be implemented using this technique by generating several closely spaced IF frequencies with each IF frequency corresponding to an RF frequency within the RF bandwidth needed to provide the required angular coverage. Thus, each IF frequency will correspond to a separate beam location. It is important to remember that as the RF bandwidth is increased to allow winder angular coverage, the beam will "smear" or broaden accordingly in the orthogonal plane.

3.0 CURRENT STATE-OF-THE-ART OF PHASED ARRAY ANTENNA TECHNOLOGY

Phased array antenna technology has developed rapidly over the last 15 years, primarily due to the ever increasing need for large, two-dimensionally scanning antennas for the present day radar systems. These antennas, for the most part, are designed for high gain and high power handling capability. Also, they are, in general, space-fed apertures which are usually large and cumbersome, and require excessive amounts of power to operate. The development of phased arrays for radiometric systems, i.e., low loss, high beam efficiency antennas, has not been as extensive.

In general, the phased array developed for radiometric applications, must meet rigid specifications as to peak sidelobe level, beam efficiency, low loss, and polarization purity. For the purposes of this study some of the more significant radiometric phased arrays developed to date will be presented along with design goals, measured performance, and technical problem areas.

3.1 NIMBUS-D ANTENNA - AEROJET-GENERAL CORPORATION

The Nimbus-D antenna is an electronically scanned phased array which operates at a center frequency of 19.35 GHz. The antenna consists of a two-dimensional array of slotted linear waveguide elements. It is fed by a traveling wave feed array which couples energy to the linear arrays via ported slots. The linear arrays are also traveling wave arrays which radiate through resonant-length slots cut into the narrow wall of the waveguide.

The coupling coefficients of the slots on both the linear arrays and the feed array are designed to produce a Dolph- Chebyshev amplitude distribution with a theoretical peak sidelobe level of -35 dB. The arrays are designed to radiate 97 percent

of the input energy and absorb 3 percent into matched terminations. The slot coupling is controlled by adjusting the slot angle.

Scan is achieved by varying the phase progression along the feed array via ferrite phase shifters inserted at each feed port. The phase shifters are Reggia-Spencer type analog phase shifters which provide up to 360 degrees of phase shift. The antenna scans $\pm$50 degrees in a plane broadside to the arrays.

The polarization of the array is linear and is oriented parallel to the longitudinal axes of the linear array waveguides. The cross polarized lobes are suppressed by adjusting the height of the ground plane relative to the radiating surface providing a "choke" like effect to reduce the surface currents which support the radiation of the cross polarized lobes.

The design specifications and measured performance of the Nimbus-D array are tabulated in Figure 3-1. Figures 3-2 and 3-3 show the orthogonal plane patterns of the array for the beam scanned to broadside and for the beam scanned to +49.3 degrees.

3.2 NIMBUS-E ANTENNA - AEROJET-GENERAL CORPORATION

The Nimbus-E antenna is an enlarged version of the Nimbus-D antenna utilizing Taylor amplitude distributions instead of Dolph-Chebyshev distributions. The only significant technical difference between the two arrays, aside from size, is the slot orientation in the feed array. The slots in the feed array of the Nimbus-E antenna are all inclined in the same direction with phase reversal achieved by alternating the inclination of slots between adjacent linear arrays as shown in Figure 3-4.

A summary of system parameters is presented in Figure 3-5 and a comparison of design goals with measured performance is shown in Figure 3-6. Principal plane

FREQUENCY	19.35 GHz
APERTURE SIZE	16"X16"
NUMBER LINEAR ELEMENTS	49
NUMBER SLOTS	36
AMPLITUDE DISTRIBUTION LINEAR ARRAY	-35 dB
AMPLITUDE DISTRIBUTION FEED ARRAY	-35 dB
BEAMWIDTH	$2.7^{\circ}X3.0^{\circ}$
SCAN ANGLE	$\pm 50^{\circ}$
BEAM SQUINT ANGLE	-3.2°
BEAM EFFICIENCY	88-93%
INSERTION LOSS DESIGN	1.4 dB
MEASURED	2 dB

Figure3-1. Antenna System Parameters Nimbus-D

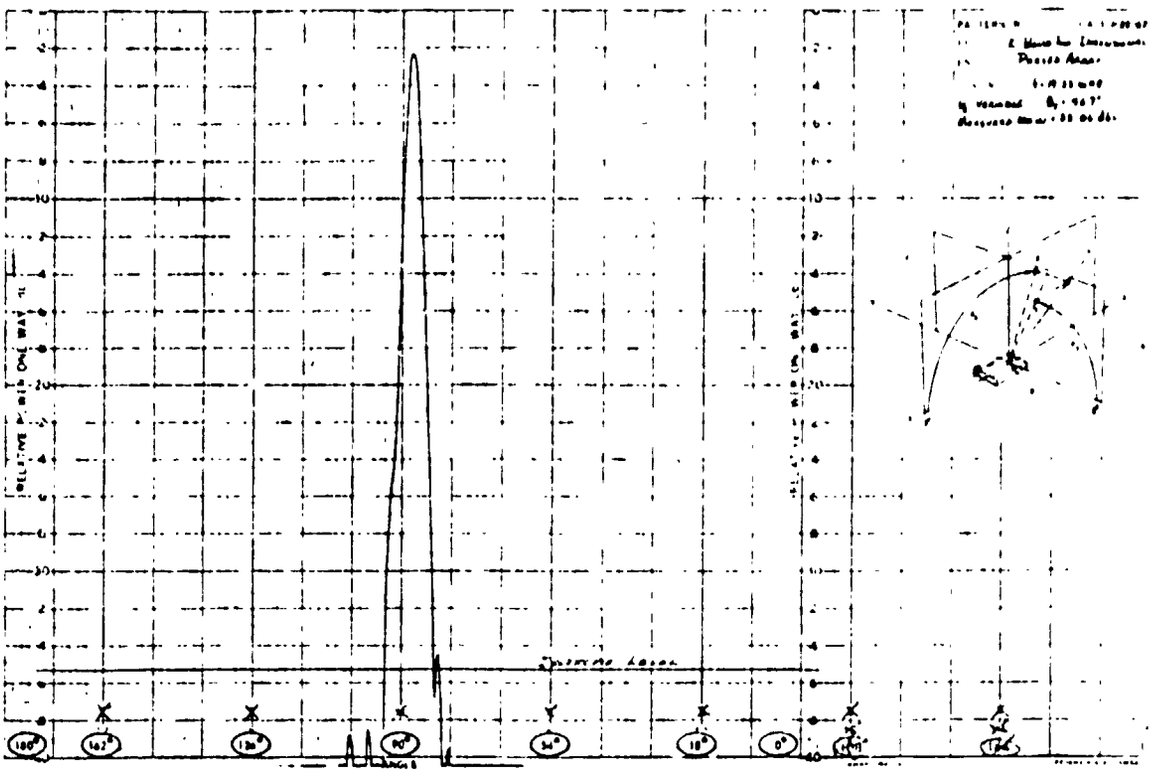

Figure 3-2a. Antenna Pattern, $\theta_x = 86.8^\circ$, θ_y Variable, Nimbus-D

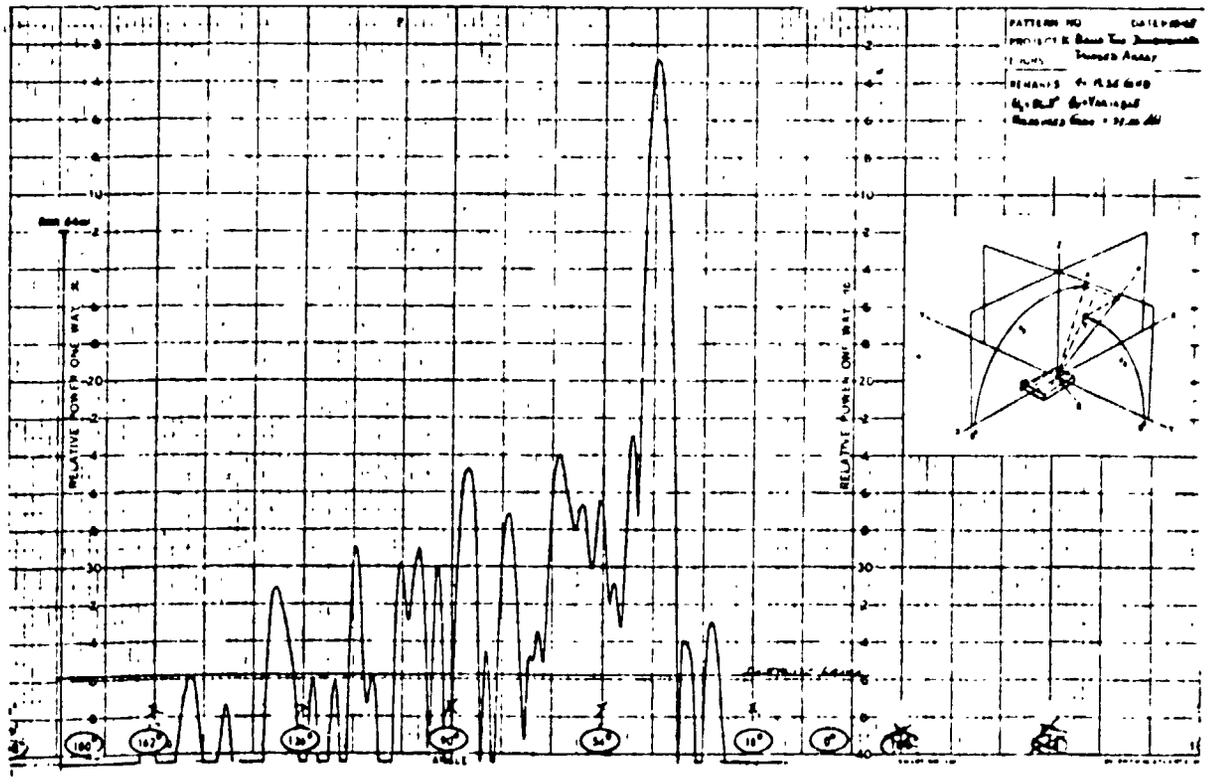

Figure 3-2b. Antenna Pattern, θ_x Variable, $\theta_y = 40.7^\circ$, Nimbus-D

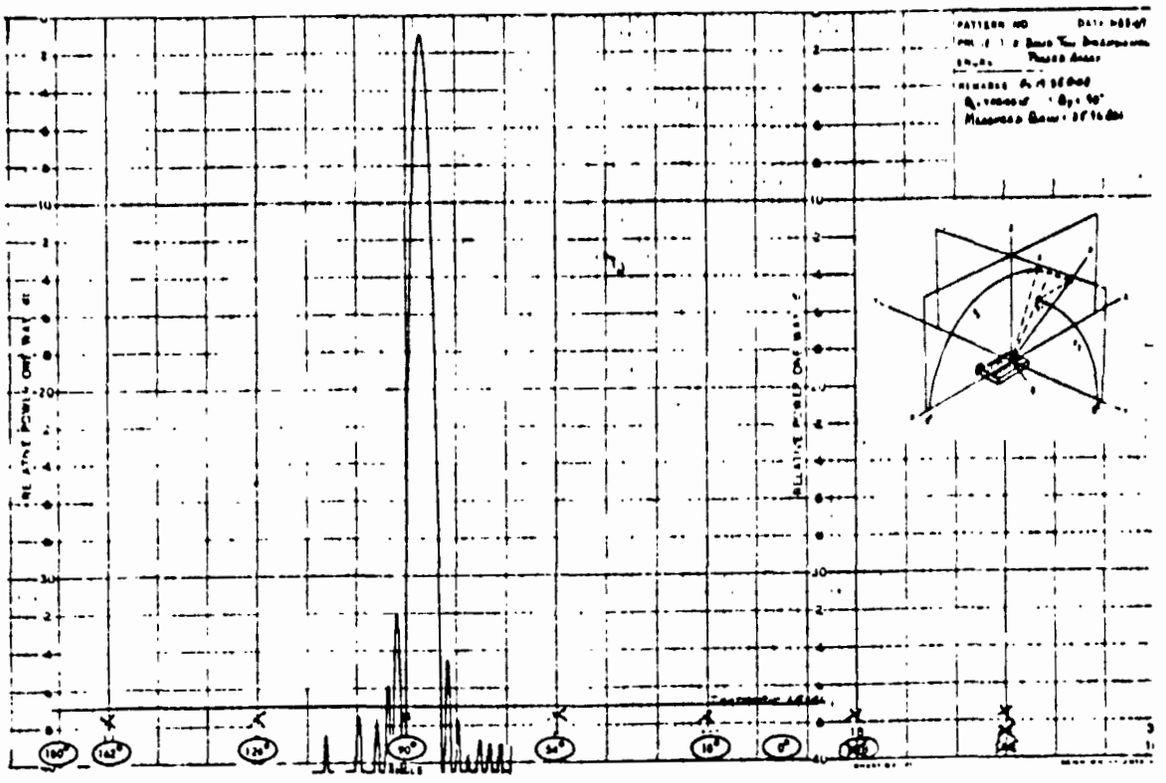

Figure 3-3a. Antenna Pattern, $\theta_x = 86.8^\circ$, θ_y Variable, Nimbus-D

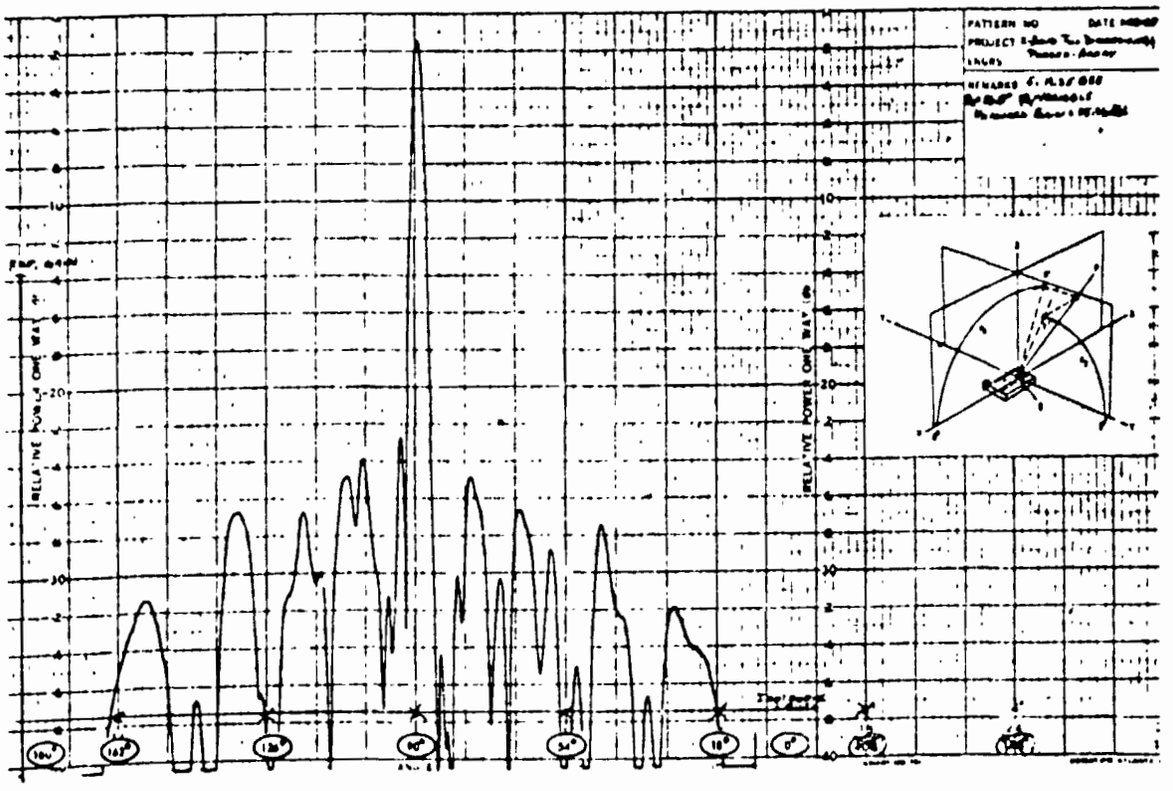

Figure 3-3b. Antenna Pattern, θ_x Variable, $\theta_y = 90^\circ$, Nimbus-D

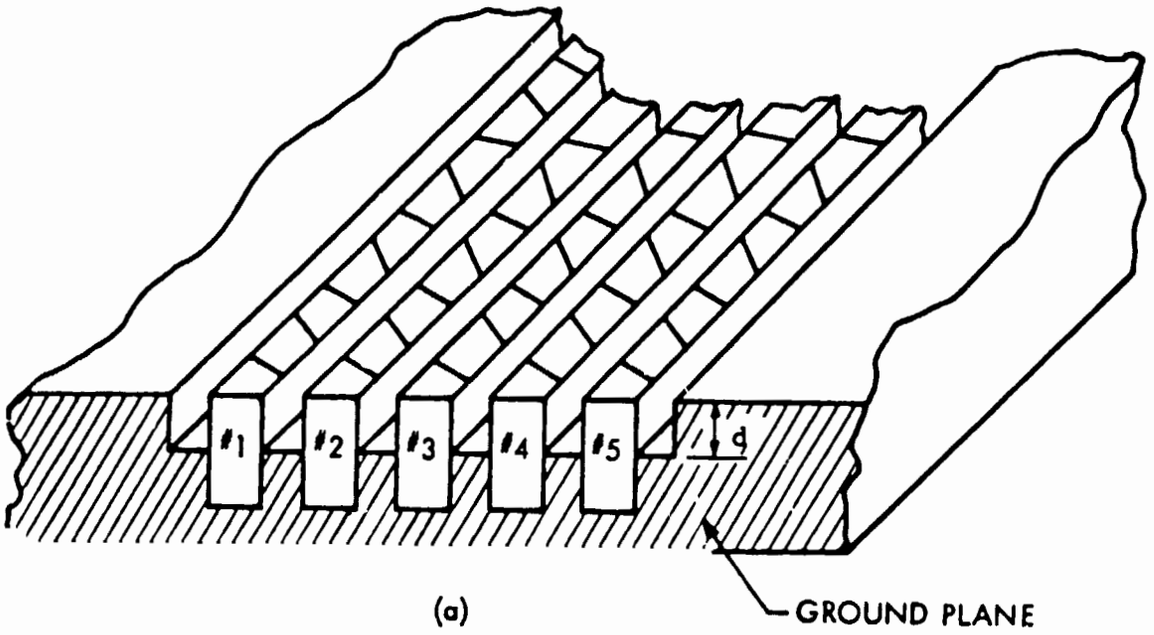

(a)

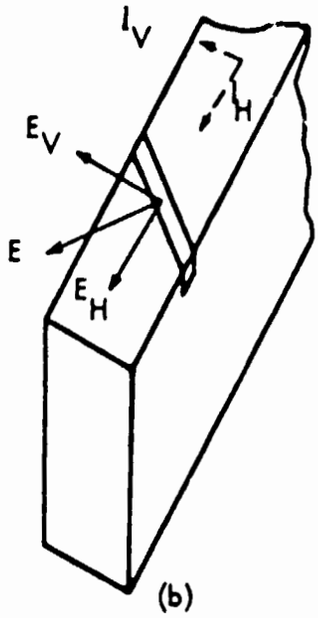

(b)

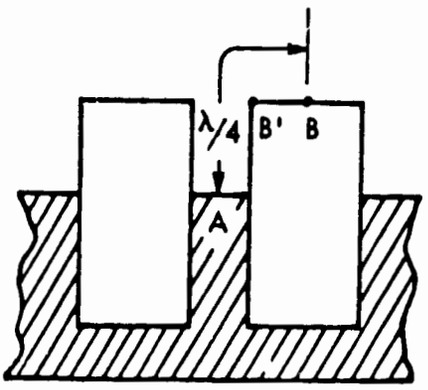

(c)

Figure 3-4. Antenna Nimbus-D

FREQUENCY	19.35 GHz
APERTURE SIZE LINEAR ARRAY DIMENSION	32.80 INCHES
APERTURE SIZE FEED ARRAY DIMENSION	33.66 INCHES
NUMBER OF LINEAR ELEMENTS	103
NUMBER OF SLOTS	81
AMPLITUDE DISTRIBUTION LINEAR ARRAY	-40 dB SIDELOBE TAYLOR DISTRIBUTION
AMPLITUDE DISTRIBUTION FEED ARRAY	-35 dB SIDELOBE TAYLOR DISTRIBUTION
BROADSIDE HALF POWER BEAMWIDTH	1.4 DEGREES
NUMBER OF BEAM POSITIONS	78
ANTENNA BEAM EFFICIENCY	90% to 92.7%
BEAM SCAN ANGLE	$\pm$51 DEGREES
ANTENNA LOSS	1.7 dB
BEAM SQUINT ANGLE	-3.2 DEGREES NOMINAL
CROSS-POLARIZATION	-25 to -36 dB

Figure 3 -5. Antenna System Parameters Nimbus-E

SPECIFICATION	DESIGN GOAL	MEASURED
PEAK SIDELOBE LEVEL		
SCAN PLANE	-35 dB	-21 dB
LINEAR ARRAY PLANE	-40 dB	-37 dB
HALF POWER BEAMWIDTH		
SCAN PLANE	1.4°	1.4°
LINEAR ARRAY PLANE	1.4°	1.4°
BEAM EFFICIENCY	≥95%	90 to 93%
ANTENNA LOSS	1.6 dB	1.7 dB
PEAK CROSS POLARIZED LOBE	-25 to -36 dB	-5 to 10% of Energy

Figure 3-6. ESMR Performunce Nimbus-E

patterns for the broadside beam position are shown in Figures 3-7 and 3-8. Beam efficiency, loss, and VSWR data are presented in Figures 3-9, 3-10 and 3-11, respectively.

3.3 PMIS ANTENNA SYSTEM - AEROJET-GENERAL CORPORATION

The PMIS antenna is a dual-polarized, electronically steered array. It is designed to be mounted in a vertical plane with the beam scanning conically about the vertical axis of the array. The array is composed of 51 linear slotted-waveguide sections forming an aperture 43 x 36 inches.

The linear array waveguide is square in cross-section and is designed to propagate two orthogonal modes, namely TE_{10} and TE_{01}. Energy is radiated from the waveguide via crossed slots with each arm of the slot coupling to a waveguide mode. The horizontal arm of the slot couples vertically polarized energy and the vertical arm couples horizontally polarized energy.

The separation between adjacent slots along each waveguide produces a fixed slot-to-slot phase shift which causes the beam to squint off-axis. The squint angle in this case is 40.5 degrees measured from broadside. When the antenna is scanned in the orthogonal plane the beam will scan conically along the surface of a cone whose apex half-angle is 49.5 degrees.

The positioning of the beam around the surface of the cone is accomplished by controlling the waveguide-to-waveguide phase shift. This phase control is achieved by analog ferrite phase shifters. Since such phase shifters can only support one polarization, the two polarizations that propagate down each slotted waveguide are separated by a group of dual-mode transducers, one for each waveguide. Two banks of phase shifters are used, one coupling to the horizontally polarized outputs of the dual-mode

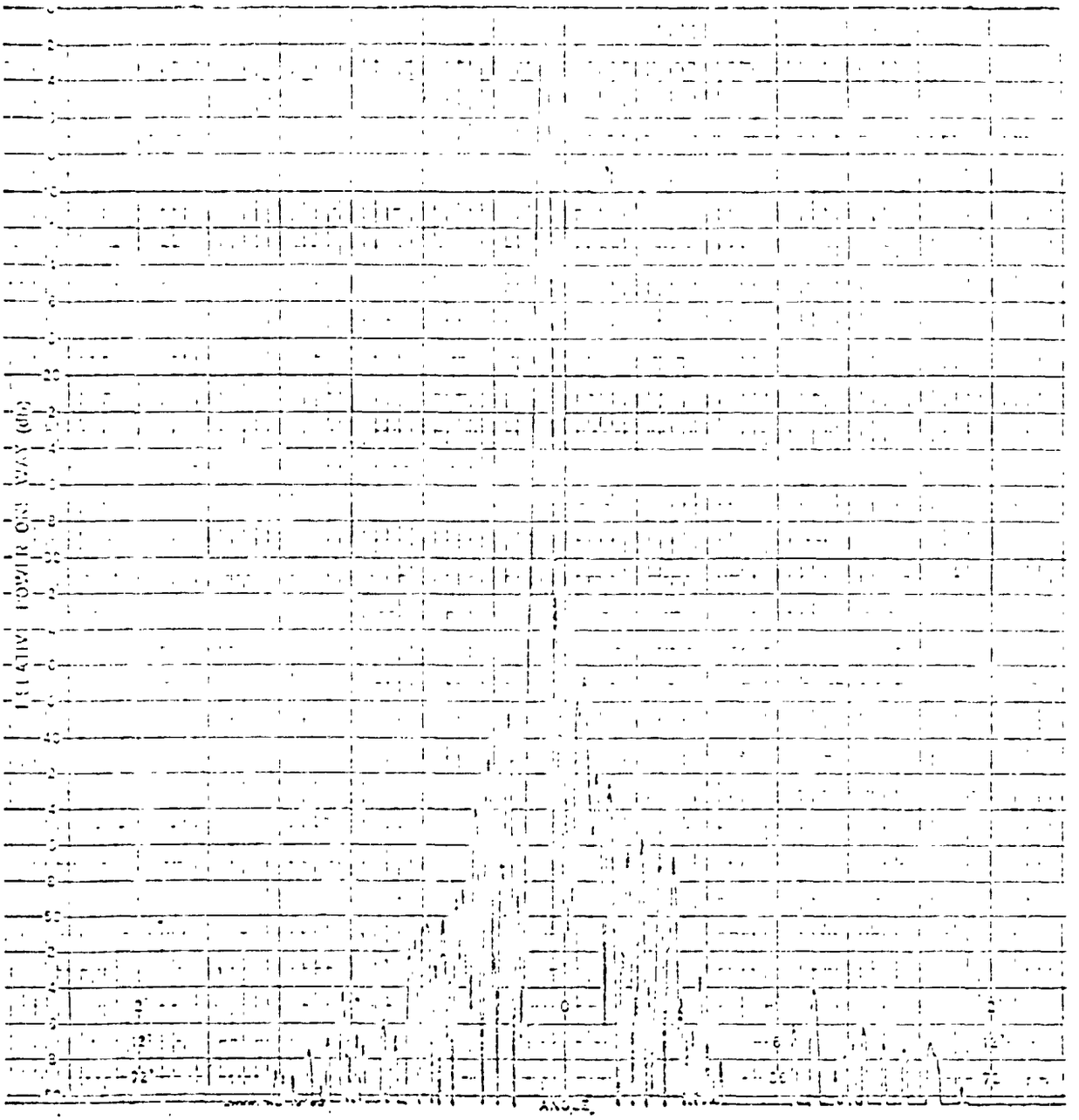

Figure 3-7. Element Plane Beam Position 39 Nimbus-E

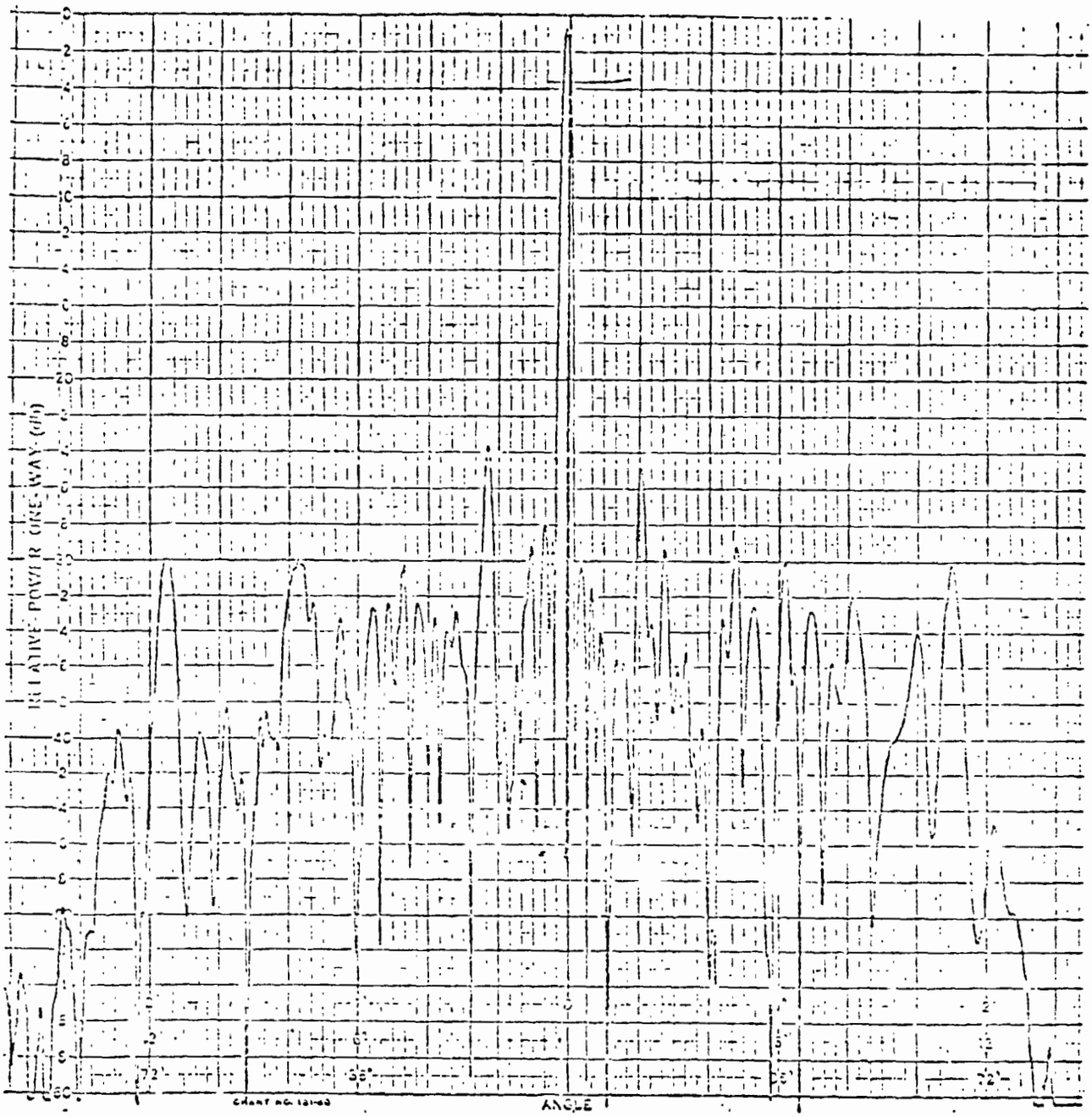

Figure 3-8. Scan Plane Beam Position 39 Nimbus-E

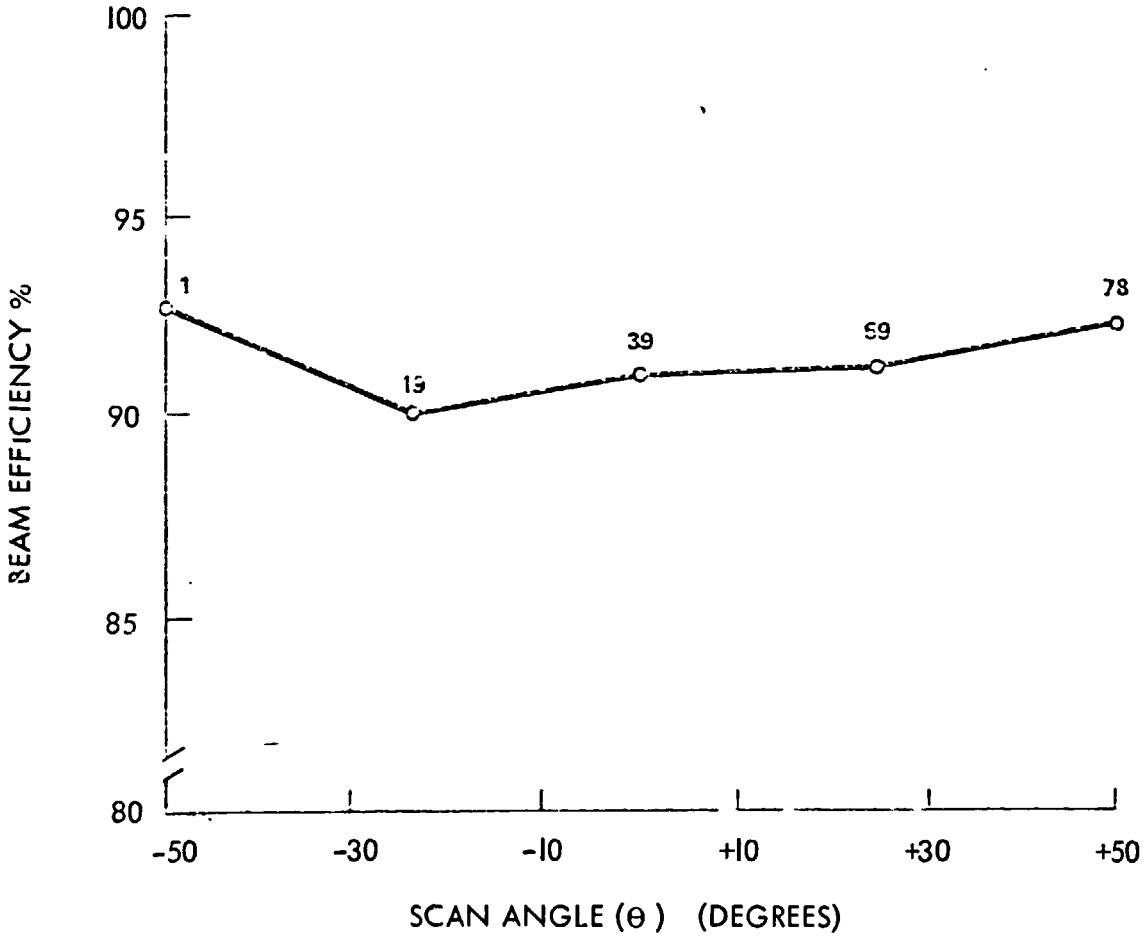

Figure 3-9. Beam Efficiency Versus Scan Angle Engineering Model

TEMP °C	FEED	FEED TERMINATION	PHASE SHIFTERS	W/G BENDS AND CONNECTORS	LINEAR ARRAY	LINEAR ARRAY TERMINATION	CALCULATED ANTENNA LOSS (dB)	MEASURED LOSS (dB)
0	.298	.222	.699	.110	.206	.157	1.692	
5	.298	.222	.690	.110	.206	.157	1.684	
10	.298	.222	.680	.110	.207	.158	1.675	
15	.298	.222	.667	.111	.207	.158	1.663	1.6 - 1.7
20	.298	.222	.654	.111	.208	.159	1.652	
25	.298	.222	.639	.112	.209	.159	1.639	
30	.298	.222	.623	.112	.210	.160	1.626	
35	.298	.222	.606	.113	.211	.161	1.611	

Figure 3-10. Antenna System Loss (dB) versus Temperature
Nimbus-E

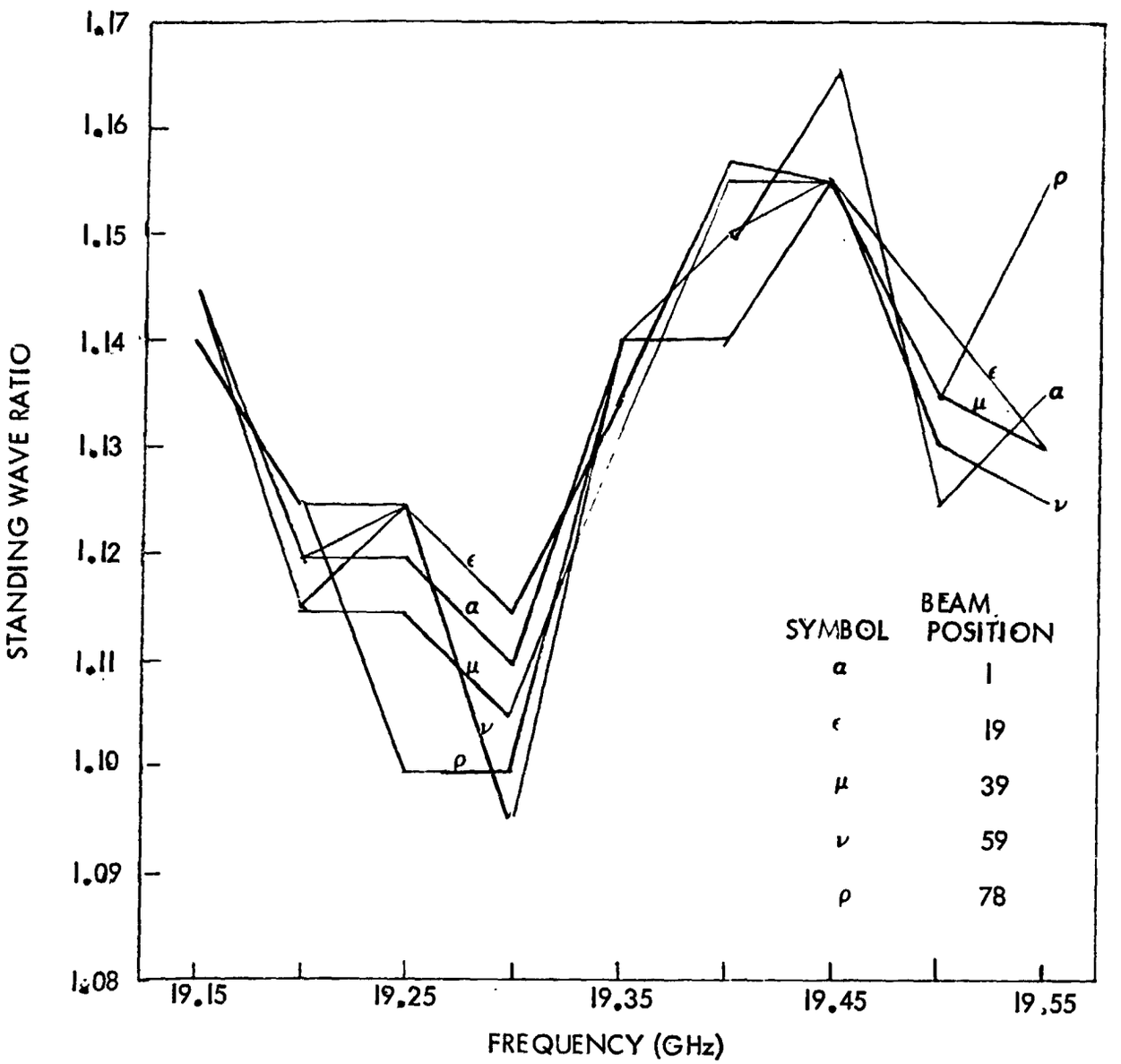

Figure 3-11. VSWR Versus Frequency For 5 Beam Positions Nimbus-E Engineering Model

transducers, and the other coupling to the vertically polarized outputs. The antenna has the capability of scanning to any one of 44 discrete positions which cover the range ±35 degrees from the broadside position.

The PMIS antenna system parameters are tabulated in Figure 3-12. Patterns showing the beam scanned to broadside are presented for both orthogonal planes and both polarizations in Figures 3-13 through 3-16. The peak sidelobe levels measured for the vertical and horizontal polarizations are plotted as a function of beam position in Figures 3-17 and 3-18, respectively. Beam efficiency data is given in Figure 3-19.

3.4 NIMBUS-F ANTENNA - AEROJET-GENERAL CORPORATION

The Nimbus-F antenna is a dual polarized electronically scanned array basically identical in design to the PMIS antenna except that it operates at a center frequency of 37.0 GHz. The beam is scanned conically on the surface of a cone whose apex half-angle is 45 degrees. The scan range is ±35 degrees from the array broadside. Spacing limitations were such however, that at scan angles past ±31 degrees, the grating lobe moves into the visible region.

A comparison of the system specifications with measured antenna performance is given in Figure 3-20. Antenna patterns taken of the broadside beam position for both polarizations are shown in Figures 3-21 through 3-24. Antenna insertion loss as a function of beam position is shown for both ports in Figure 3-25.

3.5 SUMMARY OF PROBLEMS

The following section will discuss briefly the problem areas encountered in the design and development of the four Aerojet-General antenna systems. Although all four of the antennas are traveling wave fed, waveguide arrays, the problem areas are applicable in general, to all types of phased arrays.

FREQUENCY		10.69 GHz
APERTURE SIZE		43" X36"
NUMBER LINEAR ELEMENTS		51
NUMBER SLOTS		59
AMPLITUDE DISTRIBUTION		-35 dB
BROADSIDE HALF POWER BEAMWIDTH		2.6°X1.6°
NUMBER BEAM POSITIONS		44
BEAM SCAN ANGLE		±30°
BEAM CONE ANGLE		49.5°
BEAM EFFICIENCY MEASURED		75 to 91%
VSWR		1.02 to 1.15
CROSS POLARIZATION	0°	-34 dB
	±30°	-10 dB

Figure 3-12. Antenna Parameters PMIS Dual Polarized

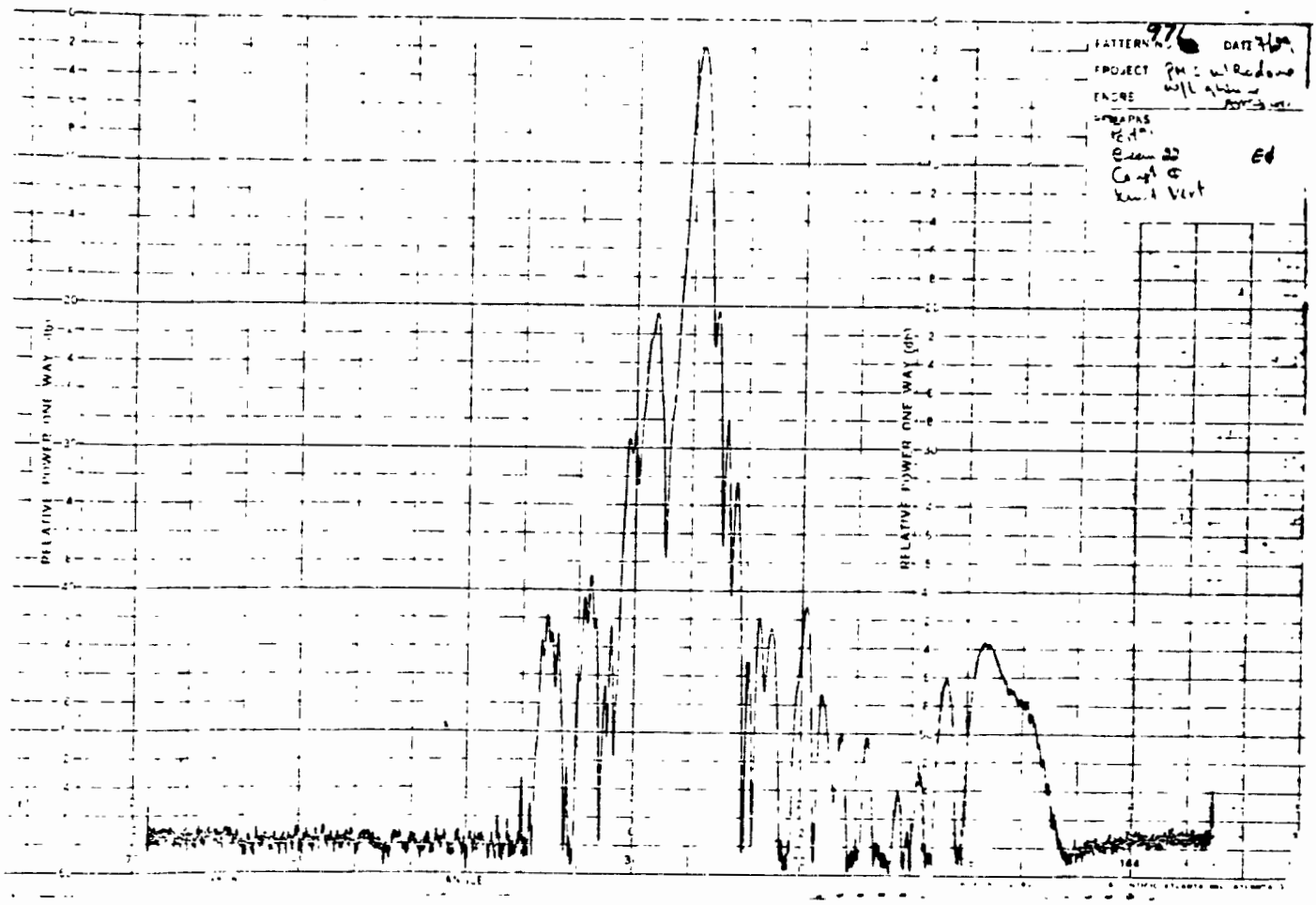

Figure 3-13. PMIS Beam 22 Horizontal Element Plane

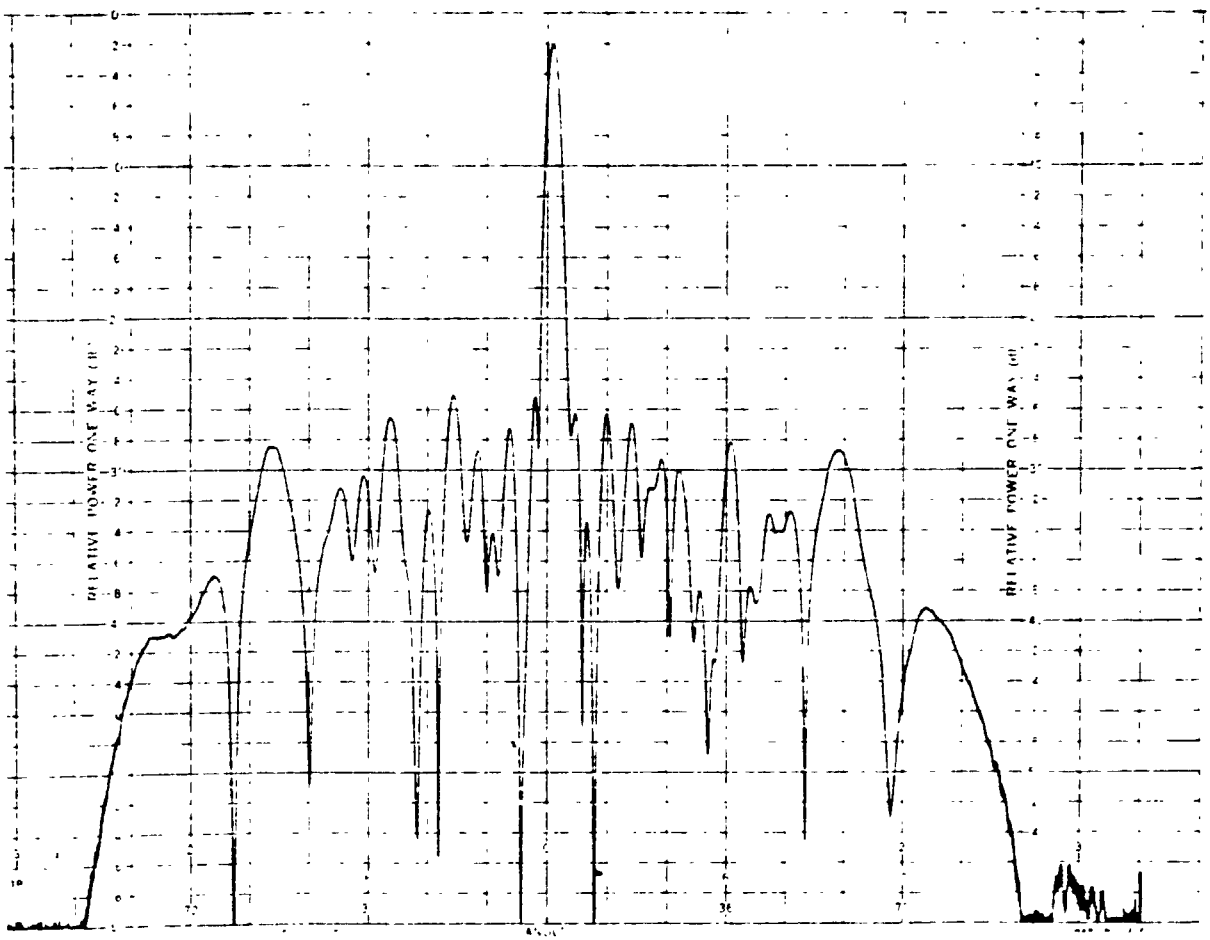

Figure 3-14. PMIS Beam 22 Horizontal Scan Plane

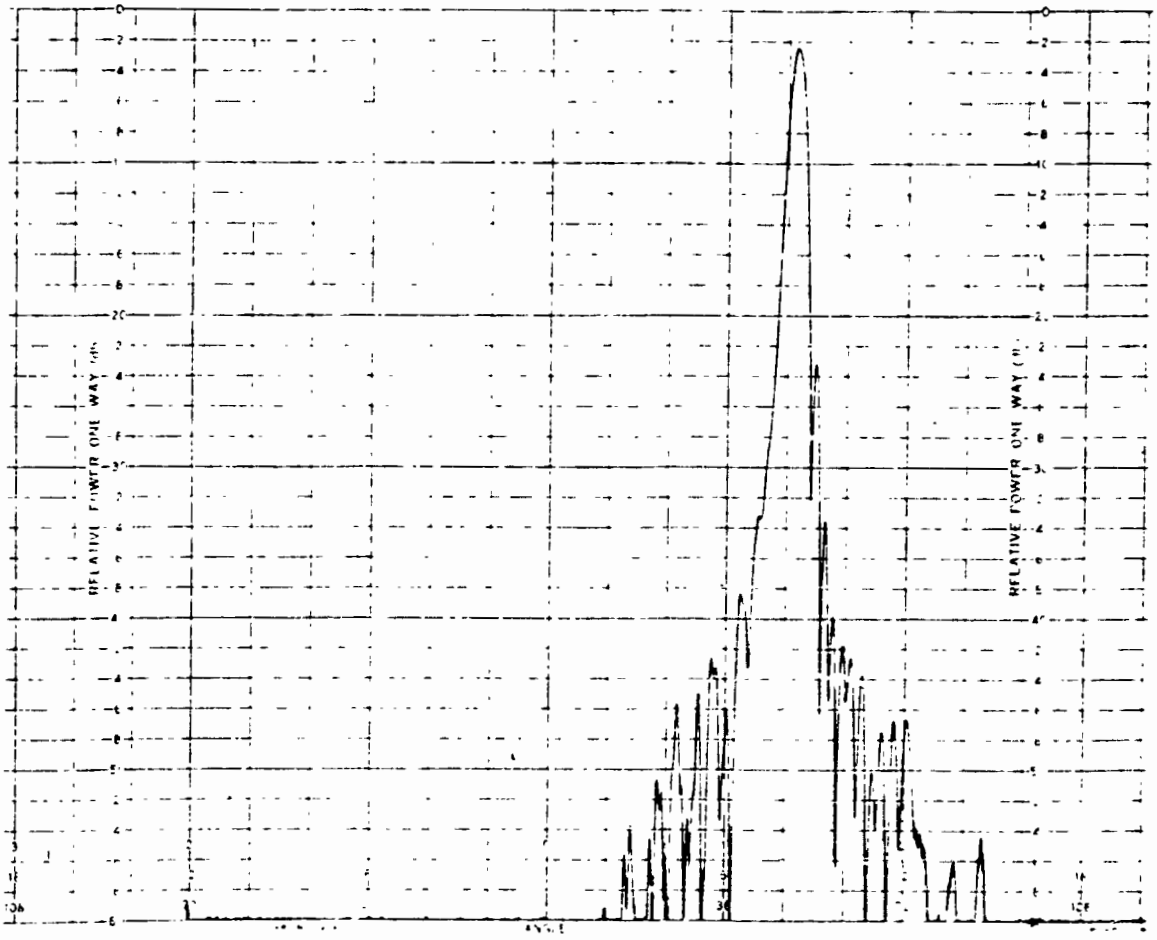

Figure 3-15. PMIS Beam 22 Vertical Element Plane

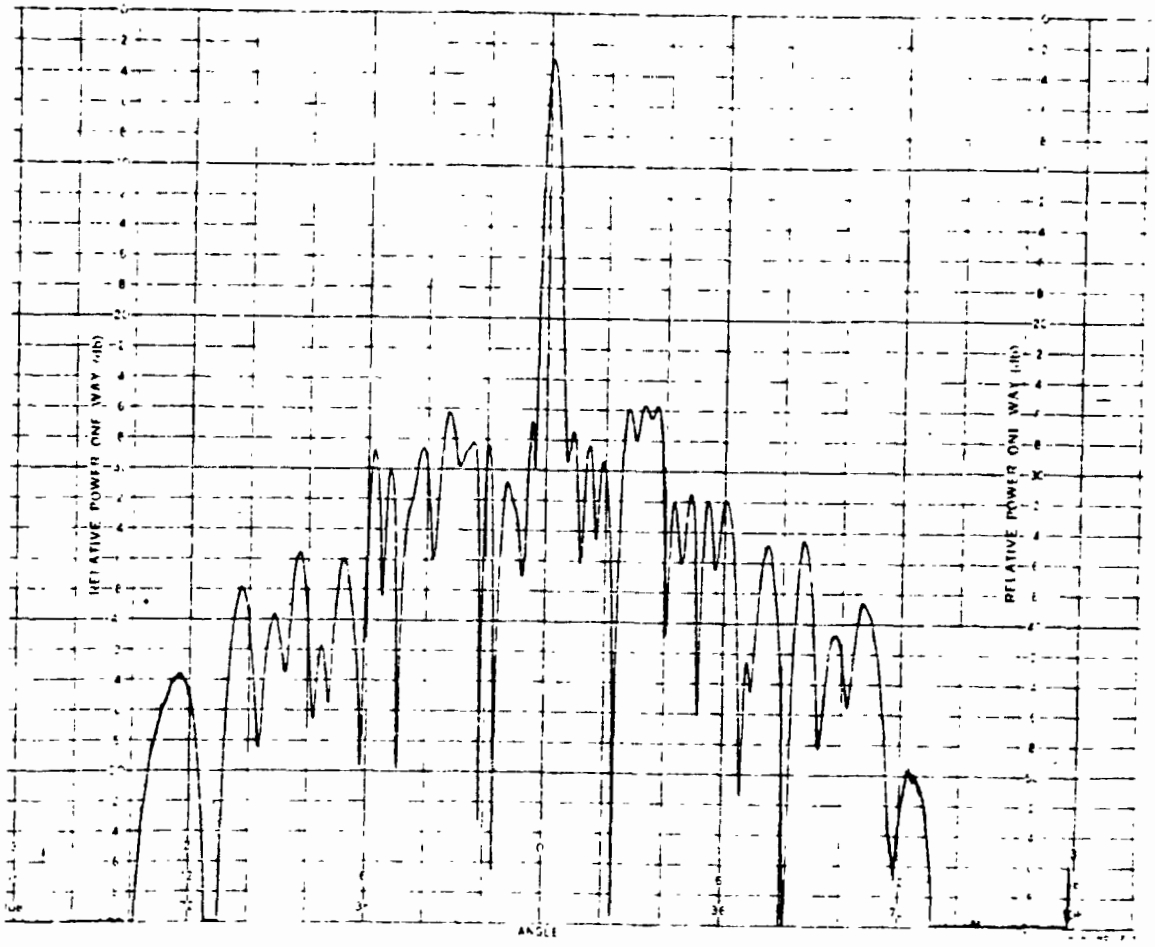

Figure 3-16. PMIS Beam 22 Vertical Scan Plane

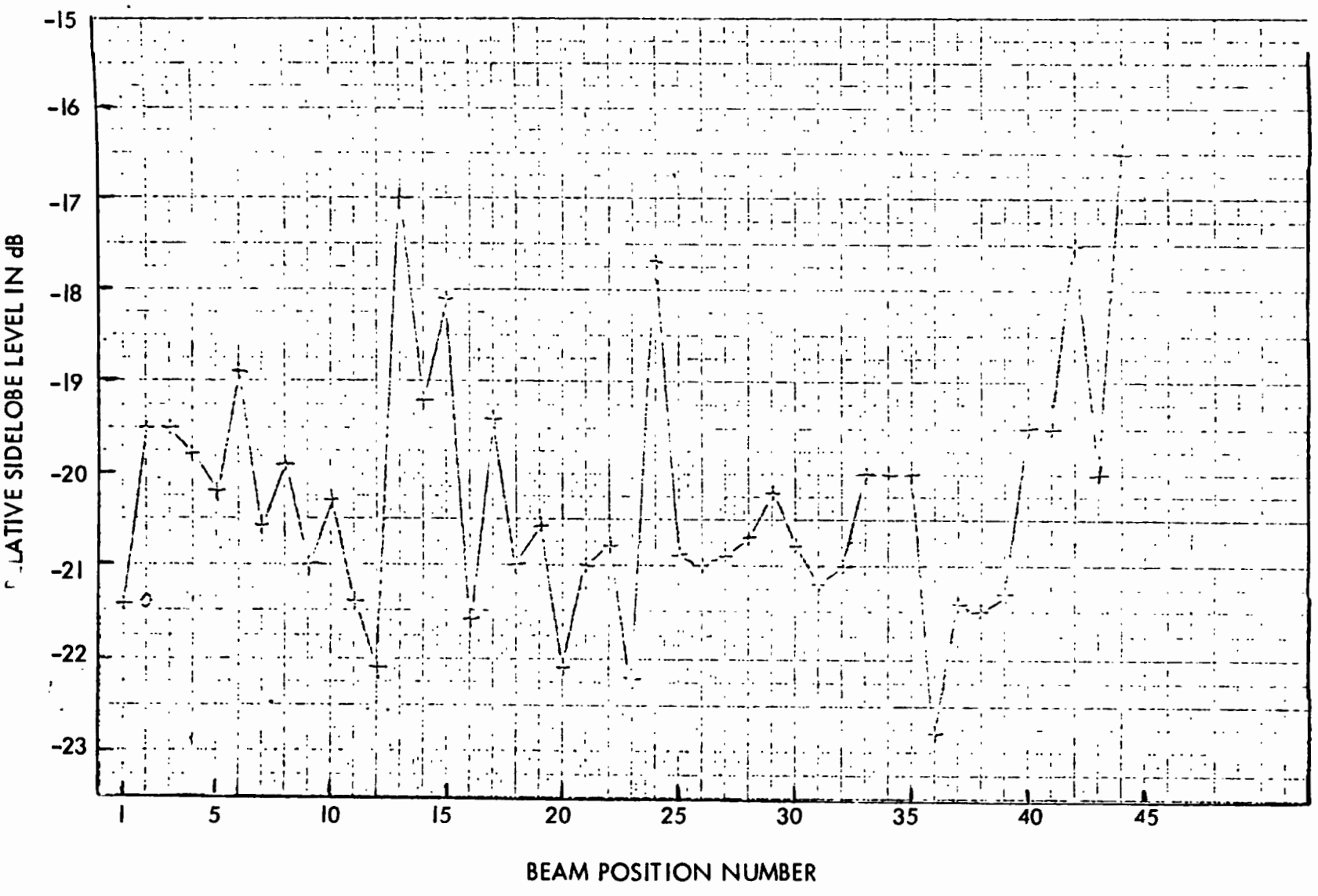

Figure 3-17. Sidelobe Level Vertical Port

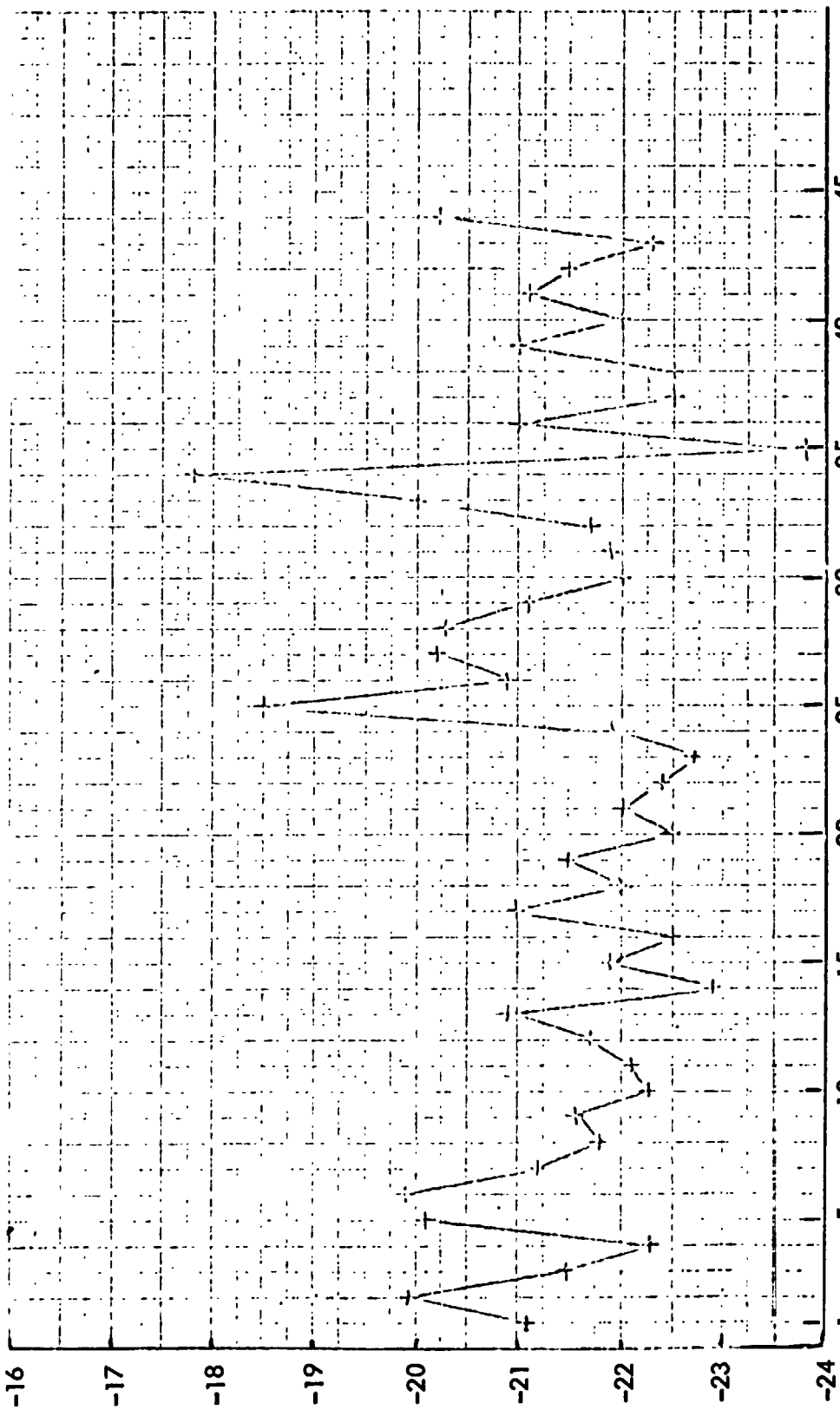

Figure 3-18. Sidelobe Level Horizontal Port

BEAM POSITION	PORT 1	PORT 2
I	83.6%	77.3%
II	86.3%	81.7%
22	78.5%	83.2%
34	78.5%	81.7%
44	90.8%	75.7%

Figure 3-19. Beam Efficiency PMIS

	ORIGINAL SPECIFICATION	ENGINEERING	PROTOFLIGHT
FREQUENCY	37 GHz	37 GHz	37 GHz
POLARIZATION	DUAL	DUAL	DUAL
APERTURE SIZE	30.45"x31.75"	30.45"x31.75"	30.45"x31.75"
RESOLUTION, BROADSIDE (3 dB BW)	1.10°x0.73°	1.17°x0.73°	1.17°x0.73°
RESOLUTION, 35° (3 dB BW)	1.10°x0.84°	0.98°x0.88°	0.98°x0.88°
BEAM TILT ANGLE	45° FROM ARRAY NORMAL	45° NOMINAL	45° NOMINAL
EARTH INCIDENCE BROADSIDE TO 35° (5° ARRAY TILT)	49° - 50.4°	49° - 50.4°	49° - 50.4°
BEAM EFFICIENCY	90% TO 31° SCAN	$\geq$60% TO $\pm 31^{\circ}$ SCAN	$\geq$86% TO $\pm 31^{\circ}$ SCAN
LOSS	< 2.4 dB	$\leq$ 2.8 dB	$\leq$ 2.8 dB
SCAN ANGLE	$\pm 35^{\circ}$	$\pm 35^{\circ}$	$\pm 35^{\circ}$

Figure 3-20. Antenna Parameters Nimbus-F

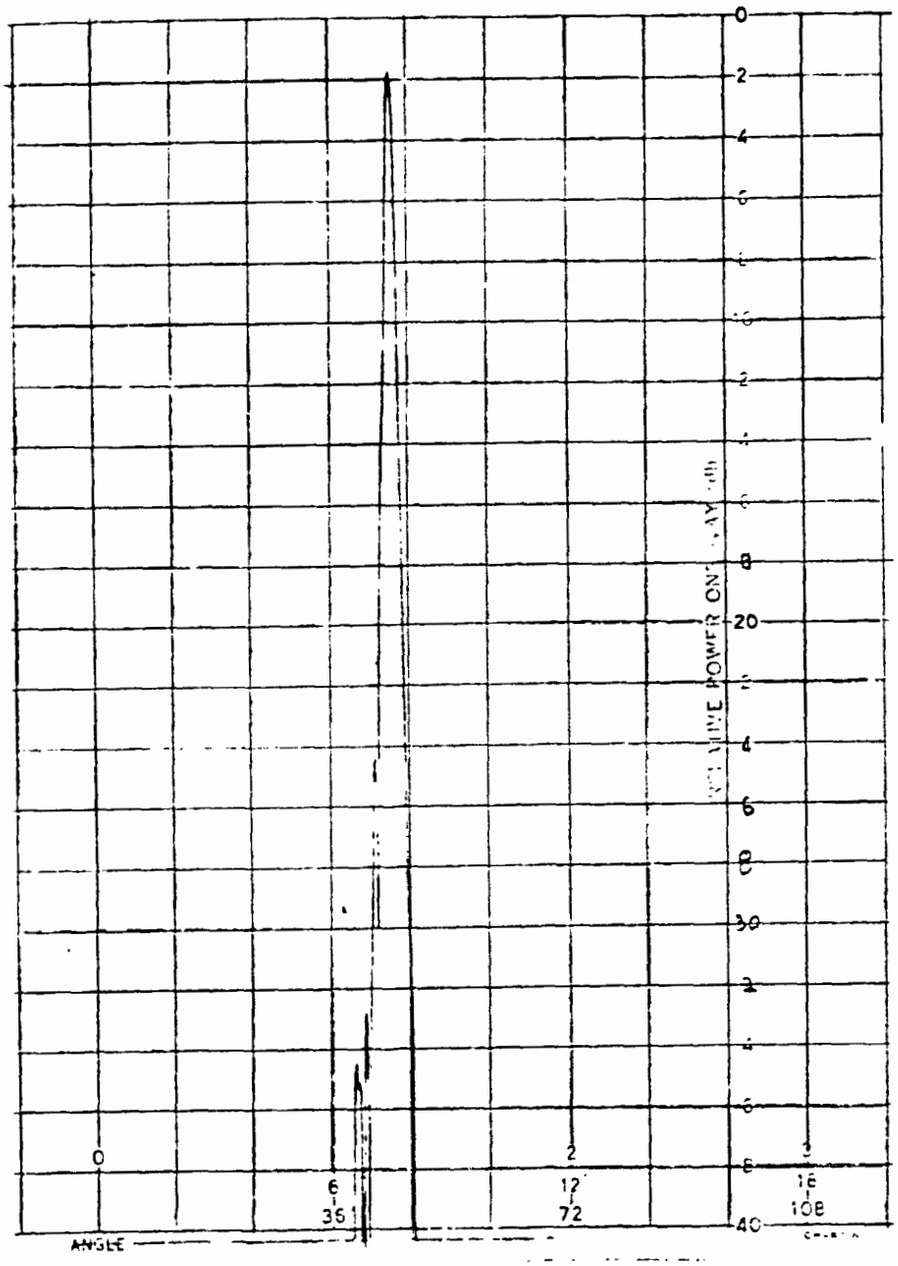

Figure 3-21. Element Plane Pattern Beam Position 36 Horizontal Polorarization Engineering Model Nimbus-F

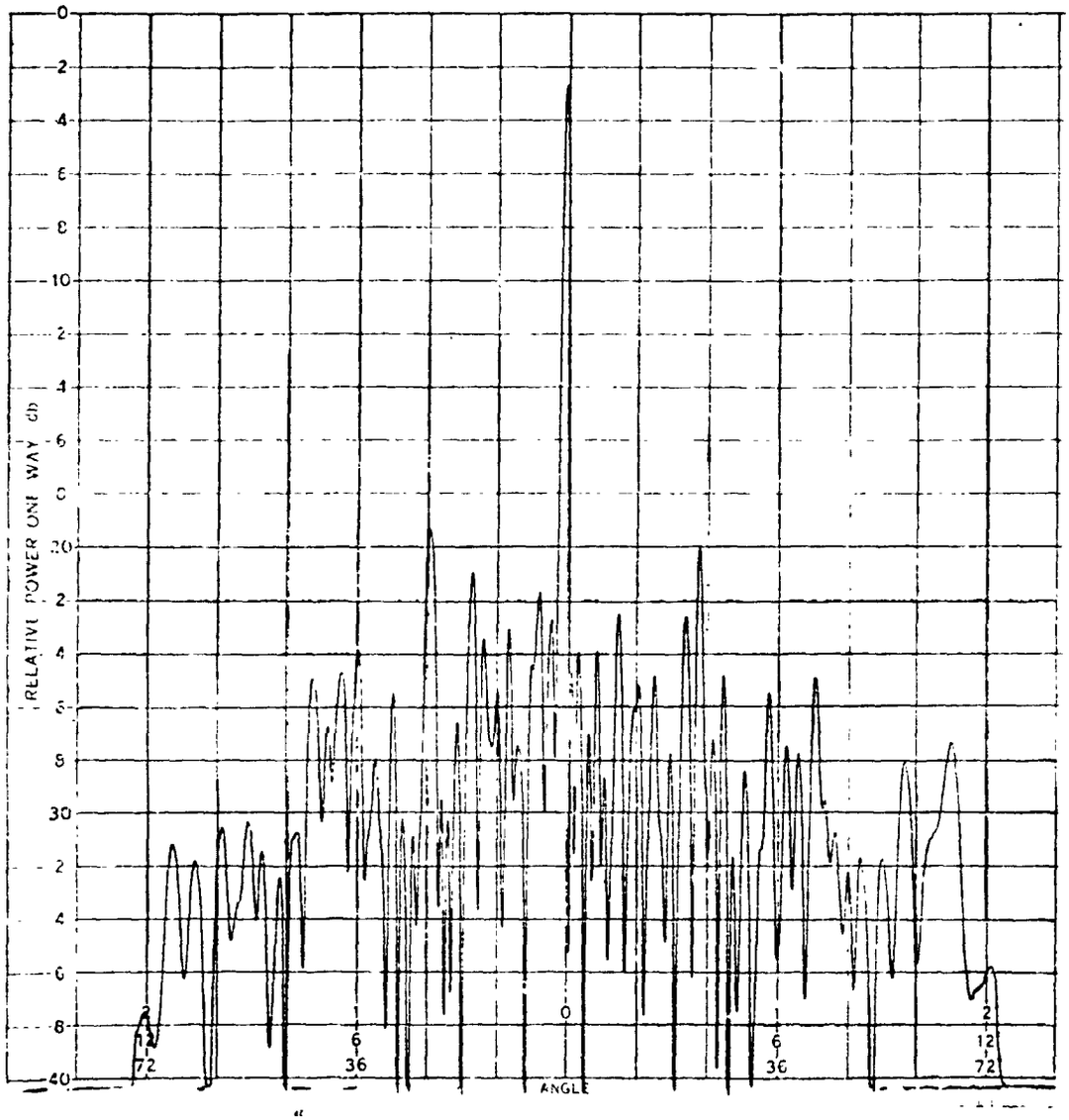

Figure 3-22. Scan Plane Pattern Beam Position 36 Horizontal Polarization Engineering Model Nimbus-F

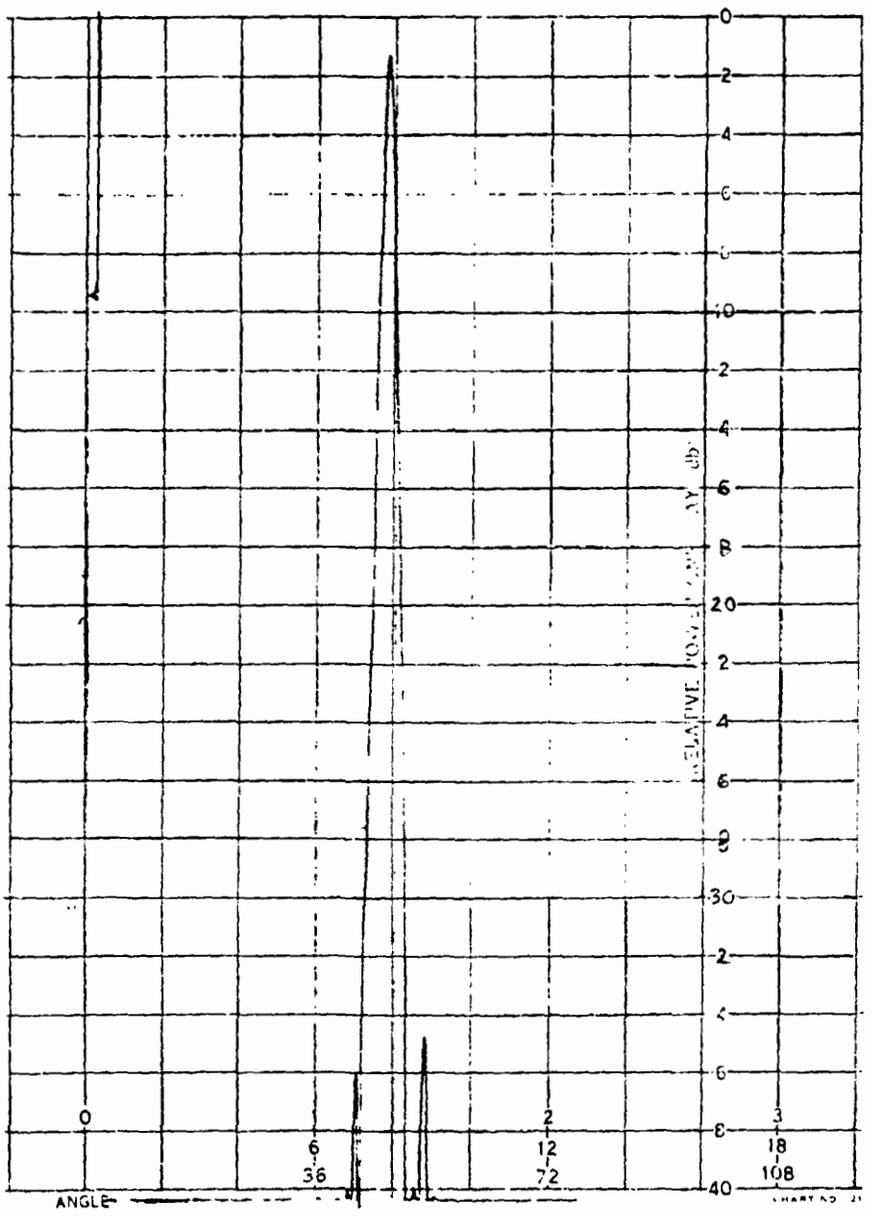

Figure 3-23. Element Plane Beam Position 36 Vertical Port Engineering Model Nimbus-F

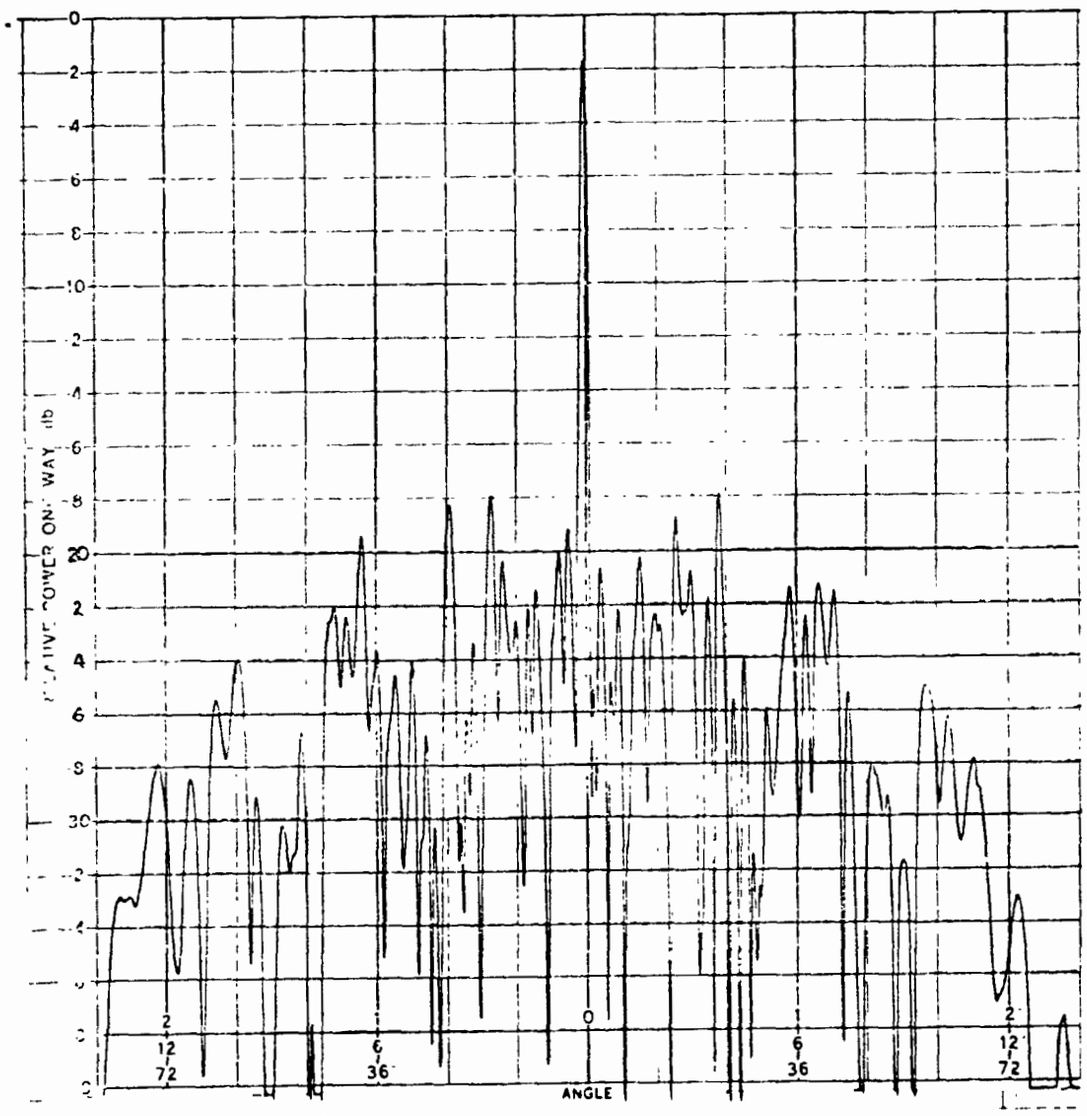

Figure 3-24. Scan Plane Pattern Beam Position 36 Vertical Polarization Engineering Model Nimbus-F

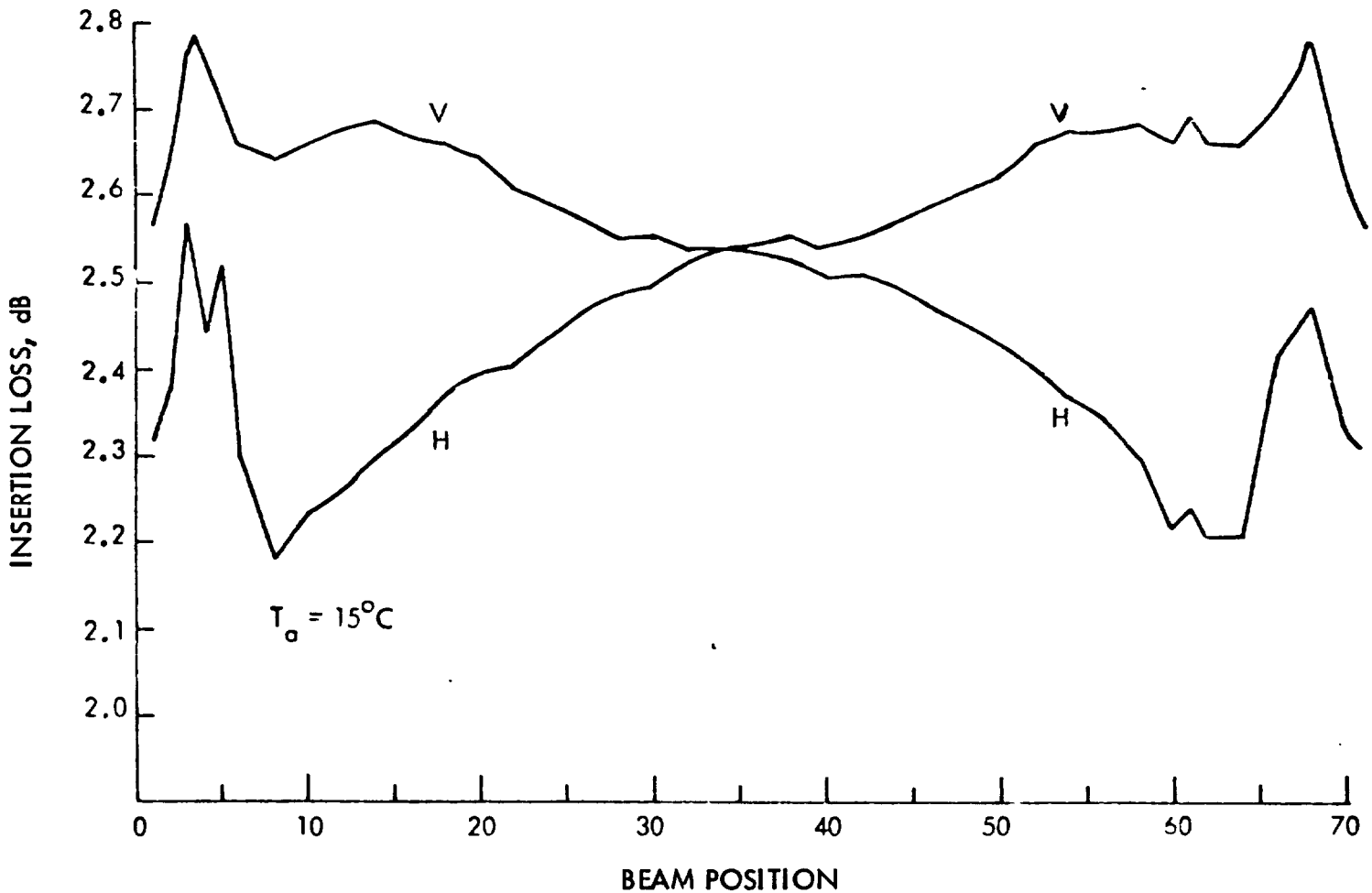

Figure 3-25. Antenna Insertion Loss Engineering Model Nimbus-F

3.5.1 SIDELOBE LEVEL

Looking at the representative antenna patterns included in the above sections, it can be seen that while the sidelobes formed in the linear array plane of the antenna show good agreement with the design level, the peak sidelobes formed in the feed plane average 10 to 15 dB above the design level. Since the feed plane incorporates ferrite phase shifters for phase control and beam scanning, it is reasonable to assume that phase errors associated with the phase shifters are responsible for the increased sidelobe levels.

A good example of the effect of phase shifters on sidelobe level is shown in Figures 3-26 and 3-27. Figure 3-26 shows the feed plane pattern of the Nimbus-F antenna before the phase shifters were inserted. The peak sidelobe level is -25 dB and the average sidelobe level is ~ -31 dB. With the phase shifters inserted, Figure 3-27, the peak sidelobe level is -20.6 dB and the average level has risen to ~ -25 dB.

While phase errors may well account for most of this increase in sidelobe level, amplitude errors associated with the phase shifters can also have an effect. Indeed, measurements taken on phase shifters over the 360 degree range of phase shift have shown up to 0.3 dB variation in insertion loss. However, for the example shown in Figure 3-27 the beam is in its quiescent position, i.e., the position of the beam when all phase shifters are set to zero degrees phase shift for comparison with the no phase shifter case, Figure 3-26. Thus, in effect, the amplitude errors associated with the phase shifters should be at a minimum for this example.

Referring again to the "no phase shifter" case of Figure 3-26, the average sidelobe level of ~ -31 dB is still significantly above the design level of -35 dB. This increase in sidelobe level can be attributed to two factors, namely mechanical tolerance errors and mutual coupling between waveguide arrays. Since it has been demonstrated that mechanical tolerances can be held to within $\pm$.001 inches, or .0063 λ at 37 GHz,

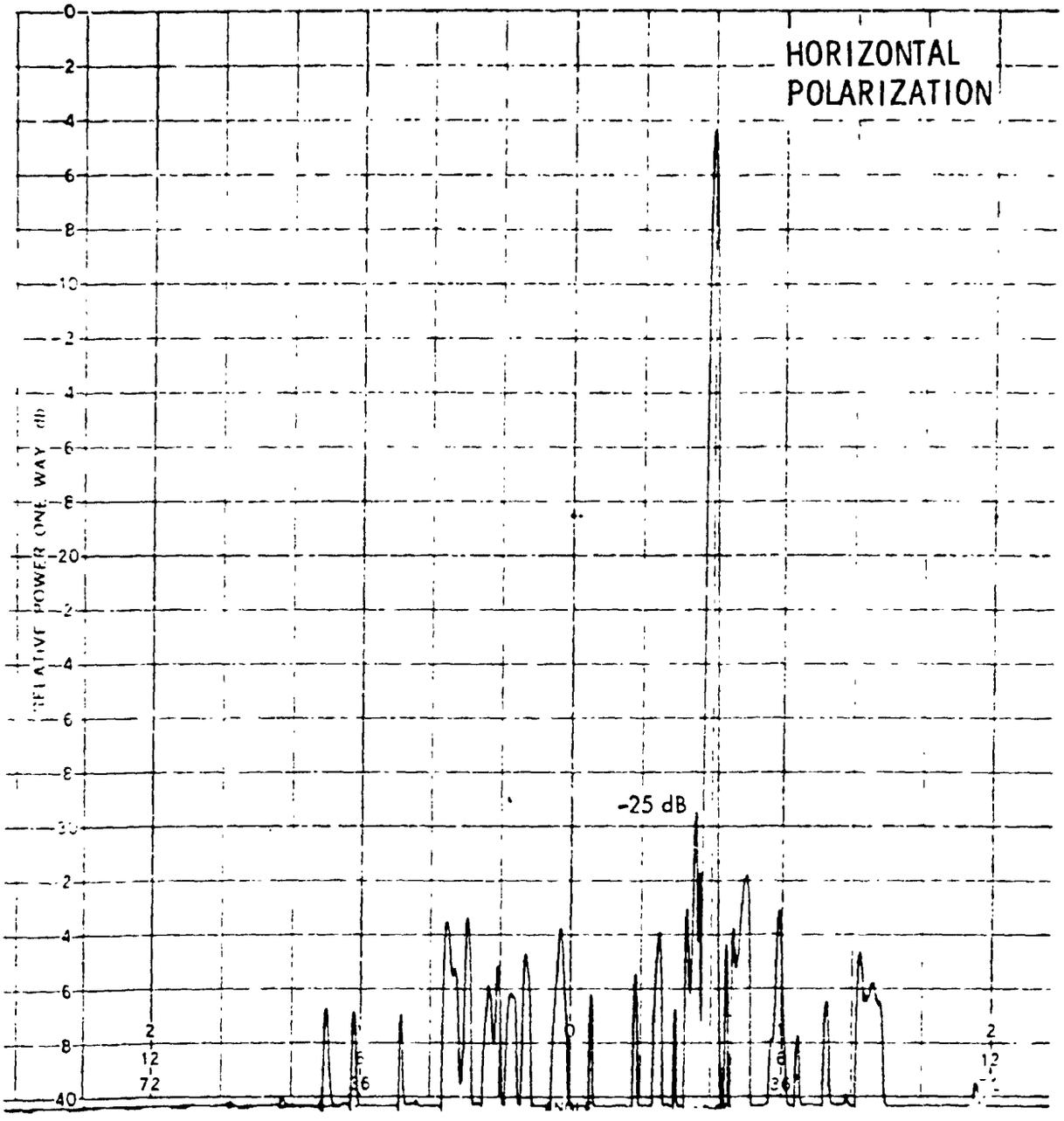

Figure 3-26. Antenna Scan Plane Pattern No Phase Shifters Prototype Model Nimbus F

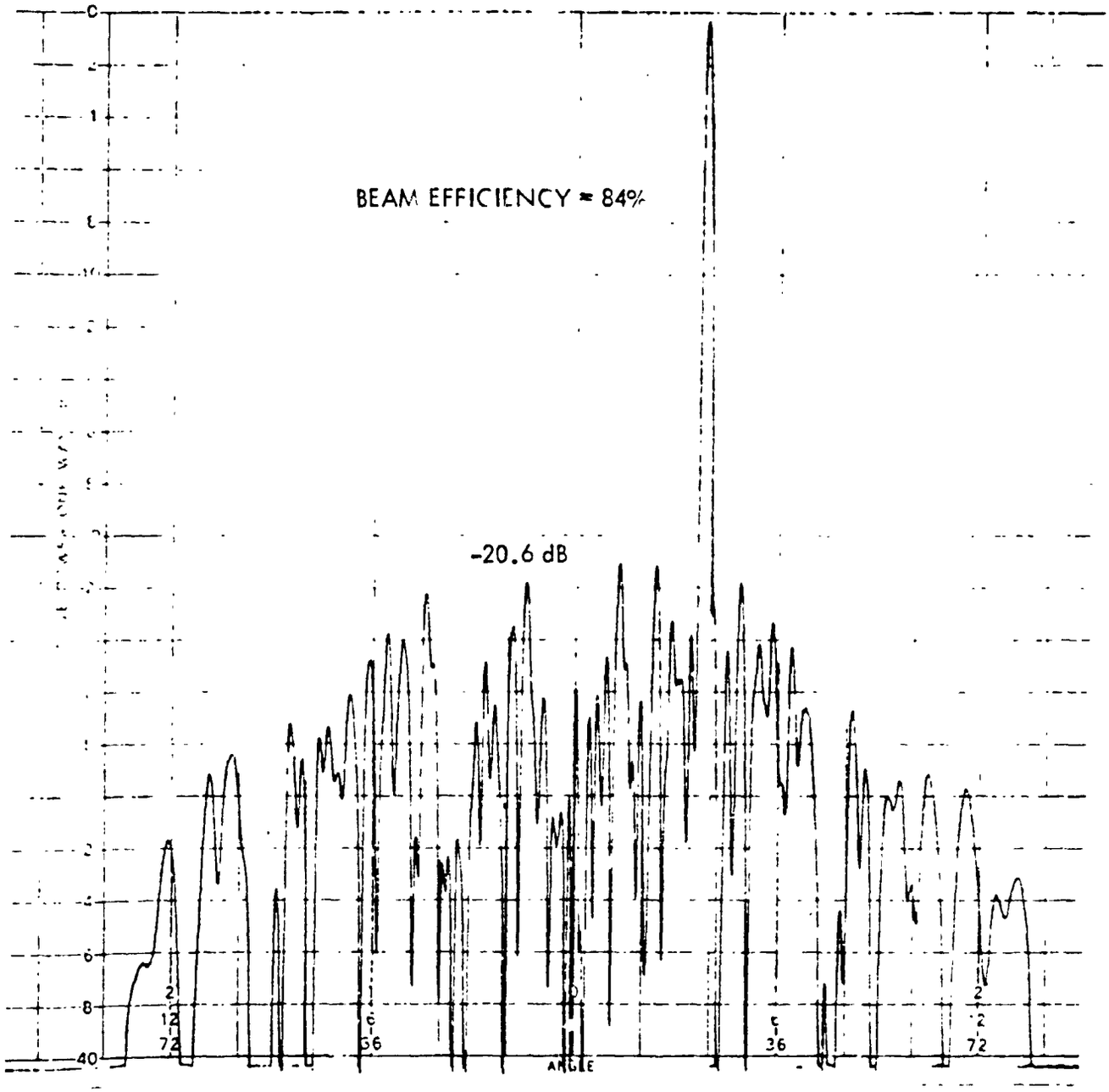

Figure 3-27. Antenna Patterns After Phase Shifters Prototype Model Nimbus F

it appears likely that the sidelobe level increase is due primarily to mutual coupling effects.

It can be concluded from the above discussions that the measured sidelobe level of a phased array in comparison with the design level represents an indication of the combined effects of mechanical and electrical tolerance errors incorporated into the final antenna system. Each of the mechanisms which combine to produce these errors along with other problem areas will be discussed in the following sections.

3.5.2 PHASE SHIFTERS

The phase shifter used in all of the above antennas is the Reggia-Spencer non-reciprocal analog ferrite phase shifter. This phase shifter consists of a section of rectangular waveguide with a cylindrical ferrite rod held in place in the center of the waveguide by a pair of dielectric supports. Each support also acts as an impedance transformer to match the ferrite rod to the waveguide. A coil is wound around the waveguide and provides the longitudinal magnetic field required to drive the device.

The partially ferrite filled waveguide behaves like a dielectric loaded waveguide where the RF energy is concentrated around the ferrite rod. The variation of the longitudinal magnetic field changes the effective permeability of the ferrite thereby producing a phase shift of the RF energy propagating through the device.

Ideally, the phase shifter should be capable of being repeatably reset to exactly the desired amount of phase shift and should have little or no insertion loss (at worst the insertion loss should be constant with changing phase shift). The Reggia-Spencer phase shifter is, of course, not an ideal device. It has been found that the repeatability of the device is in part dependent on the frequency of operation and type of ferrite material used and also on the method of recycling the device between phase changes.

Ferrite devices are also affected to some degree by thermal changes. In the ferrite phase shifter, a temperature change will produce a corresponding change in the absolute phase shift through the device. By operating the phase shifters over the linear portions of their phase curves the effect of thermal variations can be minimized. This is true if the phase shifters in any array are all affected uniformly by the temperature change, however, if a thermal gradient exists over the feed array, errors over the phase front can become quite significant.

The Reggia-Spencer phase shifter is, then, a source of both random phase error and random amplitude error. The degree to which these errors will affect the sidelobe level of the array is dependent on their magnitude. Repeatability measurements of the phase shifters used in the above arrays have shown typically that they can be reset to within 6 degrees RMS of the required phase shift. Also over a 360 degree phase shift range, the insertion loss varies in general about 0.3 dB.

3.5.3 MUTUAL COUPLING

Mutual coupling refers to the fact that energy radiated from one radiating element is capable of being coupled into the adjacent radiating elements. This effect produces changes in effective impedance of the radiating elements thus distorting the intended amplitude distributions along the array. In the linear slotted waveguide array, mutual coupling between slots along the waveguide is usually accounted for by the method in which slot impedance data is measured. However, mutual coupling from waveguide to waveguide is generally more difficult to handle requiring measurements to be made on several waveguides simultaneously with some sort of feed array. Fortunately, mutual coupling between waveguides with radiating slots cut into the narrow wall of the waveguide as in the Nimbus-E antenna, is relatively minor having little effect on the radiation patterns.

The square waveguide array with crossed slot radiators, as in the Nimbus-F antenna, presented more of a problem with surface currents propagating over the surface of the array coupling one waveguide with another. The mutual coupling in this case was reduced by adjusting the height of the ground plane relative to the radiating surface and effectively "choking" off the surface currents.

3.5.4 INSERTION LOSS

Insertion loss of an array as discussed in Section 3.7 is a parameter that can be determined quite accurately before the antenna is fabricated and in fact during the design phase if waveguide and phase shifter losses are known accurately and if it is assumed that mutual coupling between waveguides will have a negligible effect on the waveguide power-to-the-load parameter of the linear array. Generally, the insertion loss of an array is determined largely by the transmission line loss of the array elements and by the phase shifter loss. However, for the dual polarized square waveguide arrays the power-to-the-load parameter becomes significant since typically 10 percent of the input power is dissipated in the load.

Thus, it is important to note that when specifying the loss of a phased array system, consideration should be given to the size of the array, the type of transmission line making up the array, and the loss characteristics of the devices used to scan the array. These numbers will set a realistic limit on the level at which the overall loss can be held.

3.5.5 CROSS POLARIZATION

The antenna designed for radiometric applications is typically linearly polarized and in some instances is dual linearly polarized. In both cases, however,

any cross polarized energy coupled to the antenna output port represents an error signal. For this reason the antenna's ability to suppress cross polarized lobes is an important parameter.

In the Nimbus-D and Nimbus-E type of array, the orientation of the radiating slot is responsible for the radiation of cross polarized energy. The electric field vector across inclined slots, as shown below, are rotated with respect to the plane of principal polarization in such a manner that a space quadrature component of polarization is present in the array pattern. The intensity of the cross polarized lobes depends on the magnitude of slot inclination. The position of the cross polarized lobes is of course a function of the relative phasing of the cross polarized field vectors from slot to slot.

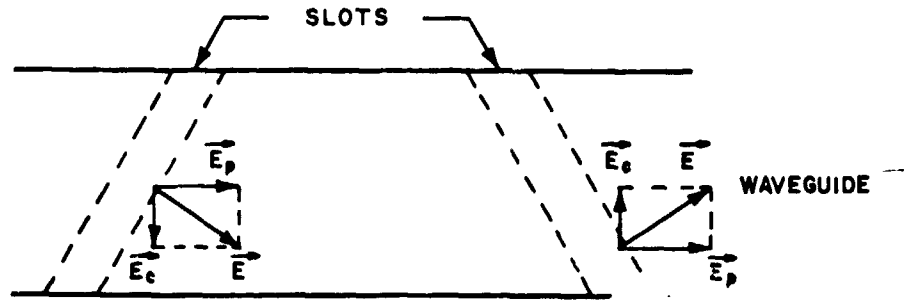

It is apparent from the above drawing that the principally polarized electric field vectors, $\vec{E}_p$, will add in phase when the slots are spaced $\lambda g/2$ apart while the cross polarized electric field vectors $\vec{E}_c$ will be 180 degrees out of phase. For this configuration the cross polarized lobes will form at approximately ± 45 degrees from the array broadside. If the linear array elements are fed by a feed array whose slots are oriented in a similar manner as in the Nimbus-D antenna, then the cross polarized lobes will form in the same plane as the principal lobe and will scan with the principal lobe.

In the Nimbus-E antenna the slots in the feed array are all inclined in the same direction but the relative inclination of slots from waveguide-to-waveguide is

reversed. This configuration produces cross polarized lobes positioned as shown in Figure 3-28. The obvious advantage of this configuration is that for a portion of the scan range, i.e., near broadside, the cross polarized lobes are formed outside of the visible region.

The crossed slots of the PMIS and Nimbus-F type of antennas are oriented perpendicular to the planes of principal polarization, hence, theoretically, producing no cross polarized radiation. Since the beam is scanned conically, it is apparent that the transverse arm of the crossed slot will not remain perpendicular to the plane of principal polarization as the beam is scanned off broadside, thus producing a cross polarized lobe, which increases in magnitude as the beam is scanned. This effect is shown for the PMIS antenna in Figure 3-29.

3.5.6 MECHANICAL TOLERANCES

Mechanical tolerances for arrays of this type can be grouped into the following categories (1) tolerances on the raw waveguide stock, (2) slot dimensional tolerances, (3) array assembly tolerances, i.e., the spacing of the linear array waveguide and the flatness of the radiating surface), and (4) tolerances on related components (i.e., phase shifters, connectors, bends, etc.)

In general, standard size waveguide is fabricated to meet the military specification, MIL-W-85C, which provides sufficient control on waveguide tolerances. It has been found, however, that square waveguide purchased for applications such as the PMIS and Nimbus-F antennas must be rigidly specified with regard to the "sqareness" or perpendicularity of the inner waveguide walls. This is due to the requirement for mode isolation within the waveguide which should be at least -40 dB. In one batch of waveguide ordered for the Nimbus-F antenna, mode isolations varied from -40 dB to -9 dB and at least 50 percent of the waveguide had to be rejected.

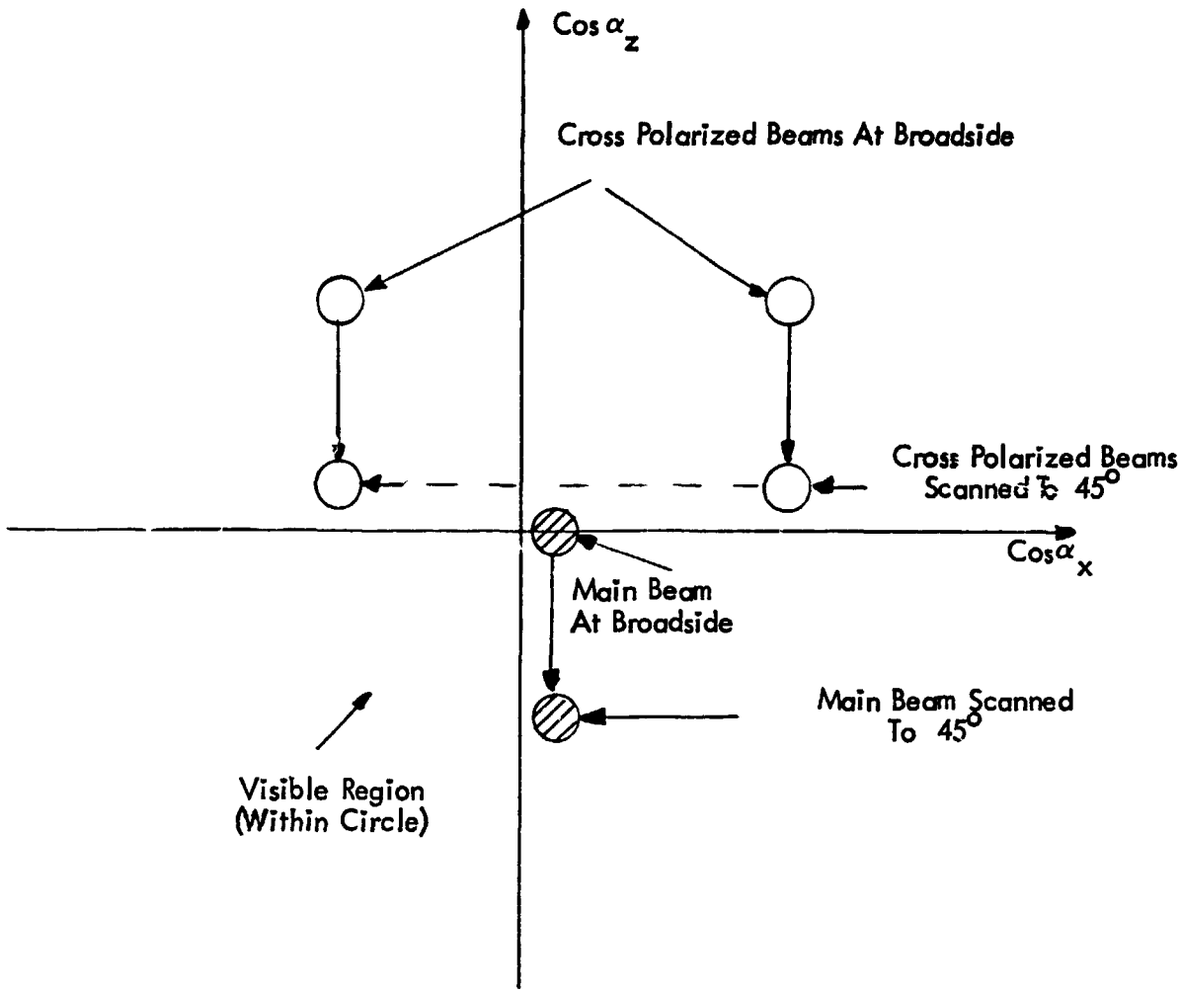

Figure 3-28. Cross Polarized Lobes Location And Movement With Scan Nimbus-E

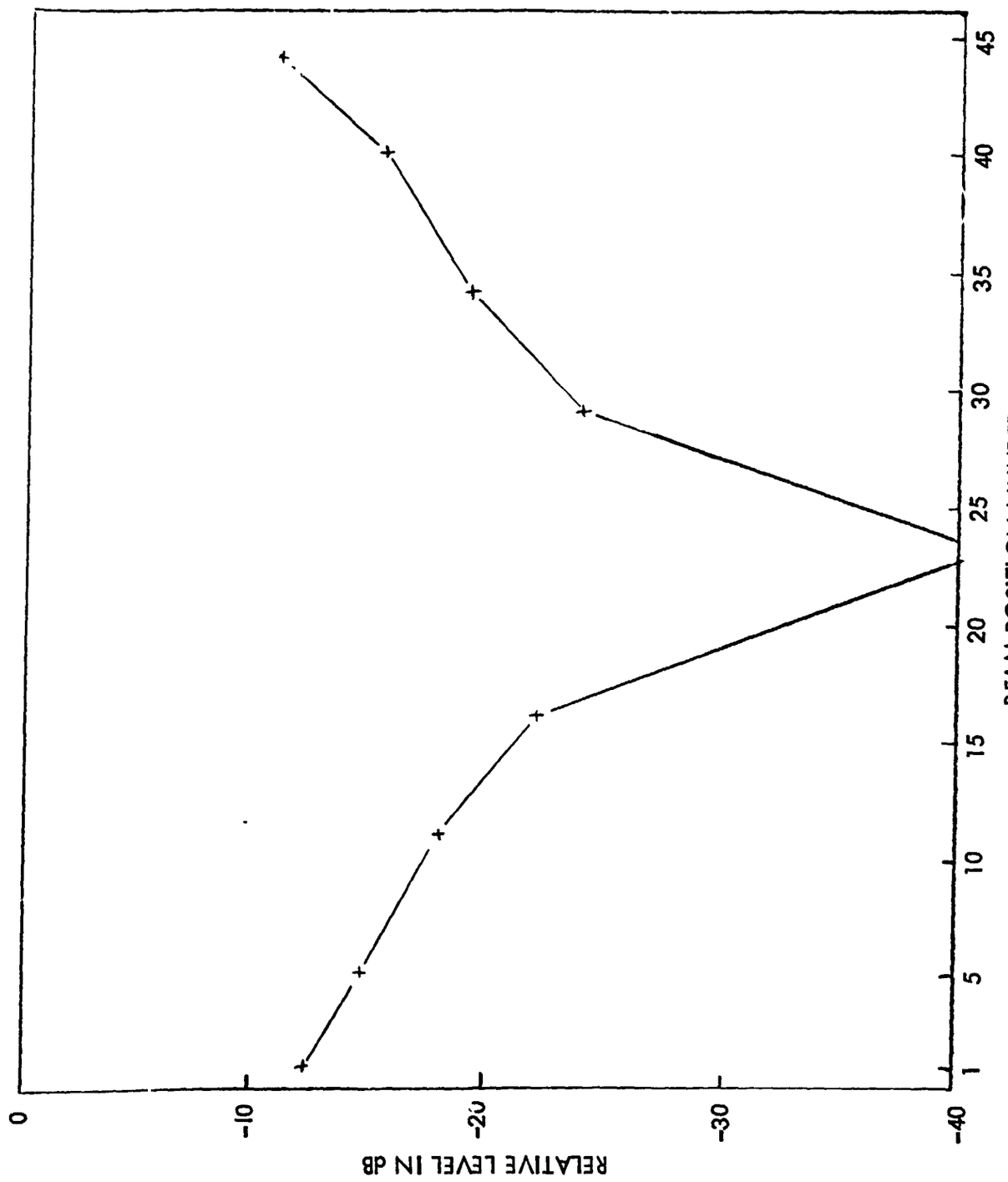

Figure 3-29. PMIS Cross Polarization Horizontal Port

Slot dimensional tolerances are very critical in a phased array since both interelement phasing and the accuracy of the amplitude distribution are determined by the slot characteristics. It has been found, however, in the fabrication of the above antennas that by using precise tooling fixtures and careful machining techniques, slot dimensions and spacings can be held to a non-accumulative tolerance of $\pm$0.001 inch.

Array assembly tolerances can also be controlled adequately through the use of precision tooling fixtures. Waveguide-to-waveguide spacing can be held to within $\pm$.001 inch and array flatness to within $\pm$.002 inch in the arrays discussed above.

With larger arrays the flatness will be the most difficult dimension to maintain.

3.5.7 THERMAL TOLERANCES

Thermal tolerances affect principally the operation of the ferrite phase shifters. An attempt is made to keep this effect minimal by operating the phase shifters in their linear phase region, thereby producing a uniform phase deviation over the entire array with change in temperature. If all the phase shifters produce the same phase shift in response to a change in temperature, then the interelement phase difference will not change, hence there will be little or no effect on the antenna patterns.

It was found for the phase shifters of the PMIS antenna that temperature effects did produce a noticeable change in sidelobe levels. This effect was minimized by adding individual heating elements to each phase shifter which were thermostatically controlled to keep all of the phase shifters at a uniform temperature of approximately 20°C.

3.5.8 BEAM EFFICIENCY

The beam efficiency of an antenna is a parameter which in effect provides a measure of the antenna's ability to discriminate between the desired signal (i.e., the main beam) and the unwanted signals, i.e., sidelobes and cross polarized lobes. Thus, the beam efficiencies of the above four antenna systems is a good indication of the extent to which the problem areas discussed previously have affected the individual antenna performance.

Figure 3-30 presents again the beam efficiency curves derived in Section 2.5 plotted as a function of average sidelobe level and beamwidth. Superimposed on these curves are vertical bars representing the measured beam efficiencies of the four antenna systems. The range of average sidelobe level encompassed by each of the bars shows good correlation with the measured average sidelobe levels.

The relatively poor beam efficiencies of the PMIS antenna system are indicative of the phase shifter problems, i.e., poor repeatability and thermal sensitivity, encountered during the design and development stages. The Nimbus-F engineering model had both phase shifter problems and fabrication problems resulting in the low beam efficiencies shown in Figure 3-30. Elimination of these problems resulted in the significant increase in beam efficiency shown for the Nimbus-F flight model antenna.

3.6 OTHER ARRAY IMAGERS

The discussion of state-of-the-art phased array antennas has emphasized Aerojet-General developed antennas because more data was available especially in the area pertaining to design and development problems. Two other radiometric imager antennas which use entirely different methods of beam forming and/or beam scanning will be briefly described.

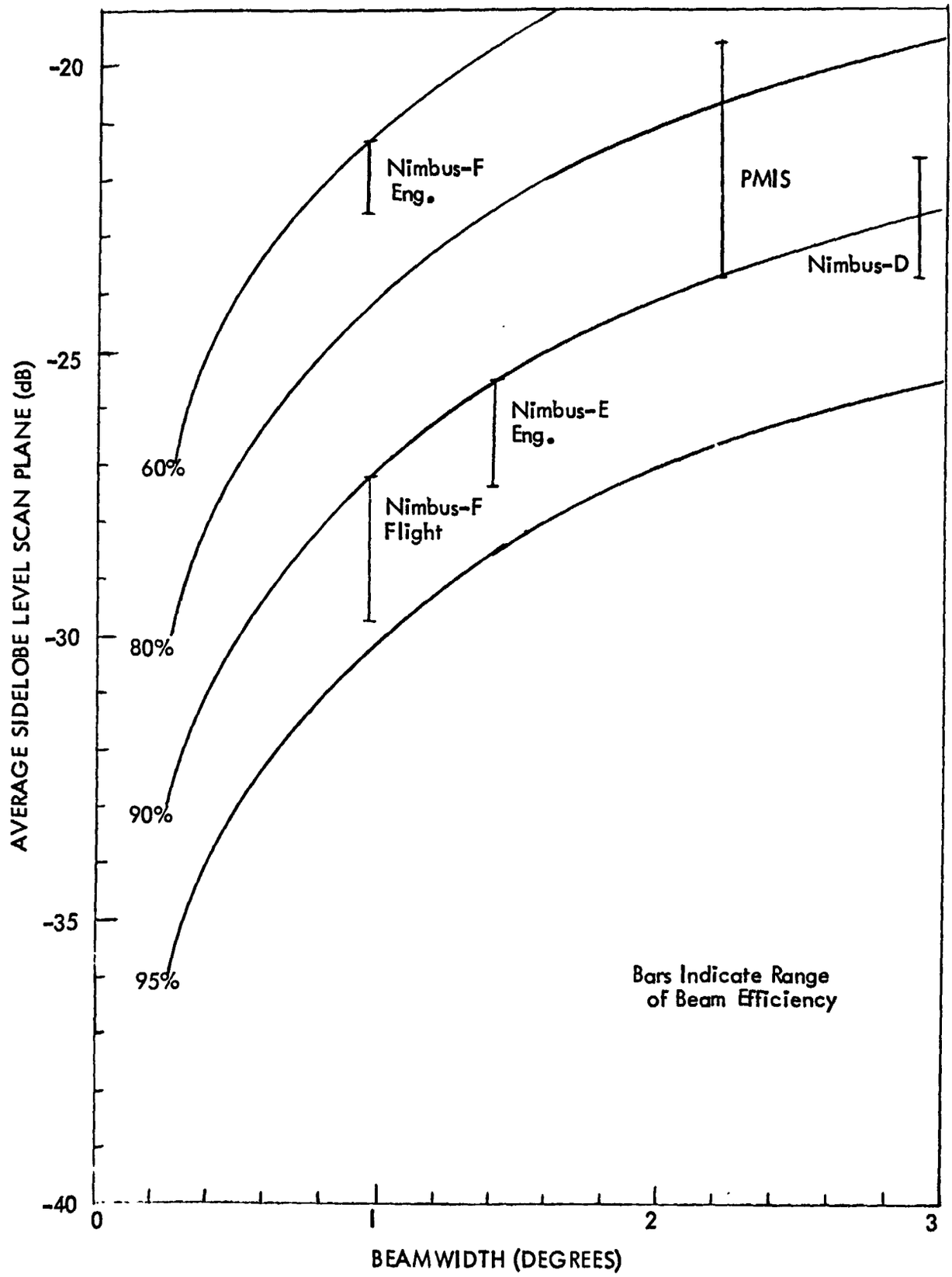

Figure 3-30. Antenna Beam Efficiencies

3.6.1 FREQUENCY SCANNED ARRAY - NORTH AMERICAN

The North American frequency scanned array operates at X-band and utilizes a four foot aperture to form a main beam approximately one degree wide at the half power points. The array is capable of scanning the beam approximately ±45 degrees. The beam scans with frequency at about one degree per 1/2 percent frequency change. The known parameters of the array are tabulated in Figure 3-31.

3.6.2 LENS TYPE PHASED ARRAY - RADIATION, INC.

The lens type phased array manufactured by Radiation, Inc., utilizes a parallel plate metallic lens to feed a two dimensional array of slotted waveguide radiators. The lens is designed so that when a source is placed on the focal arc of the lens, the energy will form a plane phase front across the array aperture. The linear phase progression across the phase front is determined by the location of the source on the focal arc. Movement of the source (or feed horn) around the focal arc causes the beam to scan. A picture of the antenna along with a schematic diagram and typical radiation pattern is shown in Figure 3-32. The array parameters are tabulated in Figure 3-33.

MANUFACTURER	NORTH AMERICAN
WAVELENGTH	2.5 - 4.2 cm
SIZE	4'X4'
SCAN	45°
SCAN IN DIRECTION OF ELEMENTS	
LENS TO COLLECT ELEMENTS	
ARRAY ELEMENTS	Cross Track
1/2% FREQUENCY ≈1° SCAN	
ELEMENTS "HUNNY RADIATOR"	

Figure 3-31. Frequency Scanned Array

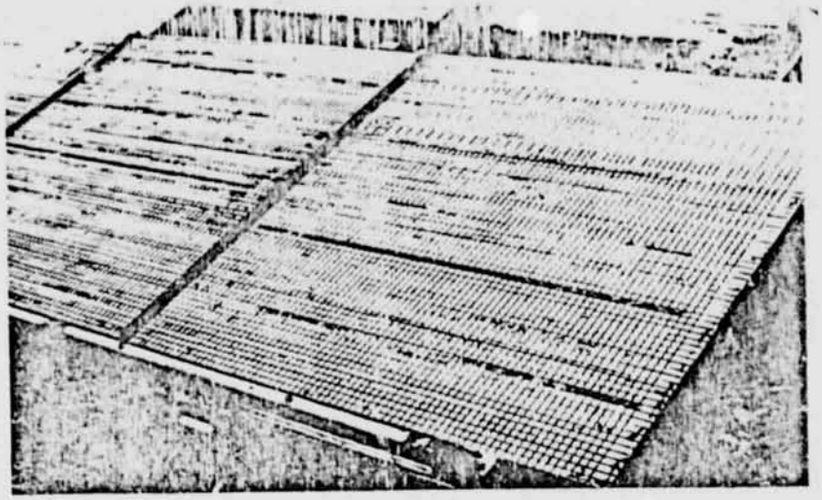

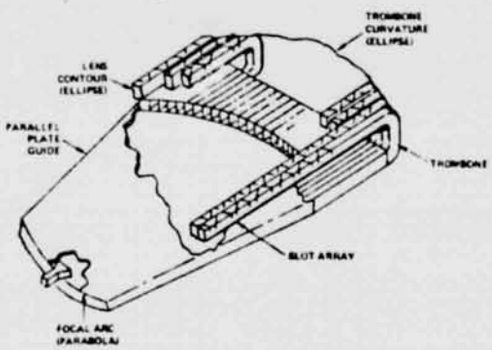

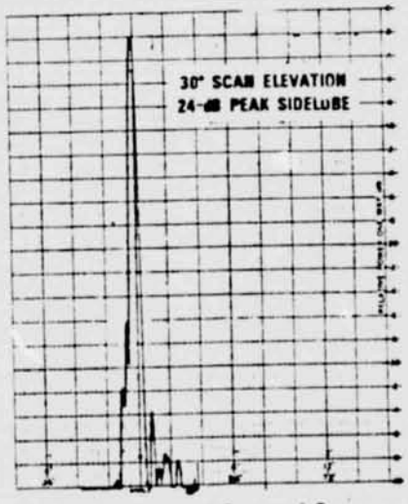

Figure 3-32. Lens Type Phased Array

MANUFACTURER	RADIATION, INC.
WAVELENGTH	4.2 cm
SIZE	1.5 X 4.5 Meters
WEIGHT	120 Kgms
SCAN	$\pm 15^{o}$
TOTAL LOSS	1.0 dB
TERMINATION LOSS	0.5 dB
SIDELOBE (AVE) BEAM SQUINT	23 dB
TAPER	$(\cos)^2$ On Pedestal
SINGLE BEAM	
$\frac{L}{\lambda}$	36 X 107

Figure 3-33. Lens Type Phased Array

4.0 PERFORMANCE CHARACTERISTICS AND POTENTIAL PROBLEM AREAS TO BE EXPECTED WITH INCREASE IN SIZE OF ARRAY ANTENNAS

The size of a phased array aperture controls the beamwidth of the array and hence the resolution of the imaging system. For most systems applications the maximum resolution consistent with a physically realizable antenna is desired. To obtain the optimum system, it is necessary to understand not only the relationship of aperture size to beamwidth, but also the effect of aperture size on such design parameters as sidelobe level, accuracy, insertion loss (aperture efficiency) and beam efficiency.

4.1 BEAMWIDTH VERSUS APERTURE SIZE

As shown in Section 2.4 the beamwidth of an antenna for a given aperture size is dependent on the amplitude distribution imposed on the array aperture. The relationship between beamwidth and aperture size for various distributions was shown in Figure 2-10.

The beamwidth versus aperture size shown in Figure 4-1 is plotted for the various wavelengths of interest. A Taylor amplitude distribution with peak sidelobe level of -40 dB is assumed in each case. The maximum aperture size plotted is 20 meters consistent with the physical size limitations of the space vehicle.

4.2 SIDELOBE LEVEL VERSUS APERTURE SIZE

Since the peak sidelobe level selected for a given amplitude distribution and a given aperture length affects the beamwidth of the array, it is possible to relate aperture length to sidelobe level. Also since beam efficiency is related to average sidelobe level and beamwidth, it follows that beam efficiency and average sidelobe level can be related to aperture length. In Figure 4-2, average sidelobe

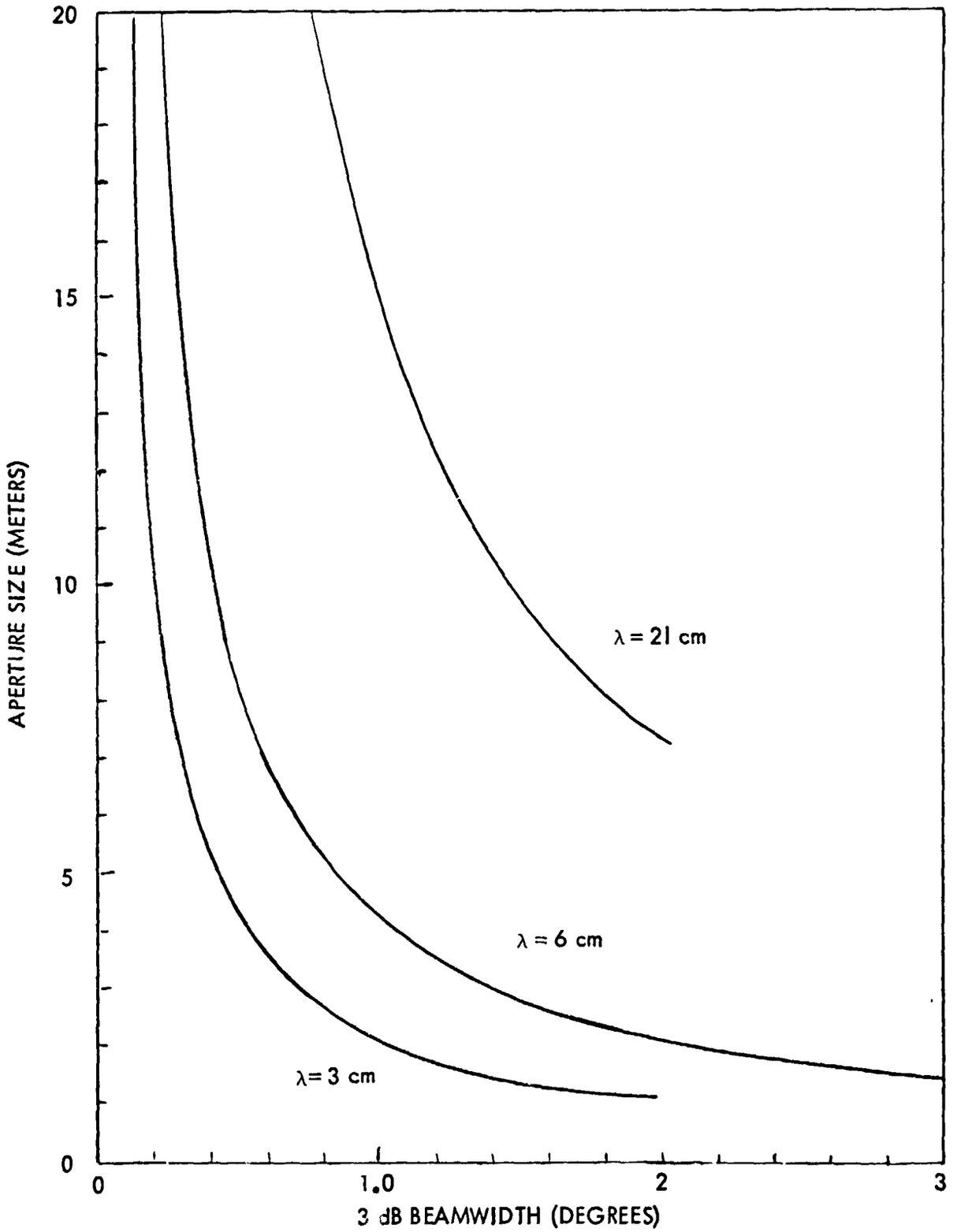

Figure 4-1. Aperture Size Versus Beamwidth

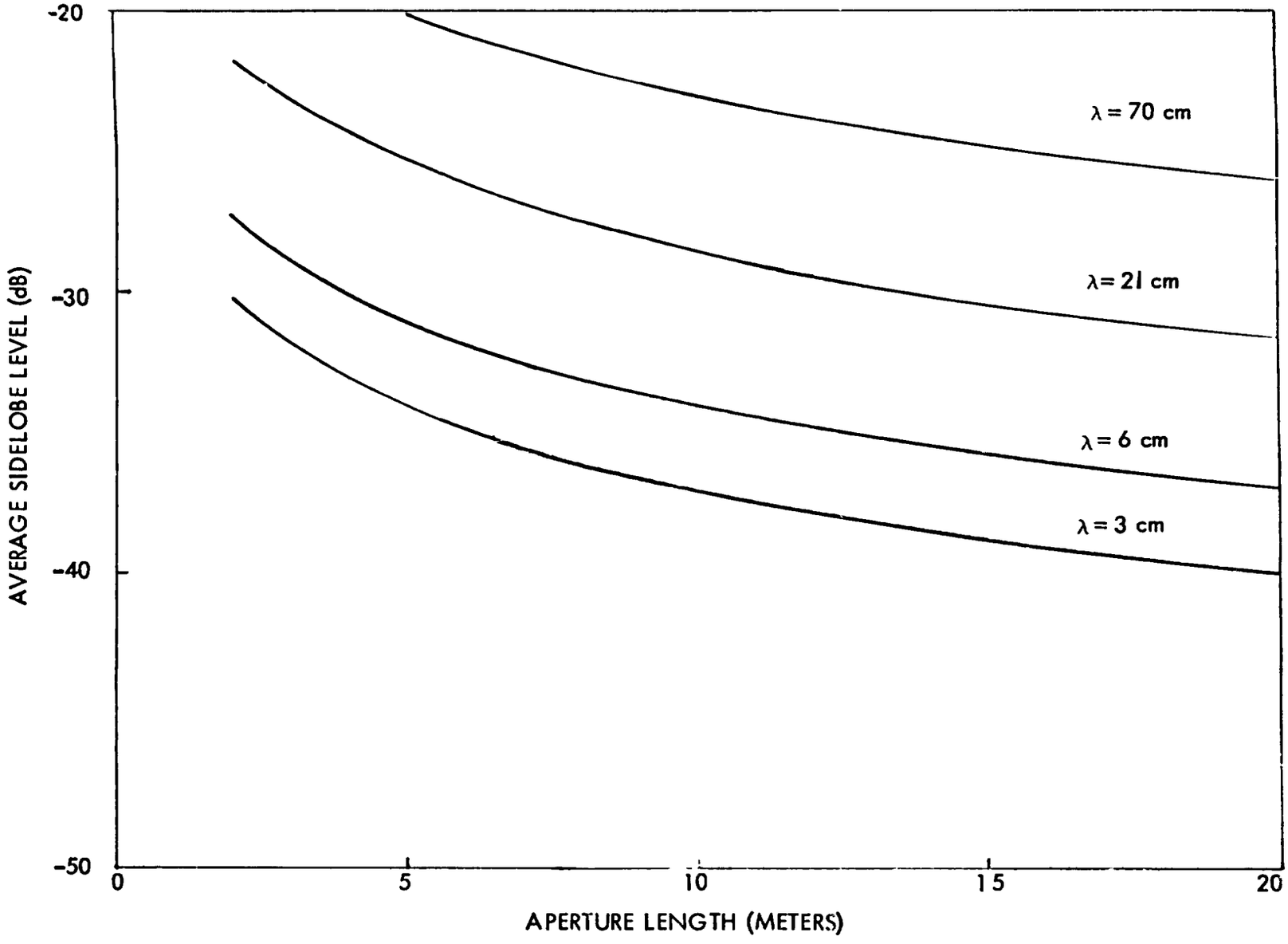

Figure 4-2. Sidelobe Level Versus Length For 90% Efficiency

level is plotted versus aperture length for various wavelengths assuming 90 percent beam efficiency.

4.3 APERTURE ACCURACY VERSUS ARRAY SIZE

The most significant errors which affect the performance of a phased array are phase errors. By relating phase errors to wavelength it is possible to measure array accuracy in terms of fractions of a wavelength. Thus, for an aperture 10 wavelengths long, a phase error of 0.02 wavelengths corresponds to an aperture accuracy of one part in 500.

In order to achieve 90 percent beam efficiency from a phased array, it is necessary to limit phase errors to a maximum of 0.05 wavelengths. Using this criteria a plot of aperture accuracy versus aperture length was generated for various wavelengths. This graph is shown in Figure 4-3.

4.4 INSERTION LOSS VERSUS APERTURE SIZE

Insertion loss of an array is primarily dependent on the type and length of transmission line used in the array. Equations for insertion loss as a function of length for various types of transmission line have already been discussed in Section 2.7. Using the equation for loss derived for a coaxial transmission line, a graph has been drawn to show attenuation as a function of length for various size coaxial transmission lines operating at various frequencies. This graph is shown in Figure 4-4.

The loss of a waveguide planar array has been calculated for two beamwidths, 0.5 degree and one degree, and plotted as a function of wavelength in Figure 4-5. It is interesting to note that as the frequency decreases the difference in loss between the the two arrays decreases indicatint that at the lower frequencies the insertion loss of an array is less sensitive to array size.

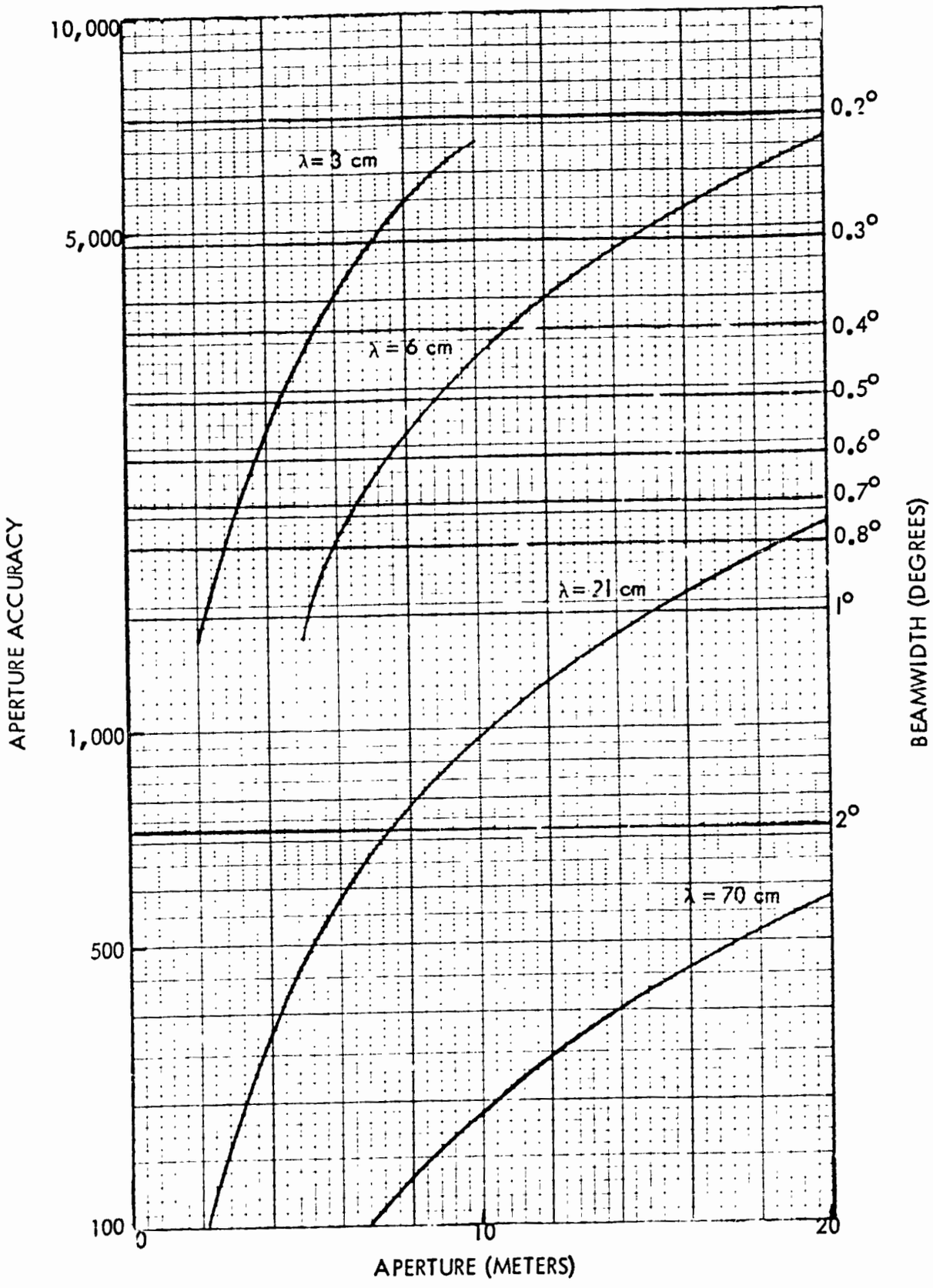

Figure 4-3. Aperture Accuracy - 90% Beam Efficiency

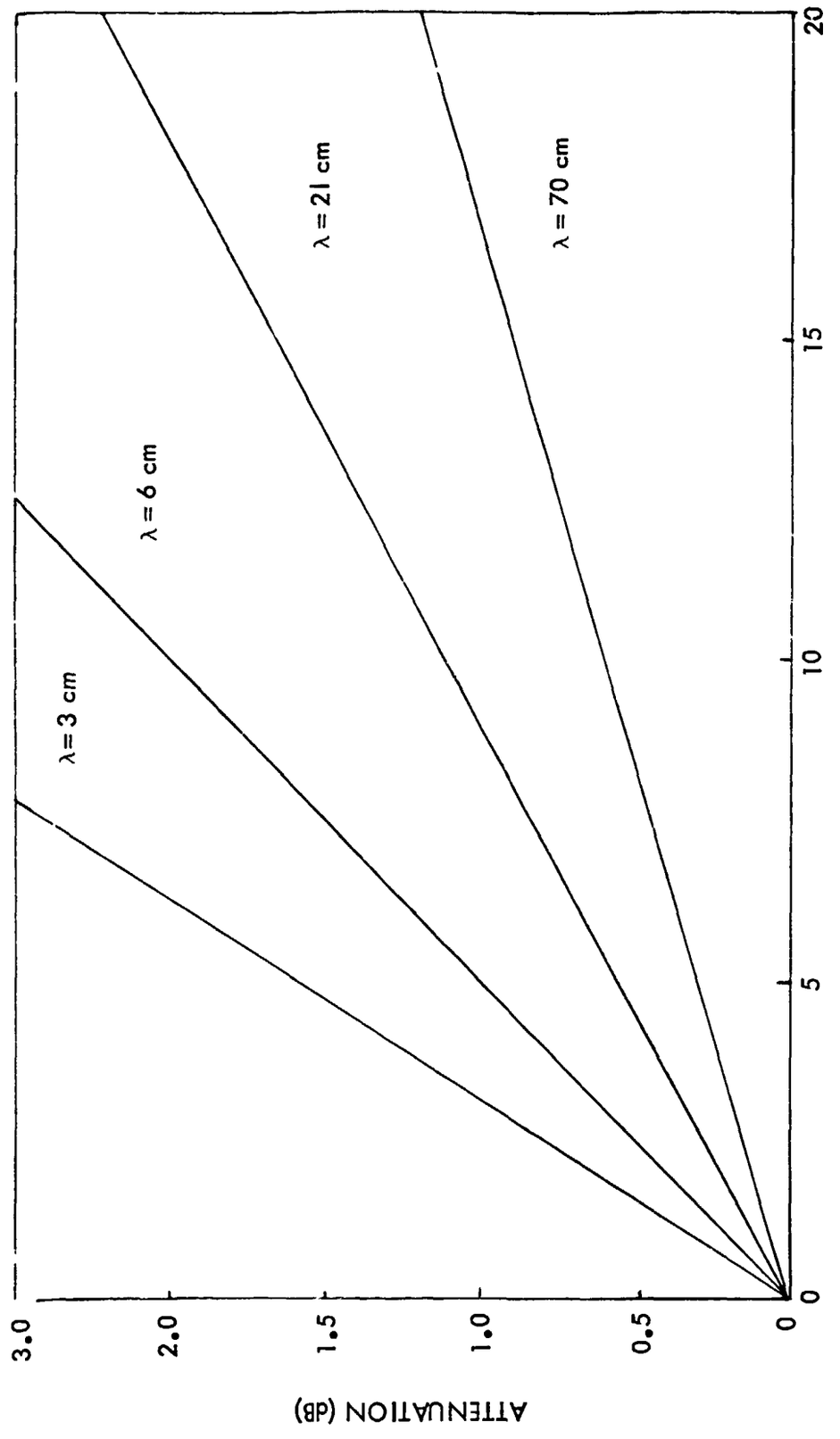

Figure 4-4. 1/2 Inch Coax Attenuation Versus Length

Figure 4-5. Linear And Feed Element Waveguide Loss For A Planar Array

5.0 MULTIFREQUENCY OPERATION

To achieve multifrequency operation from a planar phased array, it is necessary either to use a very broadband transmission line, e.g., coaxial line, together with broadband radiating elements, or to interlace two or more single frequency arrays together to form a common aperture. In either case, the array element spacing is the primary limiting factor in the array design. The problem is basically to arrange the radiating element such that all the elements operating at a common frequency satisfy the spacing criteria comensurate with grating lobe suppression and scan plane requirements.

Once the element spacing criteria have been established, it is necessary to look at the types of radiating elements which can be implemented at each frequency band, and compare their sizes to the available element spacings. Examples of multifrequency array designs can then be discussed together with possible design problem areas.

5.1 ARRAY ELEMENT SPACING

Array element spacing is dependent on two factors, grating lobe suppression and the desired squint angle or scan plane of the main beam. If two arrays operating at different frequencies are to be interlaced to form a single aperture, then the element spacing must be at a maximum. Thus, the practicality of interlacing two arrays depends on the required scan range of the array, and the plane in which the beam is to be scanned.

It is assumed for this discussion that the beam is to be scanned in a broadside or near-broadside plane over a range of ± 30 degrees. To achieve a broadside scan the array must be resonant. Since a resonant array is inherently a very narrow bandwidth

system, the emphasis here will be placed over the non-resonant array and near-broadside scan.

To achieve near-broadside scan with a non-resonant waveguide array, there must be phase reversal between elements in the non-scanned plane. In this case the position of the beam relative to broadside is given by the equation

$$\theta = \sin^{-1}\left[\lambda/\lambda_g - \lambda/2d\right]$$

where θ is the beam pointing angle, λ_g is the guide wavelength and d is the inter-element spacing.

It is apparent that the beam will be at broadside for $\lambda/\lambda_g = \lambda/2d$. Since a broadside beam will result in a high VSWR in a non-resonant array, normal practice calls for placing the beam one null beamwidth off broadside, hence

$$\lambda/\lambda_g - \lambda/2d = \sin(\theta_n)$$

where θ_n is the null beamwidth of the array. However, for the purpose of comparing relative element spacing as it pertains to the interlacing of arrays, θ_n will be assumed to be approximately zero and

$$\lambda/\lambda_g = \lambda/2d$$

or

$$d = \lambda_g/2$$

The criteria for the suppression of grating lobes requires that

$$d/\lambda < \frac{1}{1 + |\sin \theta|}$$

If θ is zero degrees for the broadsize case, then d/λ must be less than one and $\lambda_g/2$ must be less than λ. Thus, in the non-scanned plane of the array, the radiating elements must be spaced either slightly more than or slightly less than one-half guide wavelength apart, and the guide wavelength must be less than twice the free space wavelength.

In the scanned plane the element spacing is governed either by the grating lobe suppression criteria. Thus, for a ± 30 degree scan range, the spacing is limited to

$$d/\lambda < \frac{1}{1 + \left[\sin (30^{\circ})\right]}$$

or

$$d/\lambda < 0.666$$

From the above equations it can be seen that the maximum spacing of elements in the scan plane is 0.667λ and in the non-scan plane is approximately $\lambda_g/2$ with λ_g a function of waveguide geometry. In a frequency scanning array the beam is usually designed to be at broadside at the center frequency. This implies that the element spacing in both the scan plane and the non-scan plane must be approximately $\lambda_g/2$.

The guide wavelength for waveguide is given by

$$\lambda_g = \frac{\lambda}{\sqrt{1 - (\lambda/2a)^2}}$$

where "a" is the broad dimension of the guide. By decreasing the dimension "a" or in effect operating near the cutoff wavelength at the waveguide, the guide wavelength, λ_g, can be increased thus increasing the element spacing. The minimum value to which "a" can be reduced is that which produces the maximum value of spacing commensurate with suppression of the grating lobes or in equation form for the non-scan plane.

Assume

$$d = \lambda_g/2$$ (spacing required for a broadside beam)

and

$$d < \lambda$$ (spacing limitation for suppression of grating lobes - non-scan plane)

then

$$\lambda_g/2 < \lambda$$

substituting for

$$\lambda_g$$

$$\frac{\lambda}{2\sqrt{1-(\lambda/2a)^2}} < \lambda$$

or

$$\sqrt{1-(\lambda/2a)^2} < 1/2$$

hence

$$a < .577\,\lambda$$

It must be remembered, however, that as the dimension, "a", is decreased the waveguide attenuation increases.

Thus, it is possible to achieve element spacings of very nearly one wavelength in the non-scan plane at the expense of increased insertion loss. The element spacing in the scan plane is still controlled by the grating lobe criteria for the given scan range of $\pm$30 degrees, i.e., $d < .667\,\lambda$.

5.2 ARRAY RADIATOR ELEMENT TYPES

Brief descriptions of some of the more common radiating elements will be given in the following sections with emphasis placed on the size of the elements as a function of wavelength.

5.2.1 DIPOLE

The dipole is a radiator with good polarization characteristics generally used at frequencies below X-band. It is typically fed by either stripline or coaxial transmission line. It must operate above a ground plane and can be characterized as to physical size by the sketch shown in Figure 5-1. The primary disadvantage of the dipole is the face that it extends above the ground plane. This gives rise not only to packaging problems, but also enhances mutual coupling effects between elements especially as the beam is scanned off broadside.

5.2.2 YAGI DIPOLE

The Yagi dipole is essentially a dipole with added elements to increase the gain. These elements, i.e., the director and reflector elements, can also be used to provide multifrequency operation. An example of a dual frequency Yagi is shown below.

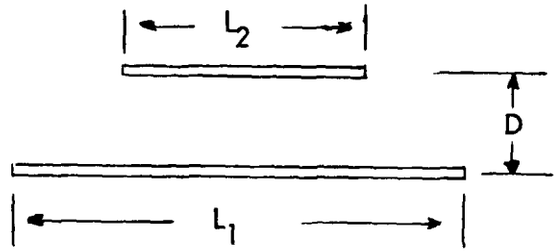

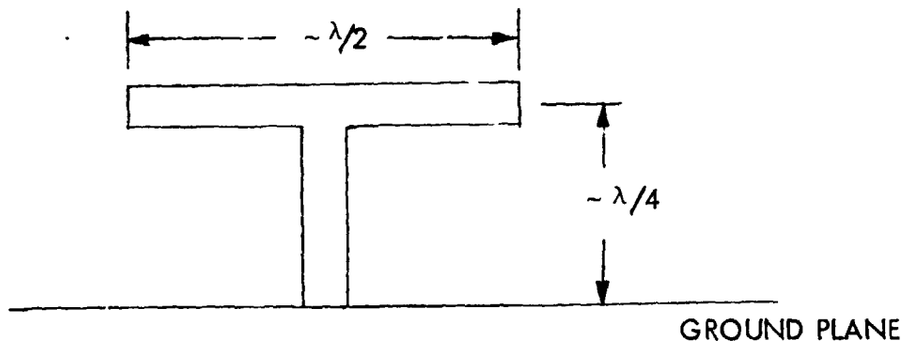

Figure 5-1. Dipole Radiator

At frequency f_1, the element L_1 is the radiating element with L_2 acting as a director. At frequency, f_2, the element L_2 is the radiator and L_1 is a reflector element. The relative sizes are

L_2 as a director	$L_2 < L_1$
	$D \sim \lambda_1/12$
L_1 as a radiator	$L_1 \sim \lambda_1/2$
L_1 as a reflector	$L_2 < L_1$
	$D \sim \lambda_2/6$
L_2 as a radiator	$L_2 \sim \lambda_2/2$

The Yagi dipole also operates above a ground plane and has the same disadvantages as the dipole.

5.2.3 LOG PERIODIC RADIATOR

The log periodic radiator is a wide bandwidth antenna operated typically at frequencies below X-band. This element radiates in essentially an end fire direction requiring the antenna to be oriented with its longitudinal axis perpendicular to the plane of the array. Its configuration is shown in Figure 5-2.

λ_L in this sketch is the wavelength of the lowest frequency and λ_S is the wavelength of the highest frequency. Once again the greatest drawback of this type of radiator is the height above the plane of the array required by each element.

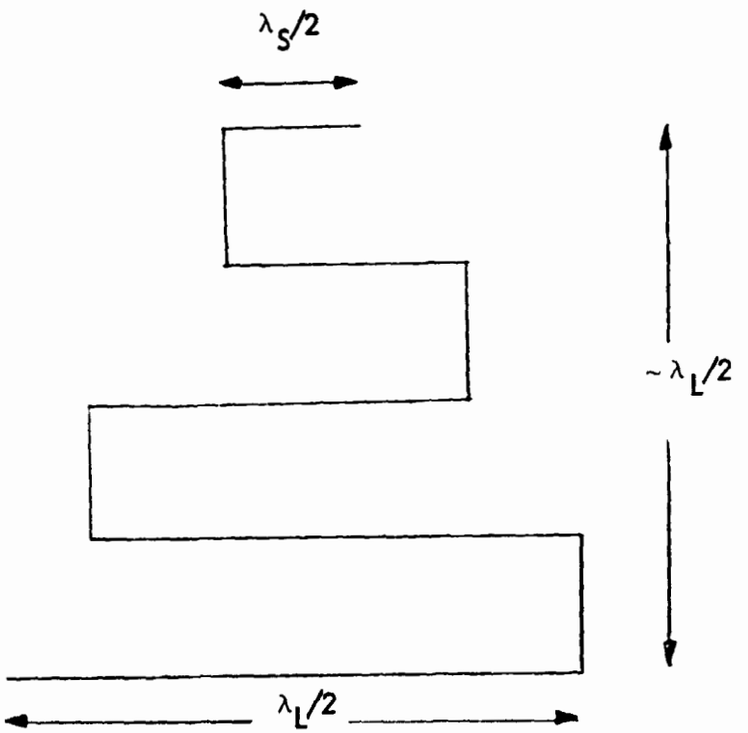

Figure 5-2. Log Periodic Radiator

5.2.4 SPIRAL RADIATOR

The spiral radiator is a broadband element whose bandwidth is determined by the diameter of the spiral. This element can be designed in a flat two dimensional configuration as shown in Figure 5-3. λ_L is the wavelength at the lowest frequency. The spiral radiator radiates a circularly polarized wave.

5.2.5 SLOT RADIATORS

Slot radiators can be used with either waveguide or stripline transmission lines. Waveguide slot radiators have been described previously in Section 1.3.3. Stripline slot radiators consist of slots approximately $\lambda/2$ in length cut through the conducting surface of one side of a dielectric filled triplate stripline configuration. The slot is fed by a center conductor sandwiched between two copper clad dielectric boards. The stripline slot radiates in a manner similar to the dipole radiating element. It has the advantage, however, of being located in the plane of the array surface, thus considerably reducing the packaging problem.

The transmission loss through stripline is the primary disadvantage of this type of element increasing significantly for frequencies above X-band. This loss problem can be reduced by interconnecting individual stripline radiators with low loss coaxial transmission line.

5.2.6 DIELECTRIC ROD RADIATORS

The dielectric rod radiator is an end-fire type antenna which typically consists of tapered dielectric rod fed by a section of waveguide as shown below.

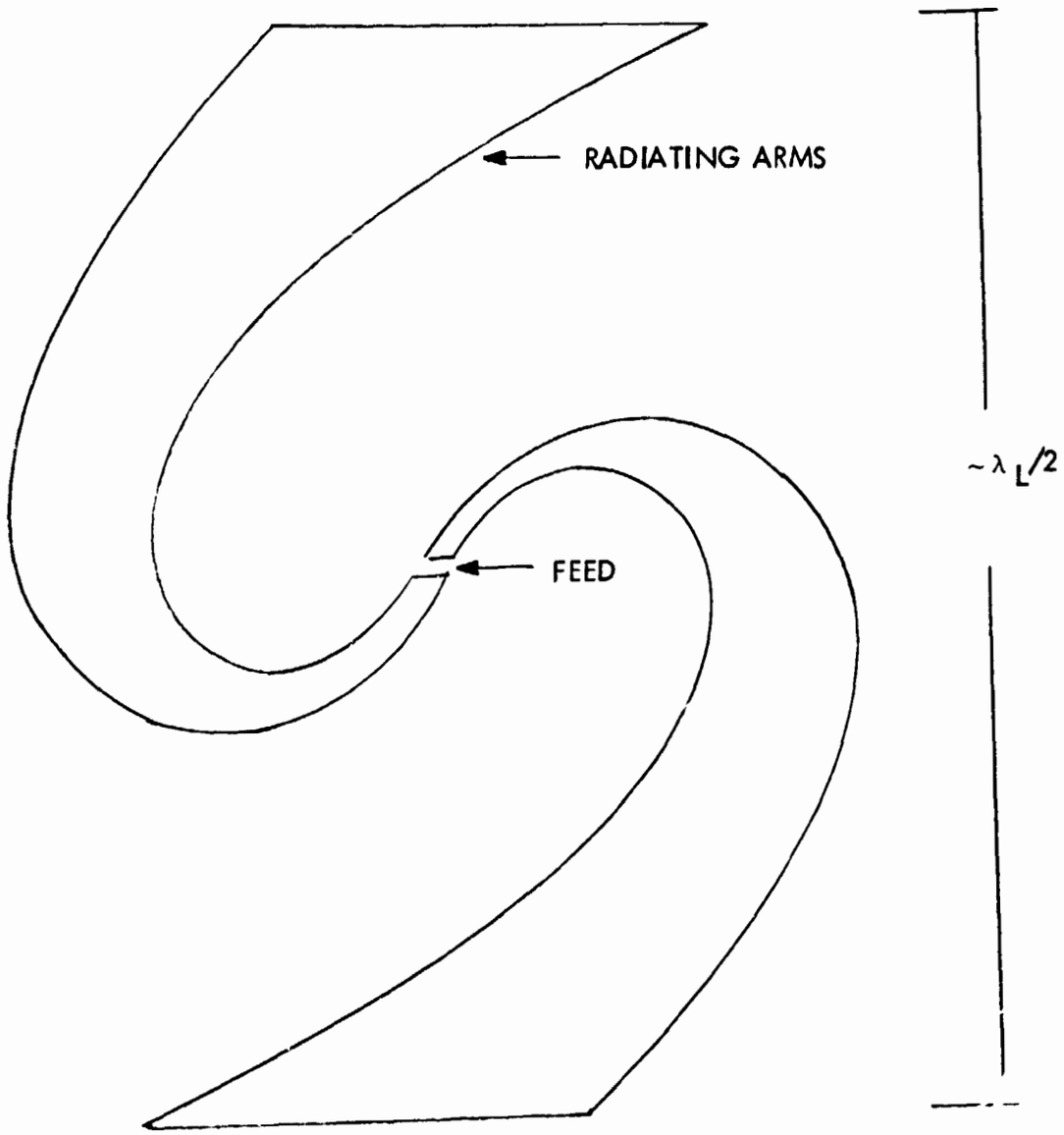

Figure 5-3. Spiral Radiator

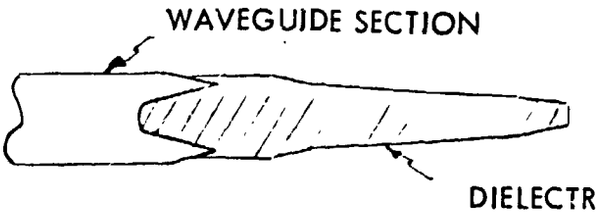

The dielectric rod supports surface waves which by proper tapering of the rod will radiate off the end of the rod with a well defined pattern shape. The gain or beamwidth of the radiated pattern is a function of the length of the rod. Proper selection of this length in conjunction with the dielectric constant of the material should result in an acceptable array element pattern.

5.3 MULTIFREQUENCY ARRAYS: EXAMPLES AND DESIGN PROBLEMS

The first example of a multifrequency array to be discussed will be the interlacing of three arrays operating at wavelengths of 70 cm, 21 cm, and 6 cm. The 6 cm array will be dual linearly polarized and all arrays will be constrained to scan ± 30 degrees in a plane broadside to the array surface.

To reduce transmission line loss and keep volume to a minimum, the feed lines for all arrays will be assumed to be 1 cm air filled coax. Since the wavelength in an air filled coax is equal to the free space wavelength, the spacing criteria of Section 5.1 reduces to a maximum spacing in both planes of the array of $\sim \lambda/2$. This means that the radiating elements for the three arrays will be spaced 35 cm, 10.5 cm and 3 cm apart. The 6 cm, or C-band, array will consist of two orthogonally polarized arrays interlaced to form a dual polarized array.

While it is conceivable that the feed lines for the four separate arrays (the 6 cm array consists of two separate feeding structures) could be interlaced, the major

problem area is the interlacing of the actual radiating elements. Assuming that the elements could be located so that there is enough room for them physically to exist side-by-side, the problem of aperture blockage remains. One possible design would be the use of dual frequency dielectric rod radiators for the C-band and L-band arrays assuming that the wavelengths were adjusted to be integer multiples of each other and that some method could be designed for coupling both frequencies to the single radiating element. This would reduce the problem to the interlacing of three arrays, the UHF (70 cm) array, the combined L-band/C-band array, and the orthogonally polarized C-band array. Even at this reduced level, the problem of aperture blockage and mutual coupling could have a significant effect on the beam efficiences of the arrays.

Based on these problems, it is apparent that a more practical solution is to separate the C-band array (which is already an interlaced array) from the UHF and L-band arrays. Interlacing of the UHF and L-band arrays is feasible and the use of thin dipole elements at UHF would minimize aperture blockage of the L-band antenna. By orienting the dipoles of the two arrays in orthogonal directions, the problem of physical placement of the individual radiators should be minimal.

6.1 SYSTEM DESCRIPTION

The recommended antenna system will consist of five phased array antennas. These antennas are (1) a UHF/L-band interlaced array, (2) a dual polarized C-band array, (3) an X-band linearly polarized array, (4) a linearly polarized K-band array and (5) a linearly polarized Ka-Band array. The design parameters of each of these arrays will be discussed in the following sections.

6.1.1 UHF/L-BAND INTERLACED ARRAY

The UHF-L-band array is visualized as a 15 m x 15 m antenna consisting of interlaced traveling wave phased arrays operating at wavelengths of 70 cm and 21 cm, respectively. Both arrays are linearly polarized. The radiating elements in both arrays will be spaced approximately one-half wavelength apart, allowing scan angles of up to $\pm$30 degrees from broadside scanned in a plane normal to the array surface. The quiescent or non-scanned (fail safe) position of the beam will be near broadside in both planes.

The 15 m aperture length will produce half power beamwidths at broadside of 1.0 degrees and 3.3 degrees for the L-band and UHF arrays, respectively, assuming a 40 dB Taylor distribution. As the beam is scanned to $\pm$30 degrees, the beams will broaden to 1.15 degrees due to aperture foreshortening. Frequency dispersive effects will broaden the beam an additional 2.0 percent for an assumed bandwidth of 35 MHz.

The radiating elements will be fed by 1/2 inch coaxial transmission lines. These coax lines will be air-filled coax with the transmission line wavelength equal to the free space wavelength. Each of these coaxial transmission lines will be coupled via directional couplers and variable phase shifters to a common feed line. The

directional couplers will be adjusted to provide the proper amplitude distribution in the feed plane. The variable phase shifters will be electronically controlled to produce phase scanning of the antenna beam.

The nature of the radiating elements for the two arrays will require some design trade-off study. From the standpoint of ease of design, dipole elements for both arrays appear most practical at least for the non-scan case. However, a dipole array when scanned, has inherent difficulties arising from increased mutual coupling and the apperance of "blind spots" in the same pattern. Also, the dipole array consisting of elements raised above the array surface, can be a source of mechanical problems, e.g., resonance points under vibration and packaging difficulties.

The stripline slot radiator is an attractive alternation to the dipole because of its low silhouette and relative ease of fabrication after the design has been finalized. The problems with a stripline radiator are its relatively high loss and the difficulty of making each element small enough to allow interlacing of the two arrays. The loss problem is significantly reduced by leading each element in parallel from a common coaxial feed line. Further design effort is needed to determine the feasibility of reducing the size of the stripline slot radiator sufficiently to allow the interlacing of two arrays.

Another possible configuration would be the interlacing of an array of dielectric rod radiators through an array of stripline slot radiators. While this method appears feasible from the standpoint of element spacing, the problem of feeding dielectric rod radiators from coaxial transmission line requires further study.

The overall insertion loss of the array, assuming stripline slot radiators and phase scanning, is predicted to be 1.8 dB for the L-band and 1.3 dB for the UHF array.

By holding the average sidelobe levels to a maximum of -25 dB for the UHF array and -30 dB for the L-band array, beam efficiencies of at least 90 percent can be expected. A table of antenna parameters is shown in Figure 6-1.

6.1.2 C-BAND DUAL POLARIZED ARRAY

The C-band antenna will consist of two interlaced waveguide arrays with each array radiating a separate orthogonal polarization. Each waveguide array will be a traveling wave array consisting of slotted linear array waveguides fed at one end by a common feed waveguide. The amplitude distributions in both planes will be adjusted by controlling the slot coupling coefficients. The beam will be phase scanned by a set of variable phase shifters located at the coupling ports of the feed waveguide.

The array will be 8.5 m square producing a broadside beamwidth of 0.5 degrees. At $\pm$30 degrees scan, the beam will broaden to approximately 0.58 degrees. The frequency dispersive proportions of the array will produce an additional 2.0 percent beam broadening assuming an RF bandwidth of 2.5 MHz.

The linear array waveguides can either be oriented so that radiation takes place from the narrow wall for both polarizations or by radiating alternately from the broad and narrow walls as shown below.

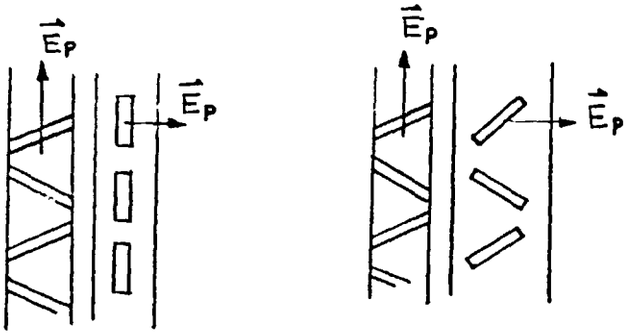

Configuration A Configuration B

Size	15 x 15 meters
λ	70, 21 cm
θ_3 dB	1°, 3.3°
Beam Broadening	1.2
θ_3' dB	1.2°, 4°
Linear Polarization, 70 cm and 21 cm	Crossed
2-1/2 Coax Feeds	
Stripline Slot Radiators or Dielectric Rod Radiators	
Phase Scan	
RF Bandwidth	35 MHz
ΔT, 1 sec, 600°K, Dicke	0.22°K
Scan 21 cm, ΔT = 1°K, Dicke	$\pm 9^\circ$
Scan ΔT = 1°K Continuous Power	$\pm 86^\circ$
ϵ	>90%
Loss λ = 21 cm	1.8 dB
λ = 70 cm	1.3 dB

Figure 6-1. Parameters for 70 cm and 21 cm Bands

It is obvious that Configuration A allows the array elements to be placed closer together, thus allowing wider scan angles. However, the longitudinal slots in Configuration A are non-resonant and do not allow any means of incorporating phase reversal between slots. This would place the beams approximately 45 degrees out of coincidence. To bring the beams into coincidence, dielectric loading of alternate slots would have to be implemented to achieve phase reversal. The elements in Configuration B will form coincident beams, but due to waveguide dimensions will significantly limit wide angle scanning.

The insertion loss of the array will be approximately 1.4 dB for both polarizations. Beam efficiencies of greater than 90 percent can be achieved if the average sidelobe is held to less than -33 dB. A table of antenna parameters is given in Figure 6-2.

6.1.3 X-BAND LINEARLY POLARIZED ARRAY

The X-band array will be a traveling wave, non-resonant waveguide array operating at a wavelength of 3 cm. The antenna will consist of slotted linear waveguide arrays fed at one end by a common feed waveguide. Slot coupling coefficients will control the amplitude distributions in both planes. The beam will be scanned by variable phase shifters located at the feed ports.

The antenna will be 3.7 m x 3.7 m producing a broadside beamwidth of 0.56 degrees. At scan angles of $\pm$30 degrees, the beam will broaden to 0.65 degrees due to foreshortening of the aperture. Frequency dispersive effects will broaden the beam an additional 20 percent assuming an RF bandwidth of 50 MHz.

The linear array waveguides will have resonant length slots cut into the narrow wall of the waveguide. This slot orientation will produce a linear polarization parallel to the longitudinal axis of the waveguides.

Size	8.5 x 8.5 meters
λ	6 cm
θ_3 dB	0.5°
Beam Broadening	1.2
θ'_3 dB	0.6°
Dual Polarized V and H	
Interlaced Waveguide	
RF Bandwidth	25 MHz
ΔT 1 sec, 600°, Dicke	0.25°K
Scan ΔT = 1°K Dicke	$\pm 4^\circ$
Scan ΔT = 1° Continuous Power	$\pm 16^\circ$
ϵ	>90 %
Loss	1.4 dB
3 Folds	

Figure 6-2. 6 cm Band

The insertion loss of the array will be approximately 1.5 dB. A beam efficiency of 90 percent can be attained if the average sidelobe level is held to less than -33 dB. The antenna parameters are tabulated in Figure 6-3.

6.1.4 K-BAND LINEARLY POLARIZED ARRAY

The K-band array is similar in nature to the X-band array described in the previous section. It will be 2.1 meters square producing a one-half degree beam. The beam will broaden 20 percent for an assumed 100 MHz RF bandwidth. The antenna parameters are tabulated in Figure 6-4.

6.1.5 Ka-BAND LINEARLY POLARIZED ARRAY

The Ka-band array is again similar in design to the X-band array. In this case the array will be 1.37 meters square, also producing a one-half degree beam. Twenty percent beam broadening for this array will occur with an assumed 150 MHz RF bandwidth. The antenna parameters are tabulated in Figure 6-5. Because of the relatively small aperture area, a separate array may be used if dual polarization is desired.

6.2 FREQUENCY SCANNING

The method of frequency scanning has been discussed briefly in Section 1. The frequency scanning method is attractive at the lower frequencies since the waveguide or coax losses are somewhat lower. Also, if a small scan angle is dictated by requirements of $\Delta T = 1^{\circ}K$ per beam position, then the required frequency range to scan is moderate. A continuous power radiometer with Dicke type stability is being developed by Sense Systems Company.* This will enable the ΔT of a phased or frequency scanned system

* Patent pending.

Size	3.7 x 3.7 meters
λ	3 cm
θ_3 dB	0.56°
Beam Broadening	1.2
θ'_3 dB	0.67°
Waveguide	
Single Polarization	
Phase Scan	
RF Bandwidth	50 MHz
ΔT 1 sec, 600° Dicke	0.18°K
Scan $\Delta T = 1°K$ Dicke	$\pm 6°$
Scan $\Delta T = 1°K$ Continuous Power	$\pm 25°$
ϵ	90%
Loss	1.5 dB
No Folds	

Figure 6-3. 3 cm Band

Size	2.1 x 2.1 meters
λ	1.5, 1.4, 1.35 cm
$\theta_{3\ dB}$	0.5°
Beam Broadening	1.2
$\theta'_{3\ dB}$	0.6°
Single Polarized	
Waveguide	
Phase Scan	
RF Bandwidth	100 MHz
ΔT 1 sec, 1200°, Dicke	$0.25^{\circ}K$
Scan$\Delta T = 1^{\circ}K$ Dicke	$\pm 8^{\circ}$
Scan$\Delta T = 1^{\circ}K$ Continuous Powe	$\pm 32^{\circ}$
	>90%
Loss	2.2 dB
No Folds	

Figure 6-4. 1.5 cm Band

Size	1.37 x 1.37 meters
λ	0.95 cm
θ_3 dB	0.5°
Beam Broadening	1.2
θ'_3 dB	0.6°
Dual Polarized	
Separate Arrays	
Phased Scanned	
RF Bandwidth	150 MHz
ΔT 1 sec, 1200°, Dicke	$0.2^\circ K$
Scan $\Delta T = 1^\circ K$, Dicke	$\pm 12^\circ$
Scan $\Delta T = 1^\circ K$, Continuous Power	$\pm 48^\circ$
ϵ	>90%
Loss	2.3 dB
No Folds	

Figure 6-5. 1 cm Band

to be improved by a factor of two. As an example, take the case of the above 6 cm system which with a Dicke system has a $\Delta T = 0.25^{\circ}K$ for a bandwidth of 25 MHz (1.2 beam broadening). This allows a scan of 16 cells for a $\Delta T = 1^{\circ}K$ since the integration time is proportionate to $(1/\Delta T)^2$. Thus, a scan of $\pm 4^{\circ}$ can be obtained.

If no loops of waveguide were in the feed line, the antenna would scan approximately $1/2^{\circ}$ for 36 MHz frequency shift thus to scan 16 cells would require approximately 600 MHz bandwidth at 5 GHz.

The antenna would also scan approximately $\pm 4^{\circ}$ in the element direction.

If a continuous power radiometer were used, four times as many or 48 cells could be scanned, producing a scan of $\pm 16^{\circ}$ which may be advantageous in some earth-observing experiments. This would require a bandwidth of approximately 2.4 GHz or 50 percent. Since this bandwidth seems excessive, the antenna becomes more frequency sensitive in the scan feed by introducing 10 λ loops of line between each linear element, making the system approximately 10 times as frequency sensitive in the scan plane. Thus to scan $+16^{\circ}$ a five percent frequency change or 250 MHz band is necessary. An added advantage may be that in the element plane the antenna scan is now $\pm 1.6^{\circ}$.

To accomplish this the feed line is now approximately 10 times longer or approximately 85 meters long. One obvious effect is to increase the insertion loss of the feed line. The loss of 8.5 meters of guide is 0.4 dB for aluminum at $\lambda = 6$ cm. This would increase to 4 dB for 85 meters, not counting the extra loss due to bends. The effective loss of the feed due to its radiation is approximately 1/2 the waveguide loss. Thus the loss of the frequency scan system is increased by approximately 2 dB. Since a phase shifter will have a loss less than 1 dB, the frequency scan system is 1 dB more lossy than a phase scan system.

In an array, the linear elements are usually spaced further apart than $\lambda/2$, thus the beam in the scan plane is off broadside, typically 20° to 30°. This situation is readily corrected in the phase scan case by the phase shift beam control network. In the frequency scan case, if the beam is to be broadside at the center frequency, a fixed phase correction will be necessary at each linear element input. This could be accomplished by cocking the feed at the appropriate angle.

One problem with frequency scan systems is the tight mechanical tolerances required to maintain a low VSWR since all of the bend VSWR's tend to add in phase. This requires precision cast bends (VSWR < 1.02 typical) and accurate joints.

The L/λ for a θ_3 dB = $1/2^\circ$ is 140 wavelengths. If we set a $\Delta\lambda/\lambda$ = 1/20 tolerance on the antenna for ϵ = 90 percent, the tolerance on the antenna is 1 part in 2800. The coefficient of thermal expansion of aluminum is $2 \times 10^{-5}/^\circ C$.

Thus for $\Delta\lambda/\lambda = 1/20$

$$\Delta t = 1\ (2.8 \times 10^3)\ (2 \times 10^{-5}) = 18^\circ C$$

Thus an $18^\circ C$ temperature variation along the array would cause a 90 percent beam efficiency for a non-frequency scanning case.

For a frequency scanning case the sensitivity would be $1.8^\circ C$.

Since in the system other errors such as mechanical will occur, it is desirable to keep the temperature stability to approximately 1/2 of the above values or approximately $1^\circ C$ for the frequency scan case.

For a phase shifter scanning array we have phase shifters that are temperature sensitive. However, these can be compensated by electronic control such as thermistors.

The phase shift scan is perhaps more versatile in being able to scan any sector or width desired on command.

In summary, both systems have their advantages and should be considered based on the versatility desired in the experiment and the instrument problems.

It has been shown in previous systems that a beam efficiency of 90 percent can be obtained with phase shifters. Since this implies that a $\Delta\lambda/\lambda$ error of 1/20 was obtained, the efficiency would remain at 90 percent due to phase shifter errors alone. With some effort, there is no reason why the phase shift error could not be reduced well below $\Delta\lambda/\lambda = 1/20$.

Since many types of errors will not be random, but systematic, the above discussion only covers the random error case and the systematic errors should be further studied.

6.3 MECHANICAL

6.3.1 VOLUME

The volume of the pallet available on the shuttle for all experiments is a cylinder approximately 20 meters long and approximately four meters in diameter. A portion of this space is available for the SIMS instrument. Based on the storage volume available and the desire to avoid as many RF joints which move as possible, a tentative configuration has been chosen. A criterion that it would be best to avoid folding the array along the linear elements if possible to minimize the moveable RF connections. Thus the arrays would be folded in the scan plane. Since the pallet is 20 meters long, a stowed length of 15 meters was chosen.

The deployed arrays are shown in Figure 6-6. There are three RF connections at (4) for the 21 cm and 70 cm arrays. The 6 cm array has two RF connections at (3)

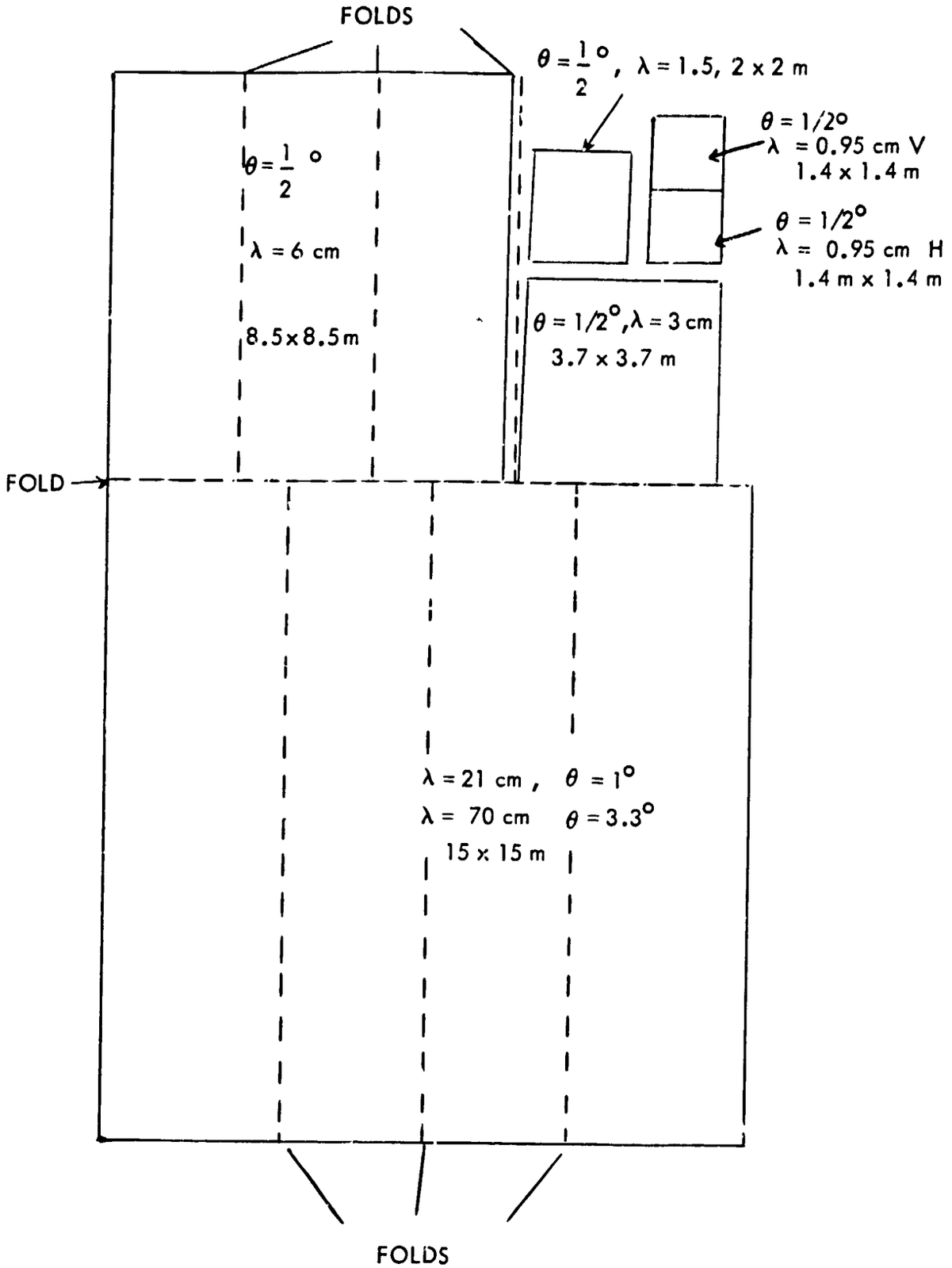

Figure 6-6. Deployed Antennas

for each polarization. The higher frequency arrays as shown require no RF folds. Figure 6-7 shows the arrays stowed on the pallet. The actual size and method of stowing requires an involved design and these configurations are to indicate that it is feasible to stow the system in the available volume. It is also clear that the selection of the radiating elements is a key design area to keep the thickness as small as possible allowing a large aperture area.

6.3.2 WEIGHT

The weight of the larger arrays must be low per area to keep the overall weight down. An estimate of the weight of the antenna is for the antenna and electronics and no support structure. Assume the 21 cm antenna consists of radiators on 10 cm x 12 cm centers with a linear element feed 12 cm apart consisting of 1 cm coax lines with a wall thickness of 0.5 mm. The coax weight is approximately 500 g/meter. Thus a total weight of 0.7 K g/meter is obtained. Since there are 8 meters of coax per square meter, the 21 cm array weighs approximately 5 Kg/meter^2 for the antenna. The electronics and associated phase shifters would weigh less than 50 kg for a total weight of approximately 1000 kg.

The 70 cm system using the same size coax and elements would weigh approximately 2 K g/m^2 or approximately 500 kg.

If thinner wall coax or smaller diameter coax can be used, it can significantly reduce the weight of the system.

Assume the 6 cm array to be 0.5 mm thick wall aluminum waveguide with a 2:1 aspect ratio with the narrow walls on the face of the array. This results in a weight of approximately 5 kilograms per square meter. The array weight is approximately 350 kilograms for a total weight of approximately 400 kilograms.

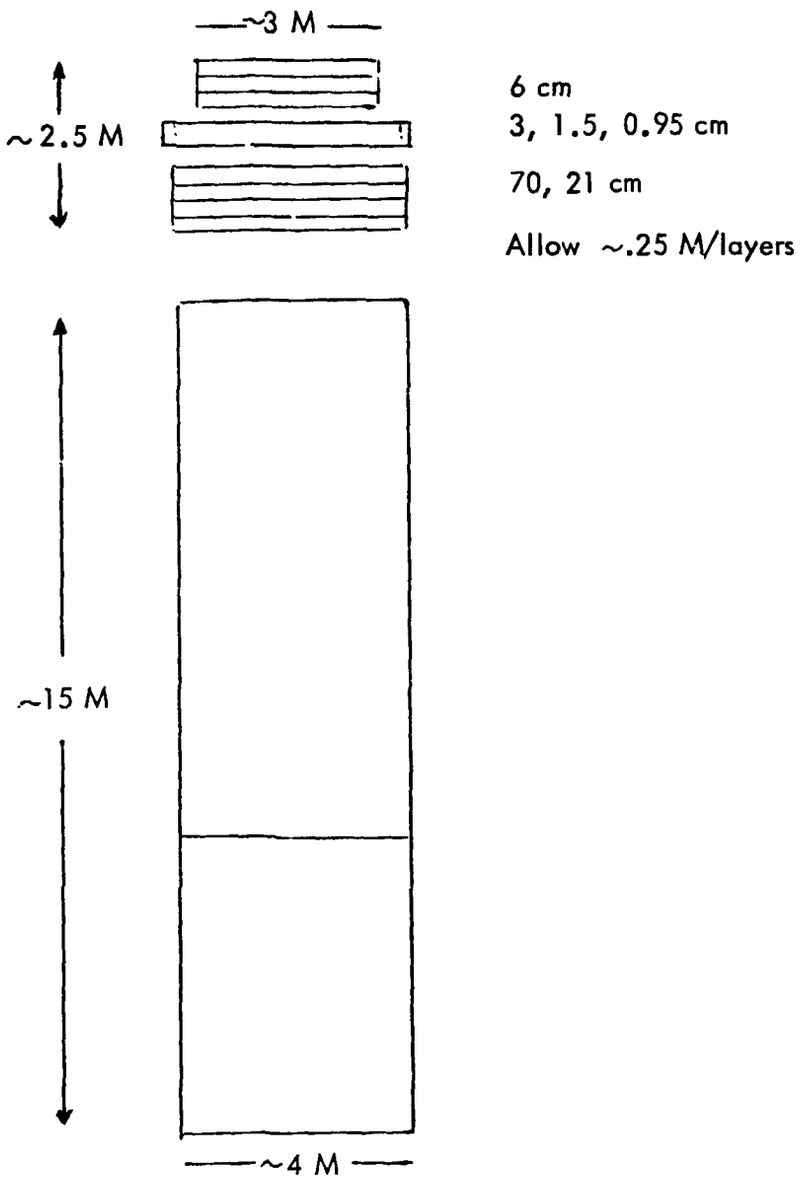

Figure 6-7. Stowed on Pallet

The 3 cm array will weigh approximately 5 kilograms per square meter or 65 kilograms for a total weight of approximately 90 kilograms.

The 1.5 cm array will weigh approximately 5 kilograms per square meter or a total of 35 kilograms.

Each 1 cm array will weigh approximately 25 kilograms.

By using thinner wall waveguide, the above weights would be further reduced.

A weight summary follows:

λ_{cm}		Weight (kg)
70		500
21		1000
6		400
3		90
1.5		35
1		50
	Total	2075 kg

6.4 POWER

The power requirements of the system increase with the increase in number of phase shifters. The Nimbus E ESMR required 35 watts of power. By using latching phase shifters and a more efficient dc-dc converter, this could be reduced to 25 watts.

The larger systems proposed will require more phase shifters raising the power to approximately 35 watts per system. If all wavelengths were used the total power requirements would be approximately 300 watts.

7.0 CONCLUSIONS AND RECOMMENDATIONS

A multiple frequency antenna system consisting of scanning planar phased arrays for the Shuttle Imaging Microwave System is feasible both from the electrical and mechanical design viewpoint. To achieve beam efficiencies or at least 90 percent at all the wavelengths of interest, it is recommended that separate apertures be used for the systems operating at frequencies of C-band and above. The L-band and UHF systems can be interlaced satisfactorily and meet the required system specifications.

The use of individual apertures at the various wavelength requires the proper selection of the individual aperture size commensurate with the desired beamwidth and total available volume. The recommended system will provide one-half degree beamwidths for the apertures operating at C-band and above with the UHF and L-band arrays producing beamwidths of 3.3 degrees and 1.0 degrees, respectively. The total system will require a volume of approximately 66 cubic meters.

Traveling wave arrays are recommended for all systems in order to optimize the input impedance and bandwidth characteristics of the arrays. It if further recommended that the arrays be one-dimensionally fed using a traveling wave feed array, or feed bus, to distribute the energy to the linear array elements. The feed array can be either end-fed or center-fed. It is recommended that the center-fed configuration be considered as a possible method of reducing insertion loss of the feed array.

Phase scanning is the recommended method of scan for all arrays if a wide angle scan is desired. Frequency scanning is a feasible alternative if limited scan angles are acceptable. For most of the arrays the 90 percent beam efficiency specification imposes stringent requirements on average sidelobe level, thus implying the need for minimal phase shifter errors. It is recommended that further study efforts be made to determine the range of maximum phase error tolerances achievable for various phase

shifter designs. Due to the thermal sensitivity of most phase shifters, it is also recommended that further study be made of thermal compensating networks for phase shifters.

It is concluded, therefore, that based on the results of this study effort, the recommended antenna system outlined in Section 5 of this report can be designed using state-of-the-art technology to meet the required specifications of the SIMS system.

REFERENCES

1. Dolph, C.L., "A Current Distribution which Optimizes the Relationship between Beamwidth and Sidelobe Level", Proc. IRE, Vol. 24, June 1946, pp.335-348.

2. Taylor, T.T., "Design of Line-Source Antennas for Narrow Beamwidth and Low Sidelobes", IRE Transactions, Jan. 1955, pp. 16-28.

3. Hanson, R.C., Microwave Scanning Antennas, Vol. II, III, Academic Press 1966.

4. Dion, Andre, "Nonresonant Slotted Arrays", IRE Transactions, Vol. AP-6, October 1968, pp. 360-365.

5. Van Aulock, "Properties of Phased Arrays", Proceedings IRE, Vol. 48, Oct. 1960, 1715,1727.

6. Ruze, J., "Antenna Tolerance Theory - A Review", Proceedings IRE, Vol. 54, No. 4, April 1966, pp. 633-640.

7. Nash, K.T., "Beam Efficiency L mitations of Large Antennas", IRE Transactions, Dec. 1964, pp. 918-923.

8. Elliot, R.S., "Mechanical and Electrical Tolerances for Two-Dimensional Scanning Antenna Arrays", IRE Transactions, Jan. 1958, pp. 114-120.

9. Moreno, Theodore, "Microwave Transmission Design Data", Dover Publications, Inc., New York, N.Y., 1958.

10. Butler, J. and Lowe, R., "Beam Forming Matrix Simplifies Design of Electronically Scanned Antennas", Electronic Design, No. 9, pp. 170-173, 1961.

11. Ruze, J., "Wide Angle Metal Plate Optics", Proceedings IRE, Jan 1950, pp. 53-59.

12. Silver, S., "Microwave Antenna Theory and Design", Vol. 12, MIT Radiation Laboratory Series, McGraw-Hill Book Company, 1949.

13. Jasik, H., "Antenna Engineering Handbook", McGraw-Hill Book Company,1961.